UNIVERSITEIT
GENT

Faculty of Medicine and Health Sciences
Department of Surgery

Integrated study of the effects of antiangiogenic therapy on microvascular physiology in human cancer models

Debergh Isabelle

Co-Promotor: Prof. Dr. P. Pattyn
Promotor: Prof. Dr. W. Ceelen

Thesis submitted in fulfilment of the requirements for the degree of
'Doctor in the Medical Sciences'
2014

Table of contents

List of Abbreviations

ADC	apparent diffusion coefficient
AF	vascular area fraction
AMel-3	Fortner's amelanotic hamster melanoma
Ang	Angiopoietin
αSMA	α-smooth muscle actin
AT	antithrombin
AUC	area under the curve
bFGF	basic fibroblast growth factor
CA	contrast agent
CE-US	contrast enhanced ultrasonography
CT	computed tomography
CRT	chemoradiation
D	microvessel diameter
DCE	dynamic contrast enhanced
DOTA	tetraazacyclododecane tetraacetic acid
DTPA	diethylenetriaminepentaacetic acid
EC	endothelial cells
ECM	extracellular matrix
FVIII	factor VIII, von Willebrand factor
FDG	^{18}F-fluorodeoxyglucose
FGF	fibroblast growth factor
FGFR	FGF receptor
FITC–dextran	fluorescein isothiocyanate–labelled dextran
FLT	^{18}F-3'-fluoro-3' deoxythymidine
Gd	gadolinium
HaP-T1	nitrosamine-induced pancreatic cancer in hamsters
HER2	human epidermal growth factor receptor 2
HIF	hypoxia inducible factor
HSPG	heparane sulphate proteoglycan
IFP	interstitial fluid pressure
IL	interleukin
i.p.	intraperitoneal
i.v.	intravenous
IVM	*in vivo* microscopy, intravital microscopy
K	Baker–Wayland factor = 1.3
kDa	kilo Dalton
L	microvessel length per area
LMWH	low molecular weight heparin

MMP	matrix metalloproteinase
MRI	magnetic resonance imaging
MVD	microvessel density
MW	molecular weight
N	number of microvessels per high-power field
NER	normalized enhancement ratio
NIR	near-infrared
PAR-2	protease-activated receptor 2
PCI	pericyte coverage index
PDGF	platelet-derived growth factor
PDGFR	PDGF receptor
PET	positron emission tomography
PlGF	placental growth factor
PS	permeability surface product
RECIST	response criteria in solid tumours
RGD	Arg-Gly-Asp, arginylglycylaspartic acid
ROI	region of interest
RT	radiotherapy
s.c.	subcutaneous
s.d., SD	standard deviation
s.e.	standard error
SEM	standard error of the mean
SPECT	single-photon emission CT
TAA	tumour associated angiogenesis
TBS	tris-buffered saline
TF	tissue factor
TFPI	tissue factor pathway inhibitor
TKI	tyrosine kinase inhibitor
TNF	tumour necrosis factor
UF	unfractionated heparin
USPIO	ultra-small superparamagnetic iron oxide nanoparticle
V	centerline red blood cell velocity
VAF	vascular area fraction
VEGF	vascular endothelial growth factor
VEGFR	VEGF receptor
VM	vasculogenic mimicry
VNI	vascular normalization index
VTE	venous thromboembolic event
VQ	volumetric blood flow
vWF	factor VIII, von Willebrand factor

Introduction

CHAPTER 1: INTRODUCTION

Malignant diseases are the second most important cause of death worldwide, accounting for well over 7 million deaths in 2008, which is 12,6% of the annual mortality. Within 15 years, due to the growth and aging of the population, the global burden is expected to grow to 21.4 million new cancer cases and 13.2 million cancer deaths [1]. Cancer research remains an intense area of investigation, and despite many efforts the underlying mechanisms of cancer development, cancer behaviour, response or resistance to treatment, metastasis, etc. are not fully elucidated. Current treatment options include surgery, chemotherapy, radiation and immunotherapy, but these regimens hold serious disadvantages and aspecific side-effects. Selective tumour-targeted delivery of drugs or contrast agents is a promising approach for patient-tailored therapy. In the following chapters and studies, we highlight some aspects of the role of neoangiogenesis in cancer, and of targeting the angiogenesis in treatment and imaging.

1.1 HALLMARKS OF CANCER

The development of cancer is dependent on 10 essential alterations in cell physiology, as reported by Hanahan and Weinberg [2,3], dictating malignant growth: sustaining proliferative signaling, evading growth supressors, avoiding immune destruction, enabling replicative immortality, tumour-promoting inflammation, activating invasion and metastasis, inducing angiogenesis, genome instability and mutation, resisting cell death, and deregulating cellular energetics (Fig. 1.1). Each of these novel functional capabilities acquired during tumour development, represents a victory on an anticancer mechanism of the host tissue. These apparently normal neighbours (fibroblasts, endothelial cells (ECs), pericytes, extracellular matrix (ECM)), play key roles in driving tumour growth through paracrine signaling.

In the next paragraphs, we focus on the ability to induce tumoural angiogenesis, and on therapeutic strategies to block angiogenesis in the battle against cancer.
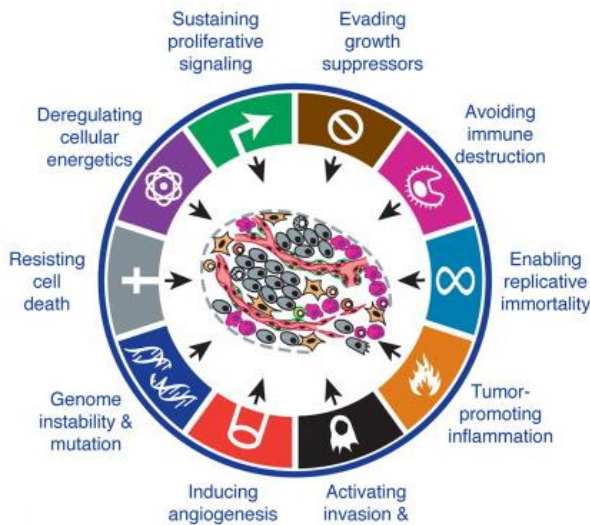

FIGURE 1.1: Acquired capabilities of cancer cells . (Adapted from Hanahan and Weinberg, 2011 [3]).

1.2 Tumour neovasculature

When neoplastic cells develop in a human body, without attack of the host immune system, multiplication of these cells will start. In this stage, all necessary nutrients and oxygen will be delivered by passive diffusion, which is sufficient for distances up to 100-200 μm. After reaching a critical mass, the formation of new blood vessels is needed to feed the tumour. The relationship between the vascular system and malignant diseases was already observed more than 100 years ago by Goldman *et al.* [4]. Several decades later, Folkman *et al.* [5] launched the idea to 'starve' tumours by blocking angiogenesis as tumour growth and metastasis rely on neovasculature.

Growing tumours develop new blood vessels through different endothelial-cell-related mechanisms (Fig. 1.2). The first one is budding and sprouting using endothelial cells in the established vascular network (sprouting angiogenesis). Secondly, intussusception expands the blood vessel system by invagination of the existing vascular lumen. Loop angiogenesis is described as expansion of translocated vessels by mechanical forces, from contracting myofibroblasts. A fourth important way to form new blood vessels is recruiting angioblastic progenitor cells from the blood stream, a process called postnatal vasculogenesis. Also, a similar process with new lymphatic vessels will take place in a tumour (lymphangiogenesis) [6].

Tumour-cell-related mechanisms include vascular mimicry (VM), mosaic vessel formation or vessel co-option (the incorporation of cancer cells into an existing vessel wall), and tumour cell differentiation into endothelial cells. Tumours with high IFP (interstitial fluid pressure) are known to have limited endothelial cell sprouting from the host tissue, but more VM channel formation [7] leading to a fraction of tumour vessels which is likely to be resistant to antiangiogenic treatment [8]. This type of neoplastic vasculature is described in lung, colon, liver cancers, sarcomas and melanoma and associated with poor overall survival in patients and metastatic disease [9].
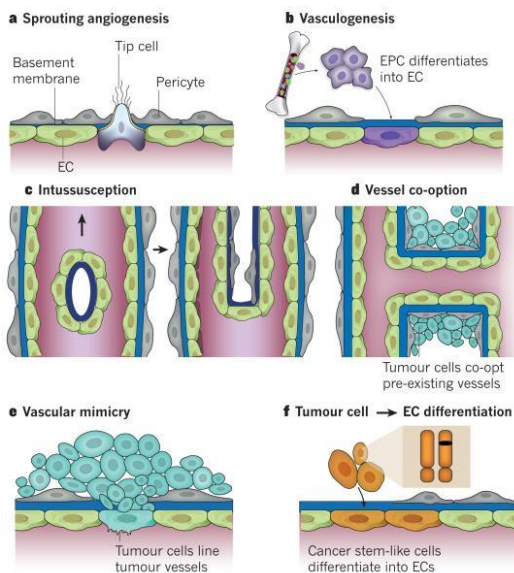

FIGURE 1.2: Sprouting angiogenesis, vasculogenesis, intussusception, vessel co-option, vascular mimicry, and tumour cell-to-endothelial cell differentiation are mechanisms for expanding the tumour vascular network. (Adapted from Carmeliet and Jain, 2011 [13]).

Unlike normal microvasculature, which has a regular and ordered structure, tumour vasculature is macroscopically chaotic, dilated, and tortuous [10,11]. Also microscopically, structural disorders are typical in these newly formed vessels. As a response to proangiogenic signals (such as vascular endothelial growth factor (VEGF) and Angiopoietin-2 (Ang-2)), pericytes detach, gaps between endothelial cells enlarge, and basement membrane remodels [12,13]. Consequently, microvascular function is abnormal, with an increased vessel leakiness and IFP [14,15]. These alterations produce spatial and temporal heterogeneity in blood flow and perfusion in tumours, leading to regional acidosis and hypoxia [16]. The abnormal microenvironment can promote tumour progression in various ways. Hypoxic conditions render cancer cells more malignant by changing the cell metabolism, promoting the epithelial-to-mesenchymal transition, and compromising the function of immune cells [17]. Another mechanism is the influence of the microenvironment on treatment resistance. In the early fifties, Gray and his group described the connection between low tissue oxygenation and tumour cell radioresistance: radiotherapy relies on the formation of oxygen radicals to kill cancer cells effectively [18]. Moreover, hypoxia inducible factor-1 (HIF-1) is known to upregulate the multidrug resistance gene (MDR1) resulting in efflux of chemotherapeutics [19]. Finally, due to increased IFP and poor perfusion, a low oncotic pressure difference across the tumor microvascular wall with high oncotic pressure in tumours, delivery of therapeutic agents to neoplastic cells will be suboptimal [14].

Taken together, the abnormal tumour vascular network results in an acid, hypoxic microenvironment with high IFP. These conditions contribute to tumour growth, metastasis and resistance to therapy. Normalizing this pathological environment could be an interesting strategy in the treatment of cancer.

1.3 Concept of vascular normalization

Antiangiogenic therapy was initially developed to target tumour blood and nutrient supply, and likewise to reduce tumour growth and metastasis by starvation [4]. Preclinical data supported this hypothesis in a mouse colorectal cancer model during anti-VEGF therapy [20]. Despite these findings, the reported beneficial effect of anti-VEGF monotherapy in clinical setting is modest [21], but reveals to be synergistic in combination with chemotherapy [22].

To explain these findings, Jain proposed the concept of vascular normalization for the first time in 2001 [23] (Fig. 1.3).

Antiangiogenic therapy could correct both structure and function of tumour vessels and as a consequence, produce a normalized microvascular environment with better prognosis and response to treatment. Indeed, several studies in different tumour models reported a positive effect on tumour oxygenation, an amelioration of delivery of systemically administered drugs into tumour and a reduction of cell shedding and metastasis [24]. Under physiological circumstances, proangiogenic factors (e.g. VEGF, basic fibroblast growth factor (bFGF), Ang-2) are in balance with antiangiogenic factors (VEGFR1, thrombospondin-1, Ang-1). In pathological conditions, such as cancer or inflammation, this balance is in favour of proangiogenic molecules: "the angiogenic switch". Therapy with antiangiogenic drugs can transiently correct this imbalance. The closure of the "window of normalization" relates to the activation of other proangiogenic

pathways in the tissue. Defining the timing and dosing of the antiangiogenic therapies in pharmacological studies is an essential next step.
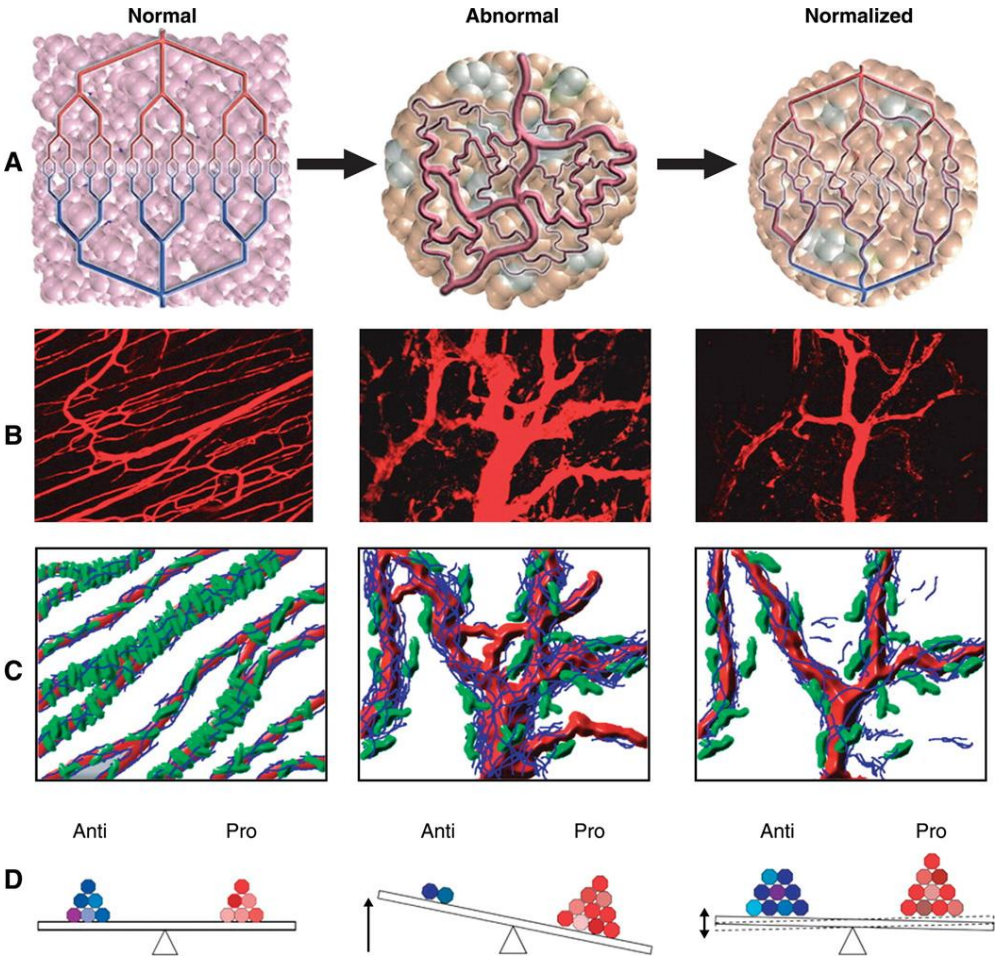
FIGURE 1.3: Proposed role of vessel normalization in the response of tumours to antiangiogenic therapy. A: tumour vasculature is structurally and functionally abnormal. It is proposed that antiangiogenic therapies initially improve both the structure and the function of tumour vessels. However, sustained or aggressive antiangiogenic regimens may eventually prune away these vessels, resulting in a vasculature that is both resistant to further treatment and inadequate for the delivery of drugs or oxygen. B: dynamics of vascular normalization induced by VEGFR2 blockade. On the left is a two-photon image showing normal blood vessels in skeletal muscle; subsequent images show human colon carcinoma vasculature in mice at day 0 and day 3 after administration of VEGR2-specific antibody. C: diagram depicting the concomitant changes in pericyte (red) and basement membrane (blue) coverage during vascular normalization. D: these phenotypic changes in the vasculature may reflect changes in the balance of pro- and antiangiogenic signaling in the tissue.
(Adapted from Goel *et al.*, 2011 [24]).

1.4 Proangiogenic molecular strategies

The principal angiogenic molecule responsible for vascular abnormalities is VEGF-A (also known as VEGF). This is produced by tumour cells in response to hypoxia/HIF, tissue factor (TF), oncogene activation, sex hormones such as estrogens and progesterones,

inflammatory cytokines. VEGF-A may also be derived from tumour-infiltrating myeloid cells, pericytes, or released from the extracellular matrix, and acts primarily via VEGFR2 on endothelial cells. In addition, VEGF-A stimulation of VEGFR2 on pericytes inhibits platelet-derived growth factor receptor (PDGFR)-mediated pericyte recruitment to endothelial cells, and causes vessel leakage. Placental growth factor (PlGF) may contribute to tumour vessel abnormalities through interaction with VEGFR1, and bFGF through interaction with fibroblast growth factor receptor (FGFR) (Fig. 1.4).

Integrins are plasma membrane receptors, upregulated on tumour cells or on activated endothelial cells, and mediate attachment between cells or the ECM, providing essential signals for cell migration and angiogenesis. Interactions between $\alpha_v\beta_3$ integrin and the FGFR and between $\alpha_v\beta_5$ integrin and VEGFR2 promote bFGF- and VEGF-mediated angiogenesis, respectively [24].

Another strategy of tumour cells to successfully permeate the ECM is to produce proteinases, e.g. heparanase or matrix metalloproteinase (MMP), with a degradation of the rigid ECM, allowing tissue invasion of both ECs and tumour cells, and metastasis. Tumour-derived growth factors bind to heparane sulphate proteoglycans (HSPGs) that are present in both the ECs and the ECM. Binding of the receptors on the endothelial wall results in proliferation and migration of ECs, leading to characteristic vessel abnormalities. HSPGs play also a crucial role in stabilizing tumour cells in the wall of vessels in VM or mosaic vessel formation [7].

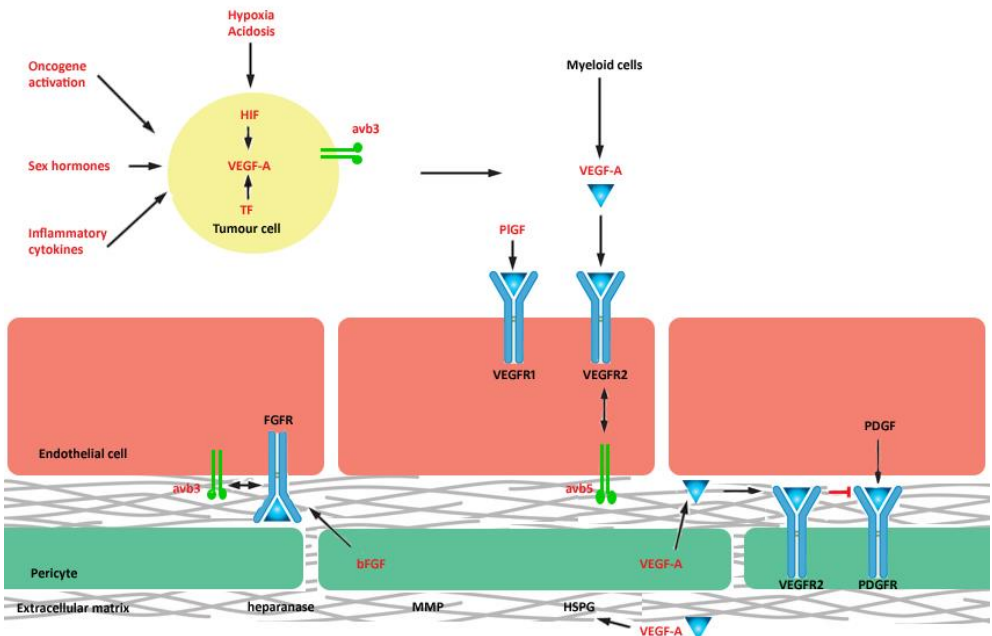**FIGURE 1.4:** Factors inhibiting the vascular normalization phenotype in tumours. This schematic depicts a tumour cell (yellow), endothelial cell (red), surrounding pericytes (green), and the extracellular matrix. (Adapted from Goel *et al.*, 2011 [24]).

All these proangiogenic strategies lead to an abnormal tumour neovasculature and an aberrant microenvironment, and contribute greatly to the malignant phenotype of

tumours. In this way, strategies to improve (or normalize) vessel structure and function through antiangiogenic therapies, may delay progression and improve delivery and efficacy of cytotoxic therapies.

1.5 Antiangiogenic therapy

1.5.1 Directly targeting VEGF pathways

VEGF-mediated signaling is important in tumour biology through its effect on angiogenesis and vascular permeability, but also on tumorigenesis [25] (Fig. 1.5). VEGF-targeted therapy is currently used for the treatment of many cancers. Dickson *et al.* [26] described after treatment with VEGF antibodies (e.g. bevacizumab) in mice bearing human neuroblastoma xenografts a decreased microvessel density (MVD), vessel length, diameter, and tortuosity. Also, an increased pericyte coverage index (PCI) was seen after therapy in these animals, which depicts maturation of vessels. Together with the structural changes in tumoral microvessels a normalized function was observed, with reduction of permeability, decrease of tumour IFP and augmented perfusion, leading to improved delivery of chemotherapeutic agents and tumour growth delay. Similar findings were reported by Gorski *et al.* [27], with synergistic effects of combining anti-VEGF treatment and radiotherapy. In clinical trials, indeed, bevacizumab has led to improved overall survival, or progression-free survival in combination with chemotherapy in well-defined groups of cancer patients [28,29].
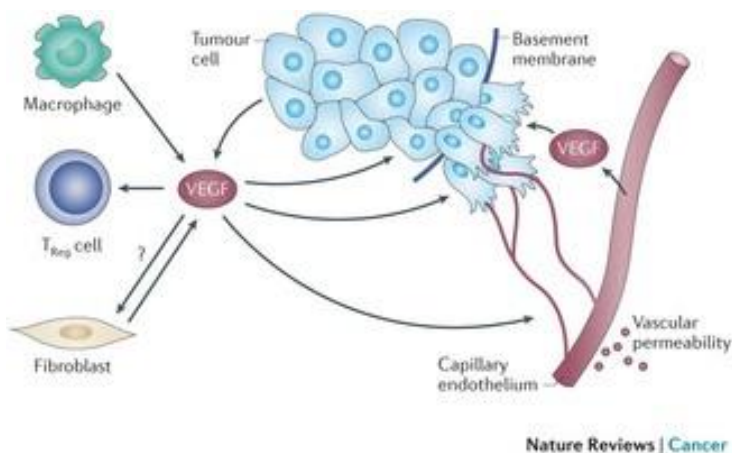
FIGURE 1.5: VEGF-functions in tumours. VEGF that is secreted by tumour and stromal cells, including macrophages, endothelial cells and fibroblasts, has multiple functions in the tumour environment, which involve the ability of VEGF to interact with VEGF-receptors that are expressed on different cell types. VEGF functions as a primary stimulus for angiogenesis, which is a process that involves the ability of VEGF-receptors to stimulate signaling pathways that induce the proliferation and the migration of endothelial cells, and the ability of these cells to degrade and to remodel the extracellular matrix. These processes culminate in sprouting angiogenesis, and the formation of new blood vessels. VEGF can also increase vascular permeability, which results in the deposition of a provisional fibrin matrix that triggers the formation of desmoplastic stoma. By contrast, VEGF secreted by tumour cells functions in an autocrine manner and promotes dedifferentiation and an epithelial-mesenchymal transition phenotype, with a consequent enhancement of tumour invasion and survival, and it can facilitate the function of cancer stem cells. VEGF can also function as a chemoattractant to recruit regulatory T-cells that inhibit an antitumour immune response. Tumour fibroblasts also secrete VEGF. (Adaptad from Goel and Mercurio, 2013 [25]).

VEGFR2 is expressed at high levels on tumour vasculature and is an interesting target to block VEGF-VEGFR2 signaling with antibodies. Tong *et al.* [15] used intravital microscopy in a mouse dorsal skinfold chamber model showing that within 3 days of therapy with VEGFR2-antibodies, a reduced MVD and diameter was seen, and an increased PCI in tumour vessels. Vessel permeability and IFP decreased, and interstitial penetration improved [15].

Similar findings were observed with receptor tyrosine kinase inhibitors (TKI); e.g. cediranib, a TKI of VEGFR1, VEGFR2, and VEGFR3, had a direct therapeutic effect in a mouse glioblastoma multiforme model with reduction of IFP and intracranial oedema due to vessel normalization, and consequently an extended survival [30]. Moreover, an increased overall survival was reported in a clinical trial comparing sorafenib with placebo in patients with hepatocellular carcinoma [31].

Another member of the VEGF family is PlGF, which has an important role in pathological conditions, such as cancer, inflammation, and cirrhosis, but not in physiological conditions. The group of Carmeliet [32] showed that anti-PlGF therapy results in tumour growth reduction, more mature vessels, a drop of tumour hypoxia and enhanced effect of cytotoxic treatments. The concept of vascular normalization after anti-PlGF treatment was also proven in mice with cirrhotic livers [33] and revealed to have better safety profiles than e.g. receptor TKI.

1.5.2 Indirectly targeting VEGF or other pathways

1.5.2.1 Integrin antagonists

The integrins are a group of evolutionary conserved heterodimeric cell surface receptors which are essential in cell-cell and cell-matrix interactions [34]. Some subtypes, such as $\alpha_v\beta_3$, $\alpha_v\beta_5$, and $\alpha_5\beta_1$, are highly overexpressed on cancer cells and play important roles in mediating tumour angiogenesis. Other subtypes, $\alpha_v\beta_6$ and $\alpha_6\beta_4$, have pivotal functions in cell migration, and hence metastasis [34] (Fig. 1.6). These interesting capacities of certain integrins, and the high level of expression on several tumour types, makes them ideal candidates for targeted therapy and imaging studies.

A potential target is $\alpha_v\beta_3$ integrin, which is overexpressed on some tumour cell types (e.g. lung cancer, ovarian cancer, breast cancer, glioblastoma multiforme [35]) and also selectively expressed on activated EC during migration through the basement membrane in the angiogenic process, such as during tumour neoangiogenesis [36,37]. This protein is not upregulated on quiescent EC [38]. Angiogenesis induced by bFGF requires the function of integrin $\alpha_v\beta_3$, whereas angiogenesis induced by VEGF requires the function of integrin $\alpha_v\beta_5$ [39]. As these integrins have key functions in tumoural metabolism, they also hold promise in tumour-targeted imaging to monitor therapy.

Cilengitide, a cyclic pentapeptide mimicking the Arg-Gly-Asp (RGD) binding site, was identified as a potent α_v integrin antagonist selectively targeting ECM components of $\alpha_v\beta_3$ and $\alpha_v\beta_5$ integrins. It is known to block bFGF- and VEGF-mediated angiogenesis, with a resulting normalization of the tumour microenvironment [40]. In preclinical models, cilengitide was synergistic with radioimmunotherapy in breast cancer and orthotopic brain tumor models [41,42]. In clinical phase III studies, however, this promising molecule still has to prove its efficacy in different cancer types [43].
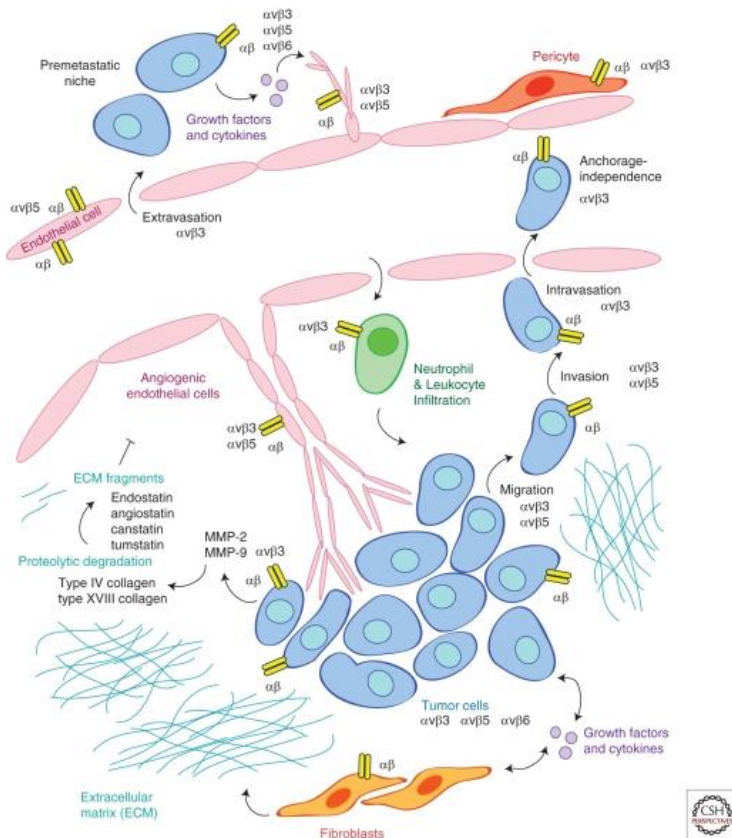
FIGURE 1.6: α_v integrins expressed on multiple cell types contribute to angiogenesis and tumour progression. Sprouting endothelial cells express a unique profile of integrins that can be targeted to suppress vascular proliferation. Tumour cells change integrin expression profiles to enhance their ability to migrate, invade, metastasize, and survive in hostile environments. Integrins signaling in fibrobla sts directs synthesis of extracellular matrix proteins and growth factors that flood the tumor stroma. Proteolytic degradation of ECM proteins creates fragments that can bind to and inhibit the function of integrins expressed by angiogenic endothelial cells. In summary, integrin expression profiles of normal cells are distinct from those within remodeling tissue. Because integrin signaling pathways can influence the behavior of multiple cell types involved in angiogenesis and cancer, selective targeting of integrin-mediated adhesion and signaling represents an attractive therapeutic strategy. (Adapted from Weis and Cheresh, 2011 [36]).

1.5.2.2 HEPARINS AND LMWHS

Different clinical studies have suggested that, independently from its effect on the incidence of venous thromboembolic events (VTEs), heparin therapy might improve survival in cancer patients [44,45] with better results for low molecular weight heparin (LMWH) than unfractionated heparin (UFH) [46]. LMWH acts through anti-factor Xa and anti-factor IIa activity (Fig. 1.7), and releases tissue factor pathway inhibitor (TFPI). Major side effects, such as bleeding, were statistically not significantly different in placebo recipients or LMWH-treated patients [47]. The potential anticancer mechanisms of LMWH administration include coagulation-dependent and coagulation-independent pathways. Effects on the formation of cancer metastasis (tumour cell heparanase), cancer cell adhesion and invasion (cell surface selectin-mediated), immune response, and angiogenesis (heparin-binding growth factors, TFPI) [48-52] are reported, independently of the anticoagulant effect of LMWH [53,54]. Some antiangiogenic effects of LMWH

rely on the effect on heparin-binding growth factors such as VEGF and bFGF. These growth factors bind to HSPGs that are present in both the ECs and the ECM. Binding of the receptors on the endothelial wall results in proliferation and migration of ECs. Soluble heparins have been shown to compete with angiogenic growth factors for ECM binding sites, and UFH therapy increases the plasma levels of certain growth factors [55]. In contrast to UFH, LMWHs inhibit binding of heparin-binding growth factors to their endothelial receptors, with larger fragments inhibiting the activity of VEGF, whereas smaller fragments reduce bFGF activity [56-58]. Similarly, in an *in vivo* assay after intraperitoneal VEGF administration, angiogenesis
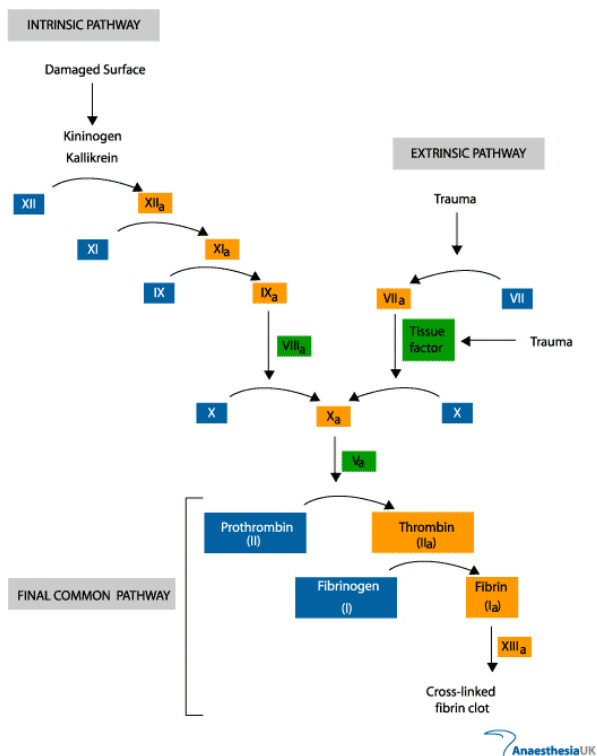
FIGURE 1.7: The coagulation cascade.

was suppressed by a 5-kDa but not by a 2.5- or 16.4-kDa heparin fraction [59].

LMWHs excert their antiangiogenic effect not only through inhibition of growth factors, but also through inhibition of heparanase and MMP [60,61]. These enzymes are overexpressed in tumours and are responsible for degradation of ECM, the release of angiogenic factors from the tumour microenvironment and are related to progression of cancer and metastasis [62]. They shed cadherins, important in tumour cell adhesion, and potentiate vascular leakage through activation of chemokines [63]. In this way, LMWHs blocking heparanase and MMP, normalize the ECM and vascular permeability.

Another documented pathway in antiangiogenesis, involves the anticoagulant property of LMWH to induce a release of TFPI from the vascular endothelium, as the inhibitory effect of tinzaparin is blocked by a monocolonal TFPI antibody [64]. Tissue factor (TF) is abundantly expressed in many tumour cell types and correlates with hypercoagulability, increased angiogenesis and higher tumor grades. TF upregulation in endothelial cells, which do not normally express TF, may be due to VEGF under tumoural conditions [65].

1.5.3 Combining antiangiogenics

Many tumours are intrinsically not sensitive for anti-angiogenic therapy or develop secondary resistance, by upregulation of other proangiogenic pathways. An answer to using antiangiogenics lies in the combination of compounds that affect different aspects of angiogenesis, if toxicity can be reduced [66].

In the preclinical setting, controlling primary tumour growth can be more effective when

a VEGFR-2 tyrosine kinase inhibitor is combined with a PDGFR tyrosine kinase inhibitor [67]. Similar findings were reported combining bevacizumab and cediranib, compared to each product alone [68]. Currently, several clinical phase I and II trials are ungoing to confirm a synergistic effect of antiangiogenic strategies and to evaluate toxicity [66].

Recently, efforts were directed to develop a LMWH derivative (targeting VEGF) undergoing chemical conjugation with cyclic Arg-Gly-Asp (RGD)-containing small peptides targeting $\alpha_v\beta_3$ integrin. Indeed, this agent has higher antiangiogenic efficiency than that of the LMWH derivative alone in *in vitro* experimental models, with significantly decreased MVD and tumour volume in *in vivo* models [69]. No additional effects on normalization of vessel function were examined.

1.6 Biomarkers for anti-angiogenic therapy

To identify patients who benefit from anti-angiogenic therapies, and to overcome resistance to anti-angiogenic strategies, which lead to the risk of developing a more malignant tumour phenotype, it is crucial to define biomarkers of tumour response in an early phase of treatment. These predictive markers could be circulating factors (VEGF, PlGF, soluble VEGFRs) [24], tissue factors in biopsies, single nucleotide polymorphisms (SNPs) in DNA of patients [70], or imaging parameters.

Easily accessible structural imaging modalities can offer images with good spatial resolution in a non-invasive way, but they share the limitation of not being able to detect lesions until the structural changes in the tissue (e.g. tumor growth or shrinkage) are large enough to be detected by these imaging technologies [71] which means crucial time is lost. Recent advances in molecular and functional imaging could be a solution.

Since the introduction of agents targeting tumour angiogenesis, increasing efforts have been invested in functional imaging of the neoplastic vascular bed. Most imaging modalities (PET, CT, ultrasonography, MRI) use contrast agents to improve visualization of tumour behaviour. Importantly, the earliest sign of response to anti-angiogenic therapy is microvessel normalization and a known hallmark of this process is a decrease in microvascular permeability. We previously showed that dynamic contrast enhanced (DCE)-MRI incorporating mathematical modelling allows to quantify early changes in microvessel permeability (K^{trans}) as well as tumour perfusion [72,73]. In studies with antiangiogenesis and antivascular agents [74] imaging biomarkers from DCE-MRI or perfusion CT (pCT), correlated with therapeutic drug dose [75-78] and efficacy, or patient survival [79,80]. Similar findings are also seen with chemotherapy [81], and radiotherapy [82].

To develop a predictor of an individual patient's progression-free and overall survival, a new biomarker was described by the group of Jain: the "vascular normalization index" (VNI), quantifying the fall in K^{trans}, the decrease of tumour microvessel volume, and the rise in plasma level of collagen IV (which is a marker of vascular basement membrane thinning) using multivariable Cox regression analyses of changes in these three parameters [83]. The VNI proved to be a good predictor for survival in cediranib-treated glioblastoma patients.

Contrast-enhanced ultrasonography (CE-US) is another functional imaging modality which is currently under investigation. Semiquantitative data analysis is possible and a

reduction in tumor vascularity parameters, measured by CE-US, can predict response to therapy in liver, renal, and gastrointestinal stromal tumors [84-87].

Finally, isotope imaging with PET is a common tool in oncology practice. The basic principle of this imaging modality is that it uses the characteristics of tumours to incorporate specific radioactive nuclides which are combined with other elements to form chemical compounds. These contrast agents provide information about tumour cell metabolism (FDG), tumour hypoxia, or tumour cell proliferation (FLT), and isotope imaging will record radiation emitting from within the body rather than radiation that is generated by external sources. For instance, ^{18}F-3'-fluoro-3'deoxythymidine (FLT)-PET is incorporated by proliferating cells in the pyrimidine salvage pathway during the S-phase. The tracer is then phosphorylated by thymidine kinase 1, after which it accumulates in the cells [88]. Several clinical studies have aimed to use FLT-PET to monitor the response to antiproliferative therapy. In breast cancer, FLT-PET enabled early response prediction, i.e. after one course of chemotherapy [89,90].

Whereas functional imaging depicts indirect signs of tumour response, molecular imaging has the advantage to give information about tumour specific details of microvasculature using probes directed against receptors expressed on the proliferating EC surface, which are detectable at nanomolar concentrations [91]. This allows not only early monitoring of therapy, but also the development of contrast agents that even could deliver drugs to the targeted tumour (vessel) receptors [92].

MRI is hereby an interesting tool, but this technique is limited by the low sensitivity to visualize these low concentrated epitopes. Therefore, efforts have been made to combine target-specific molecules with a large (super)paramagnetic payload. Several authors have used RGD-coupled liposomes containing Gd-DTPA for visualization of integrins in tumour angiogenesis [93,94], or RGD-labeled ultra-small superparamagnetic iron oxide nanoparticles (USPIO) [95-97].

On the other hand, molecular imaging using PET has a superior sensitivity, even at very low contrast agent concentrations. Radiolabeled VEGF, or other mediators of angiogenesis, can predict response to anti-VEGF treatment [98]. Radioiodinated RGD peptides reveal integrin receptor-specific tumour uptake [91]. PET scanning after administration of radiolabeled trastuzumab allowed identification and quantification of expression of HER2-positive tumors in patients with metastatic breast cancer [99].

Recently, new promising technologies with sophisticated optical probes have been developed that target with biological processes on a molecular level after being exogenously delivered. The design of such probes involves the attachment of a fluorophore to a targeting moiety, such as a peptide, an antibody or a fragment of an antibody, small molecules, and nanoparticles. Most of these fluorescent probes are completing preclinical validation in mouse models [100-104]. The advancements in nanoparticle fluorescent probe imaging will benefit open and endoscopic cancer surgery, for visualization of resection margins, jump metastases and lymph node involvement (Fig. 1.8) [105-107].

FIGURE 1.8: (A) In vivo near infra red (NIR) fluorescence imaging of tumour-bearing mice after tail vein injection of cyclicRGD NIR quantum dot bioconjugates (a non-injected mouse is used as grey control); (B) NIR imaging-guided surgery performed 48h after injection; and (C) the solid tumour precisely removed. Adapted from Li *et al.*, 2012 [102].

Taken together, identification of a validated, non-invasive biomarker is a key challenge for the future, to tailor antitumour strategies for each cancer patient, preventing unnecessary treatments, reducing the risk of toxicity and resistance, and deminishing health care costs. This important step can produce new insights in the mechanisms of antiangiogenic therapies.

1.7 References

1   World Health Organization: Cancer Facts. http://www.who.int/mediacentre/factsheets/fs297/en/index.html (accessed July 26, 2013).

2   Hanahan D and Weinberg RA. The hallmarks of cancer. *Cell.* 2000; Jan 7 (100): 57-70.

3   Hanahan D and Weinberg RA. The hallmarks of cancer: the next generation. *Cell*. 2011; Mar 4; 144(5):646-74.

4   Goldman, E. The growth of malignant disease in man and the lower animals with special reference to the vascular system. *Lancet* 1970; 2: 1236–1240.

5   Folkman J. Tumor angiogenesis: therapeutic implications. *N Engl J Med.* 1971; Nov 18; 285 (21): 1182-6.

6   Carmeliet P, Jain RK. Angiogenesis in cancer and other diseases. *Nature.* 2000; 407: 249-257.

7   Zhang S, Zhang D, Sun B. Vasculogenic mimicry: current status and future prospectives. *Cancer Letters.* 2007; 254: 157-164.

8   Carmeliet P. Angiogenesis in life, disease and medicine. *Nature.* 2005; 438: 932-936.

9   Cao Z, Bao M, Miele L, Sarkar FH, Wang Z, Zhou Q. Tumour vasculogenic mimicry is associated with poor prognosis of human cancer patients: a systemic review and meta-analysis. *Eur J Cancer.* 2013 Dec; 49(18): 3914-23.

10 Gazit Y, Baish JW, Safabakhsh N, Leunig M, Baxter LT, Jain RK. Fractal characteristics of tumor vascular architecture during tumor growth and regression. *Microcirculation.* 1997; 4: 395-402.

11 Debergh I, Van Damme N, Pattyn P, Peeters M, Ceelen W. The low-molecular-weight heparin, nadroparin, inhibits tumour angiogenesis in a rodent dorsal skinfold chamber model. *Br J Cancer.* 2010; 5 (102): 837-843.

12 Dejana E, Tournier-Lasserve E, Weinstein BM. The control of vascular integrity by endothelial cell junctions: molecular basis and pathological implications. *Dev Cell.* 2009; 16: 209-221.

13 Carmeliet P, Jain RK. Molecular mechanisms and clinical applications of angiogenesis. *Nature.* 2011; May 19; 473(7347): 298-307.

14 Stohrer M, Boucher Y, Stangassinger M, Jain RK. Oncotic pressure in solid tumors is elevated. *Cancer Res.* 2000; 60: 4251-4255.

15 Tong RT, Boucher Y, Kozin SV, Winkler F, Hicklin DJ, Jain RK. Vascular normalization by vascular endothelial growth factor receptor 2 blockade induces a pressure gradient across the vasculature and improves drug penetration in tumors. *Cancer Res.* 2004; 64: 3731-3736.

16   Helmlinger G, Yuan F, Dellian M, Jain RK. Interstitial pH and pO2 gradients in solid tumors *in vivo*: high-resolution measurements reveal a lack of correlation. *Nat Med.* 1997; 3: 177-182.

17   Semenza GL. Hypoxia-inducible factors: mediators of cancer progression and targets for cancer therapy. *Trends Pharmacol Sci.* 2012 April; 33(4): 207-214.

18   Gray LH, Conger AD, Ebert M, Hornsey S, Scott OC. The concentration of oxygen dissolved in tissues at the time of irradiation as a factor in radiotherapy. *Br J Radiol.* 1953;26:638–48.

19   Comerford KM, Wallace TJ, Karhausen J, Louis NA, Montalto MC, Colgan SP. Hypoxia-inducible factor-1-dependent regulation of the multidrug resistance (MDR1) gene. *Cancer Res.* 2002 Jun 15; 62(12): 3387-94.

20   Warren RS, Yuan H, Matli MR, Gillett NA, Ferrara N. Regulation by vascular endothelial growth factor of human colon cancer tumorigenesis in a mouse model of experimental liver metastasis. *J Clin Invest.* 1995 April; 95(4): 1789–1797.

21   Duda DG, Jain RK, Willett CG. Antiangiogenics: The Potential Role of Integrating This Novel Treatment Modality With Chemoradiation for Solid Cancers. *J Clin Oncol.* 2007 September 10; 25(26): 4033–4042.

22   Saltz LB, Clarke S, Diaz-Rubio E, Scheithauer W, Figer A, Wong R, Koski S, Lichinitser M, Yang TS, Rivera F, Couture F, Sirzen F, Cassidy J. Bevacizumab in combination with oxaliplatin-based chemotherapy as first-line therapy in metastatic colorectal cancer: a randomised phase III study. *J Clin Oncol.* 2008; 26: 2013-2019.

23   Jain RK. Normalizing tumor vasculature with anti-angiogenic therapy: a new paradigm for combination therapy. *Nat Med.* 2001; 3: 987-989.

24   Goel S, Duda DG, Xu L, Munn LL, Boucher Y, Fukumura D, Jain RK. Normalization of the vasculature for treatment of cancer and other diseases. *Physiol Rev.* 2011 July; 91(3): 1071–1121.

25   Goel HL and Mercurio AM. VEGF targets the tumour cell. *Nat Rev Cancer*. 2013 Nov 22;13(12):871-82.

26   Dickson PV, Hamner JB, Sims TL, Fraga CH, Ng CY, Rajasekeran S, Hagedorn NL, McCarville MB, Stewart CF, Davidoff AM. Bevacizumab-induced transient remodeling of the vasculature in neuroblastoma xenografts results in improved delivery and efficacy of systemically administered chemotherapy. *Clin Cancer Res.* 2007 Jul 1;13(13):3942-50.

27   Gorski DH, Beckett MA, Jaskowiak NT, Calvin DP, Mauceri HJ, Salloum RM, Seetharam S, Koons A, Hari DM, Kufe DW, Weichselbaum RR. Blockage of the vascular endothelial growth factor stress response increases the antitumor effects of ionizing radiation. *Cancer Res.* 1999 Jul 15;59(14):3374-8.

28   Hurwitz H, Fehrenbacher L, Novotny W, Cartwright T, Hainsworth J, Heim W, Berlin J, Baron A, Griffing S, Holmgren E, Ferrara N, Fyfe G, Rogers B, Ross R, Kabbinavar F. Bevacizumab plus irinotecan, fluorouracil, and leucovorin for metastatic colorectal cancer. *N Engl J Med.* 2004 Jun 3; 350(23): 2335-42.

29   Valachis A, Polyzos NP, Patsopoulos NA, Georgoulias V, Mavroudis D, Mauri D. Bevacizumab in metastatic breast cancer: a meta-analysis of randomized controlled trials. *Breast Cancer Res Treat.* 2010 Jul; 122(1):1-7.

30   Kamoun WS, Ley CD, Farrar CT, Duyverman AM, Lahdenranta J, Lacorre DA, Batchelor TT, di Tomaso E, Duda DG, Munn LL, Fukumura D, Sorensen AG, Jain RK. Edema control by cediranib, a vascular endothelial growth factor receptor-targeted kinase inhibitor, prolongs survival despite persistent brain tumor growth in mice. J *Clin Oncol.* 2009 May 20;27(15):2542-52.

31   Llovet JM, Ricci S, Mazzaferro V, Hilgard P, Gane E, Blanc JF, de Oliveira AC, Santoro A, Raoul JL, Forner A, Schwartz M, Porta C, Zeuzem S, Bolondi L, Greten TF, Galle PR, Seitz JF, Borbath I, Häussinger D, Giannaris T, Shan M, Moscovici M, Voliotis D, Bruix J; SHARP Investigators Study Group. Sorafenib in advanced hepatocellular carcinoma. *N Engl J Med.* 2008 Jul 24;359(4):378-90.

32   Fischer C, Jonckx B, Mazzone M, Zacchigna S, Loges S, Pattarini L, Chorianopoulos E, Liesenborghs L, Koch M, De Mol M, Autiero M, Wyns S, Plaisance S, Moons L, van Rooijen N, Giacca M, Stassen JM, Dewerchin M, Collen D, Carmeliet P. Anti-PlGF inhibits growth of VEGF(R)-inhibitor-resistant tumors without affecting healthy vessels. *Cell.* 2007 Nov 2;131(3):463-75.

33   Van Steenkiste C, Ribera J, Geerts A, Pauta M, Tugues S, Casteleyn C, Libbrecht L, Olievier K, Schroyen B, Reynaert H, van Grunsven LA, Blomme B, Coulon S,Heindryckx F, De Vos M, Stassen JM, Vinckier S,

Altamirano J, Bataller R, Carmeliet P, Van Vlierberghe H, Colle I, Morales-Ruiz M. Inhibition of placental growth factor activity reduces the severity of fibrosis, inflammation, and portal hypertension in cirrhotic mice. *Hepatology.* 2011 May; 53(5):1629-40.

34 Barczyk M, Carracedo S, Gullberg D. Integrins. C*ell Tissue Res.* 2010; 339: 269-280.

35 Marelli U, Rechenmacher F, Sobahi TR, Mas-Moruno C, Kessler H. Tumor targeting via integrin ligands. *Frontiers in Oncol.* 2013; 3: 1-12.

36 Weis SM and Cheresh DA. αV integrins in angiogenesis and cancer. *Cold Spring Harb Perspect Med.* 2011 Sep;1(1):a006478.

37 Meyer A, Auemheimer J, Modlinger A, Kessler H. Targeting RGD recognizing integrins: Drug development, biomaterial research, tumor imaging and targeting. *Current Pharm Design.* 2006; 12: 2723-2747.

38 Brooks PC, Clark RAF, Cheresh DA. Requirement of Vascular Integrin Alpha(V)Beta(3) for Angiogenesis. *Science.* 1994; 264: 569-571.

39 Friedlander M, Brooks PC, Shaffer RW, Kincaid CM, Varner JA, Cheresh DA. Definition of two angiogenic pathways by distinct alpha v integrins. *Science*. 1995 Dec 1;270(5241):1500-2.

40 Skuli N, Monferran S, Delmas C, Favre G, Bonnet J, Toulas C, Cohen-Jonathan Moyal E. Alphavbeta3/ alphavbeta5 integrins-FAK-RhoB: a novel pathway for hypoxia regulation in glioblastoma. *Cancer Res.* 2009 Apr 15;69(8):3308-16.

41 Burke PA, DeNardo SJ, Miers LA, Lamborn KR, Matzku S, DeNardo GL. Cilengitide targeting of alpha(v) beta(3) integrin receptor synergizes with radioimmunotherapy to increase efficacy and apoptosis in breast cancer xenografts. *Cancer Res.* 2002; 62: 4263–72.

42 MacDonald TJ, Taga T, Shimada H, Tabrizi P, Zlokovic BV, Cheresh DA, Laug WE. Preferential susceptibility of brain tumors to the antiangiogenic effects of an alpha(v) integrin antagonist. *Neurosurgery.* 2001; 48: 151–7.

43 Stupp R, Hegi ME, Gorlia T, *et al.* Cilengitide combined with standard treatment for patients with newly diagnosed glioblastoma and methylated O6-methylguanine-DNA methyltransferase (MGMT) gene promoter: Key results of the multicenter, randomized, open-label, controlled, phase III CENTRIC study. *J Clin Oncol* 31, 2013 (suppl; abstr LBA2009)

44 Carrier M, Agnes YY. Prophylactic and therapeutic anticoagulation for thrombosis-major issues in oncology. *Nat Clin Pract Oncol.* 2009; 6: 74–84.

45 Klerk CPW, Smorenburg SM, Otten HM, Lensing AWA, Prins MH, Piovella F, Prandoni P, Bos MMEM, Richel DJ, van Tienhoven G, Buller HR. The effect of low molecular weight heparin on survival in patients with advanced malignancy. *J Clin Oncol.* 2005; 23: 2130–2135.

46 von Tempelhoff GF, Harenberg J, Niemann F, Hommel G, Kirkpatrick CJ, Heilmann L. Effect of low molecular weight heparin (Certoparin) versus unfractionated heparin on cancer survival following breast and pelvic cancer surgery: A prospective randomized double-blind trial. *Int J Oncol.* 2000 Apr; 16(4):815-24.

47 Falanga A, Vignoli A, Diani E, Marchetti M. Comparative assessment of low-molecular-weight heparins in cancer from the perspective of patient outcomes and survival. *Patient Related Outcome Measures* 2011; 2: 175-188.

48 Smorenburg SM, Van Noorden CJF. The complex effects of heparins on cancer progression and metastasis in experimental studies. *Pharmacol Rev.* 2001;53:93–105.

49 Niers TMH, Klerk CPW, DiNisio M, Van Noorden CJF, Buller HR, Reitsma PH, Richel DJ. Mechanisms of heparin induced anti-cancer activity in experimental cancer models. *Crit Rev Oncol Hematol.* 2007; 61:195–207.

50 Zacharski LR, Lee AYY. Heparin as an anticancer therapeutic. *Expert Opin Investig Drugs.* 2008; 17:1029–1037.

51 Kenessey I, Simon E, Futosi K, Bereczky B, Kiss A, Erdödi F, Gallagher JT, Tímár J, Tóvári J. Antimigratory and antimetastatic effect of heparin-derived 4-18 unit oligosaccharides in a preclinical human melanoma metastasis model. *Thromb Haemost.* 2009 Dec;102(6): 1265-73.

52 Mousa SA, Petersen LJ. Anti-cancer properties of low-molecular-weight heparin: preclinical evidence. *Thromb Haemost.* 2009; 102: 258-267.

53 Mousa SA, Linhardt R, Francis JL, Amirkhosravi A. Anti-metastatic effect of a non-anticoagulant low-molecular-weight heparin versus the standard low-molecular-weight heparin, enoxaparin. *Thromb Haemost.* 2006; 96: 816-21.

54 Norrby K. Low-molecular-weight heparins and angiogenesis. *APMIS*. 2006; 114: 79-102.

55 Folkman J, Weisz PB, Joullie MM, Li WW, Ewing WR. Control of angiogenesis with synthetic heparin substitutes. *Science.* 1989; 243: 1490–1493.

56 Norrby K. Heparin and angiogenesis: a low-molecular-weight fraction inhibits and a high-molecular-weight fraction stimulates angiogenesis systemically. *Haemostasis.* 1993; 23:141–149.

57 Norrby K, Ostergaard P. Basic-fibroblast-growth-factor mediated de novo angiogenesis is more effectively suppressed by low-molecular-weight than by high-molecular-weight heparin. *Int J Microcirc Clin Exp.* 1996; 16:8–15.

58 Soker S, Goldstaub D, Svahn CM, Vlodavsky I, Levi BZ, Neufeld G. Variations in the size and sulfation of heparin modulate the effect of heparin on the binding of VEGF(165) to its receptors. *Biochem Biophys Res Comm.* 1994; 203:1339–1347.

59 Norrby K, Ostergaard P. A 5.0kDa heparin fraction systemically suppresses VEGF(165)-mediated angiogenesis. *Int J Microcirc Clin Expl.* 1997; 17:314–321.

60 Takahashi H, Ebihara S, Okazaki T, Asada M, Sasaki H, Yamaya M. A comparison of the effects of unfractionated heparin, dalteparin and danaparoid on vascular endothelial growth factor-induced tumour angiogenesis and heparanase activity. *Br J Pharmacol.* 2005 Oct; 146 (3): 333-43.

61 Lee DY, Lee SW, Kim SK, Lee M, Chang HW, Moon HT, Byun Y, Kim SY. Antiangiogenic activity of orally absorbable heparin derivative in different types of cancer cells. *Pharm Res.* 2009 Dec; 26(12): 2667-76.

62 Takahashi H, Ebihara S, Okazaki T, Suzuki S, Asada M, Kubo H, Sasaki H. Clinical significance of heparanase activity in primary resected non-small cell lung cancer. *Lung Cancer.* 2004 Aug; 45(2): 207-14.

63 Azzi S, Hebda JK, Gavard J. Vascular permeability and drug delivery in cancers. *Front Oncol.* 2013 Aug 15; 3: 211.

64 Mousa SA, Mohamed S. Anti-angiogenic mechanisms and efficacy of the low molecular weight heparin, tinzaparin: anti-cancer efficacy. *Oncol Rep.* 2004 Oct; 12(4): 683-8.

65 Amirkhosravi A, Meyer T, Amaya M, Davila M, Mousa SA, Robson T, Francis JL. The role of tissue factor pathway inhibitor in tumor growth and metastasis. *Semin Thromb Hemost.* 2007 Oct; 33(7): 643-52.

66 Moreno G V, Basu B, Molife LR, Kaye SB. Combining antiangiogenics to overcome resistance: rationale and clinical experience. *Clin Cancer Res.* 2012 Jul 15;18(14):3750-61.

67 Lu C, Kamat AA, Lin YG, Merritt WM, Landen CN, Kim TJ, Spannuth W, Arumugam T, Han LY, Jennings NB, Logsdon C, Jaffe RB, Coleman RL, Sood AK. Dual targeting of endothelial cells and pericytes in antivascular therapy for ovarian carcinoma. *Clin Cancer Res.* 2007 Jul 15;13(14):4209-17.

68 Bozec A, Gros FX, Penault-Llorca F, Formento P, Cayre A, Dental C, Etienne-Grimaldi MC, Fischel JL, Milano G. Vertical VEGF targeting: A combination of ligand blockade with receptor tyrosine kinase inhibition. *Eur J Cancer.* 2008 Sep;44(13):1922-30.

69 Adulnirath A, Chung SW, Park J, Hwang SR, Kim JY, Yang VC, Kim SY, Moon HT, Byun Y. Cyclic RGDyk-conjugated LMWH-taurocholate derivative as a targeting angiogenesis inhibitor. *J Control Release.* 2012 Nov 28;164(1):8-16.

70 Lambrechts D, Claes B, Delmar P, Reumers J, Mazzone M, Yesilyurt BT, Devlieger R, Verslype C, Tejpar S, Wildiers H, de Haas S, Carmeliet P, Scherer SJ, Van Cutsem E. VEGF pathway genetic variants as biomarkers of treatment outcome with bevacizumab: an analysis of data from the AViTA and AVOREN randomised trials. *Lancet Oncol.* 2012 Jul;13(7):724-33.

71 Weissleder R, Pittet MJ: Imaging in the era of molecular oncology. *Nature* 2008; 452: 580–589.

72 Ceelen W, Smeets P, Van Damme N, *et al.* Noninvasive monitoring of radiotherapy-induced

microvascular changes using dynamic contrast enhanced magnetic resonance imaging (DCE-MRI) in a colorectal tumor model *Int J Radiat Oncol Biol.* 2006; Phys 64: 1188-1196.

73 Ceelen W, Boterberg T, Smeets P, *et al.* Recombinant human erythropoietin alpha modulates the effects of radiotherapy on colorectal cancer microvessels. *Brit J Cancer.* 2007; 96: 692-700.

74 Galbraith SM *et al.* Combretastatin A4 phosphate has tumor antivascular activity in rat and man as demonstrated by dynamic magnetic resonance imaging. *J. Clin. Oncol.* 2003; 21:2831–2842.

75 Lockhart AC *et al.* Phase I study of intravenous vascular endothelial growth factor trap, aflibercept, in patients with advanced solid tumors. *J. Clin. Oncol.* 2010; 28: 207–214.

76 Wong CI *et al*. Phase I and biomarker study of ABT-869, a multiple receptor tyrosine kinase inhibitor, in patients with refractory solid malignancies. *J. Clin. Oncol.* 2009; 27: 4718–4726.

77 Morgan B *et al.* Dynamic contrast-enhanced magnetic resonance imaging as a biomarker for the pharmacological response of PTK787/ZK 222584, an inhibitor of the vascular endothelial growth factor receptor tyrosine kinases, in patients with advanced colorectal cancer and liver metastases: results from two phase I studies. *J. Clin. Oncol.* 2003; 21: 3955–3964.

78 Galbraith SM *et al.* Effects of 5,6-dimethylxanthenone-4-acetic acid on human tumor microcirculation assessed by dynamic contrast-enhanced magnetic resonance imaging. *J. Clin. Oncol.* 2002; 20: 3826–3840.

79 Jarnagin WR *et al.* Regional chemotherapy for unresectable primary liver cancer: results of a phase II clinical trial and assessment of DCE-MRI as a biomarker of survival. *Ann. Oncol.* 2009; 20: 1589–1595.

80 Willett CG *et al.* Direct evidence that the VEGF-specific antibody bevacizumab has antivascular effects in human rectal cancer. *Nat. Med.* 2004; 10: 145–147.

81 Delille JP *et al*. Invasive ductal breast carcinoma response to neoadjuvant chemotherapy: noninvasive monitoring with functional MR imaging pilot study. *Radiology* 2003; 228: 63–69.

82 Mayr NA *et al.* Pixel analysis of MR perfusion imaging in predicting radiation therapy outcome in cervical cancer. *J. Magn. Reson.* Imaging 2000; 12: 1027–1033.

83 Sorensen AG, Batchelor TT, Zhang WT, Chen PJ, Yeo P, Wang M, Jennings D, Wen PY, Lahdenranta J, Ancukiewicz M, di Tomaso E, Duda DG, Jain RK. A "vascular normalization index" as potential mechanistic biomarker to predict survival after a single dose of cediranib in recurrent glioblastoma patients. *Cancer Res.* 2009; Jul 1 69(13): 5296-300.

84 Lassau N *et al.* Gastrointestinal stromal tumors treated with imatinib: monitoring response with contrast-enhanced sonography. AJR Am. J. Roentgenol. 2006; 187: 1267–1273.

85 Lamuraglia M *et al.* To predict progression-free survival and overall survival in metastatic renal cancer treated with sorafenib: pilot study using dynamic contrast-enhanced Doppler ultrasound. *Eur. J. Cancer* 2006; 42: 2472–2479.

86 Averkiou M *et al.* Quantification of tumor microvascularity with respiratory gated contrast enhanced ultrasound for monitoring therapy. *Ultrasound Med. Biol.* 2010; 36: 68–77.

87 De GU, Aliberti C, Benea G, Conti M, Marangolo M. Effect of angiosonography to monitor response during imatinib treatment in patients with metastatic gastrointestinal stromal tumors. *Clin. Cancer Res.* 2005; 11: 6171–6176.

88 Alexander S, Varaha ST, John G, Vesselle H: FLT: measuring tumor cell proliferation *in vivo* with positron emission tomography and 3-deoxy-3-F-18 fluorothymidine. *Semin Nucl Med* 2007; 37: 429–439.

89 Contractor KB, Kenny LM, Stebbing J, Rosso L, Ahmad R, Jacob J, Challapalli A, Turkheimer F, Al-Nahhas A, Sharma R, Coombes RC, Aboagye EO: [(18)F]-3-Deoxy-3-fluorothymidine positron emission tomography and breast cancer response to docetaxel. *Clin Cancer Res* 2011; 17: 7664–7672.

90 Kenny L, Coombes RC, Vigushin DM, AlNahhas A, Shousha S, Aboagye EO: Imaging early changes in proliferation at 1 week post chemotherapy: a pilot study in breast cancer patients with 3-deoxy-3-[F-18]fluorothymidine positron emission tomography. *Eur J Nucl Med Mol Imaging* 2007; 34: 1339–1347.

91 Zhu L, Niu G, Fang X, Chen X. Preclinical molecular imaging of tumour angiogenesis. *Q J Nucl Med Mol Imaging.* 2010 June; 54 (3): 291-308.

92   Chen ZY, Wang YX, Lin Y, Zhang JS, Yang F, Zou QL, Liao YY. Advance of molecular imaging technology and targeted imaging agent in imaging and therapy. *Biomed Res Int.* 2014; 2014:819324.

93   Winter PM, Caruthers SD, Kassner A, *et al.* Molecular Imaging of angiogenesis in nascent vx-2 rabbit tumors using a novel alpha(v)beta(3)-targeted nanoparticle and 1.5 tesla magnetic resonance imaging. *Cancer Res*. 2003; 63: 5838-5843.

94   Mulder WJM, Strijkers GJ, Habets JW, *et al.* MR molecular imaging and fluorescence microscopy for identification of activated tumor endothelium using a bimodal lipidic nanoparticle. *FASEB J.* 2005; 19: 2008-2010.

95   Zhang CF, Jugold M, Woenne EC, *et al.* Specific targeting of tumor angiogenesis by RGD-conjugated ultrasmall superparamagnetic iron oxide particles using a clinical 1.5-T magnetic resonance scanner. *Cancer Res.* 2007; 67: 1555-1562.

96   Jiang T, Zhang CF, Zheng X, Xu XF, Xie X, Liu HC, Liu SY. Noninvasively characterizing the different alpha v beta 3 expression patterns in lung cancers with RgD-USPIO using a clinical 3.0T MR scanner. *Int J Nanomed.* 2009; 4: 241-249.

97   Kiessling F, Huppert J, Zhang CF, *et al.* RGD-labeled USPIO Inhibits Adhesion and Endocytotic Activity of alpha(v)beta(3)-Integrin-expressing Glioma Cells and Only Accumulates in the Vascular Tumor Compartment. *Radiology.* 2009; 253: 462-469.

98   Collingridge DR, *et al.* The development of [124I]-iodinated-VG76e: a novel tracer for imaging vascular endothelial growth factor *in vivo* using positron emission tomography. *Cancer Res.* 2002; 62: 5912–5919.

99   Dijkers EC, *et al.* Biodistribution of [89]Zr-trastuzumab and PET imaging of HER2-positive lesions in patients with metastatic breast cancer. *Clin. Pharmacol. Ther.* 2010; 87: 586–592.

100   Kelly K, Alencar H, Funovics M, Mahmood U, Weissleder R: Detection of invasive colon cancer using a novel, targeted, library-derived fluorescent peptide. *Cancer Res.* 2004; 64: 6247–6251.

101   Gee MS, Upadhyay R, Bergquist H, Weissleder R, Josephson L, Mahmood U: Multiparameter noninvasive assessment of treatment susceptibility, drug target inhibition and tumor response guides cancer treatment. *Int J Cancer.* 2007; 121: 2492–2500.

102   Weissleder R, Kelly K, Sun EY, Shtatland T, Josephson L: Cell-specific targeting of nanoparticles by multivalent attachment of small molecules. *Nat Biotechnol.* 2005; 23: 1418–1423.

103   Luo S, Zhang E, Su Y, Cheng T, Shi C. A review of NIR dyes in cancer targeting and imaging. *Biomaterials.* 2011; 32:7127-7138.

104   Zhang X, Bloch S, Akers W, Achilefu S. Near-infrared molecular probes for *in vivo* imaging. *Curr Protoc Cytom.* 2012 April: unit 12.27.

105   Li Y, Li Z, Wang X, Liu F, Cheng Y, Zhang B, Shi D. *In vivo* cancer targeting and imaging-guided surgery with near infrared-emitting quantum dot bioconjugates. *Theranostics.* 2012; 2(8):769-76.

106   Murahari MS, Yergeri MC. Identification and usage of fluorescent probes as nanoparticle contrast agent in detecting cancer. *Curr Pharm Des.* 2013; 19 (25): 4622-40.

107   Yi X, Wang F, Qin W, Yang X, Yuan J. Near-infrared fluorescent probes in cancer imaging and therapy: an emerging field. *Int J Nanomedicine.* 2014 Mar 5;9: 1347-65.

Objectives

CHAPTER 2: Objectives

Current cancer treatment options include surgery, chemotherapy, radiation and immunotherapy, but these regimens are known to evoke different disadvantages and aspecific side-effects. Improving the treatment specificity, leading to a patient-tailored approach, is an essential next step in treating cancer effectively. By timely discontinuation of inactive regimens, tumour resistance to therapy is prevented, quality of life of the patient is maintained by circumventing treatment toxicity, and unnecessary costs are avoided. Every single detail in the underlying mechanisms of cancer development, cancer behaviour, response or resistance to therapy, metastasis, can be a potential treatment target. In this complicated network, we focus on tumour neoangiogenesis as a target for therapy.

Overexpression of proangiogenic factors leads to formation of tumour vasculature which is chaotic, dilated, and tortuous [1]. In this heterogenous network, other structural changes take place, e.g. pericytes detach, gaps between endothelial cells enlarge, and basement membrane remodels [2,3]. Consequently, microvascular function is abnormal, with an increased vessel leakiness and IFP [4,5]. These alterations produce spatially and temporally heterogeneity in blood flow and perfusion in tumours, leading to regional acidosis and hypoxia [6], rendering the tumour phenotype more malignant. At last, due to increased IFP and poor perfusion, systemically administered drugs fail to enter tumour regions [3].

In **chapter 3.1**, we examine the vascular normalization effect of the LMWH nadroparin on tumour angiogenesis using a dorsal skinfold window chamber model in the Syrian golden hamster. Most of the experimental data on the anticancer effects of heparins were generated by cell culture experiments. *In vivo* microscopy (IVM) allows longitudinal non-invasive observation of tumour angiogenesis in the living animal, with quantification of microvessel density, red blood cell velocity, microvascular diameter and volumetric blood flow over time. Histological data, concerning microvessel density, pericyte coverage index and fractal dimension, help to evaluate the degree of vascular normalization after treatment. In this study, pancreatic carcinoma and amelanotic melanoma is studied in a hamster model. Using a human colorectal cell line, is the next logical step, which leads to the study described in **chapter 3.2**. The aim of the this experiment is to study the effects of the LMWH nadroparin and enoxaparin on colorectal angiogenesis in a mouse xenograft dorsal window chamber model using IVM studies and immunohistochemistry. Ultimately, these findings can help elucidate the behaviour of the tumour microenvironment during antiangiogenic strategies in humans. To identify patients who benefit from certain antiangiogenic therapies, and to overcome resistance, which leads to development a more malignant tumour phenotype, it is crucial to define biomarkers of tumour response in an early phase of treatment. These predictive markers could be imaging parameters.

Historically, non-invasive structural imaging modalities were used to evaluate tumour response to treatment with good spatial resolution (e.g. CT, MRI), but they assess only morphological, and not functional properties of the neoplastic tissue [7]. In **chapter 4.1** we give an overview of recent advances in molecular and functional imaging modalities, with some promising preclinical developments. Since the introduction of agents targeting

tumour angiogenesis, increasing efforts have been invested in functional imaging of the neoplastic vascular bed. One of the earliest signs of response to antiangiogenic treatment, with vascular normalization, is a decrease of vascular permeability. Dynamic contrast enhanced (DCE) magnetic resonance imaging allows to quantify these early changes in microvessel permeability as well as tumour perfusion [8,9]. Although of interest, these parameters remain indirect estimators of tumour angiogenesis. A direct method of early iconographic evaluation of tumour response requires probes directed against tumour-specific moieties expressed on the proliferating endothelial cell (EC) surface. A potential target is $\alpha_v\beta_3$ integrin, which we studied in **chapter 4.2**, with a novel $\alpha_v\beta_3$ integrin directed molecular MRI tracer (P1227) as a tool to visualize tumour angiogenesis in a colorectal xenograft mouse model. To prove specificity of the tracer, we used cilengitide, an integrin $\alpha_v\beta_3$ inhibitor, before imaging with P1227. The identification of tumour receptors through imaging allows not only the non-invasive measurement of early response to treatment, but can be a tool to develop further tumour receptor-specific delivery of drugs.

2.1 References

1 Bazit Y, Baish JW, Safabakhsh N, Leunig M, Baxter LT, Jain RK. Fractal characteristics of tumor vascular architecture during tumor growth and regression. *Microcirculation.* 1997; 4: 395-402.

2 Dejana E, Tournier-Lasserve E, Weinstein BM. The control of vascular integrity by endothelial cell junctions: molecular basis and pathological implications. *Dev Cell.* 2009; 16: 209-221.

3 Carmeliet P, Jain RK. Molecular mechanisms and clinical applications of angiogenesis. *Nature.* 2011; May 19; 473(7347): 298-307.

4 Stohrer M, Boucher Y, Stangassinger M, Jain RK. Oncotic pressure in solid tumors is elevated. *Cancer Res.* 2000; 60: 4251-4255.

5 Tong RT, Boucher Y, Kozin SV, Winkler F, Hicklin DJ, Jain RK. Vascular normalization by vascular endothelial growth factor receptor 2 blockade induces a pressure gradient across the vasculature and inproves drug penetration in tumors. *Cancer Res.* 2004; 64: 3731-3736.

6 Helmlinger G, Yuan F, Dellian M, Jain RK. Interstitial pH and pO2 gradients in solid tumors *in vivo*: high-resolution measurements reveal a lack of correlation. *Nat Med*. 1997; 3: 177-182.

7 Weissleder R, Pittet MJ: Imaging in the era of molecular oncology. *Nature* 2008; 452: 580–589.

8 Ceelen W, Smeets P, Van Damme N, *et al.* Noninvasive monitoring of radiotherapy-induced microvascular changes using dynamic contrast enhanced magnetic resonance imaging (DCE-MRI) in a colorectal tumor model *Int J Radiat Oncol Biol.* 2006; Phys 64: 1188-1196.

9 Ceelen W, Boterberg T, Smeets P, *et al.* Recombinant human erythropoietin alpha modulates the effects of radiotherapy on colorectal cancer microvessels. *Brit J Cancer.* 2007; 96: 692-700.

CHAPTER 3

Vascular normalization after LMWH-treatment in cancer

CHAPTER 3: Vascular normalization after LMWH-treatment in cancer

Chapter 3.1: The low-molecular-weight heparin, nadroparin, inhibits tumour angiogenesis in a rodent dorsal skinfold chamber model

3.1.1 Abstract

Background:
Recently, low-molecular-weight heparins (LMWHs) were found to confer a survival advantage in cancer patients. The mechanism underlying this observation is unclear, but may involve inhibition of tumour angiogenesis. We aimed to examine the effects of nadroparin on tumour angiogenesis using a dorsal skinfold window chamber model in the Syrian hamster.

Methods:
AMel-3 and HAP-T1 tumours were grown in donor animals and fragments implanted in the window chambers. Animals (N=46) were treated with 200IU of nadroparin or saline for 10 days. Repeated intravital fluorescence microscopy was performed to calculate functional microcirculatory parameters: number (N) and length (L) of microvessels, vascular area fraction (AF), and red blood cell velocity (V). Microvessel density (MVD), fractal dimension, and pericyte coverage were assessed histologically.

Results:
Active angiogenesis was observed in control animals, resulting in a significant increase in N, L, and AF. In nadroparin-treated animals, however, N and L did not increase whereas AF decreased significantly. Both groups showed an initial increase in V, but nadroparin treatment resulted in an earlier decrease in red blood cell velocity over time. Compared with control animals, nadroparin-treated animals showed a significantly lower MVD and fractal dimension but significantly higher pericyte coverage index (PCI).

Conclusions:
Taken together, these results suggest that the LMWH nadroparin inhibits tumour angiogenesis and results in microvessel normalisation.

3.1.2 Introduction

Cancer patients are at risk of venous thromboembolic events (VTEs) induced by the hypercoagulable state associated with malignancy (Mousa, 2004). There is therefore a clear rationale for prophylactic administration of unfractionated heparin (UFH) or low-molecular-weight heparin (LMWH) in these patients (Carrier and Agnes, 2009).
Recent clinical studies have suggested that, independent from its effect on the incidence of VTE, heparin therapy might alter survival in cancer patients (Kakkar *et al*, 2004; Klerk *et al*, 2005).

The potential anticancer mechanisms of LMWH administration remain incompletely understood. Suggested targets include the formation of cancer metastasis, cancer cell adhesion and invasion, immune response, and angiogenesis (Smorenburg and Van Noorden, 2001; Niers *et al,* 2007; Zacharski and Lee, 2008). Angiogenesis is a critical process in survival, growth, and metastasis of a malignant tumour, and is regulated by a number of heparin-binding growth factors such as vascular endothelial growth factor (VEGF) and basic fibroblast growth factor (bFGF). These growth factors bind to heparane sulphate proteoglycans (HSPGs) that are present in both the endothelial cells (ECs) and the extracellular matrix (ECM). Binding of the receptors on the endothelial wall results in proliferation and migration of ECs. Soluble heparins have been shown to compete with angiogenic growth factors for ECM binding sites, and UFH therapy increases the plasma levels of certain growth factors (Folkman *et al*, 1989). In contrast to UFH, LMWHs inhibit binding of heparin-binding growth factors to their endothelial receptors, an effect that depends on the molecule's number of saccharide units (Norrby, 1993; Norrby and Ostergaard, 1996). Fragments of <18 saccharides inhibit the activity of VEGF, whereas fragments smaller than 10 saccharide units reduce bFGF activity (Soker *et al*, 1994). Similarly, in an *in vivo* assay after intraperitoneal VEGF administration, angiogenesis was suppressed by a 5-kDa but not by a 2.5- or 16.4-kDa heparin fraction (Norrby and Ostergaard, 1997).

Most of the experimental data on the anticancer effects of heparins were generated by cell culture experiments. *In vivo* microscopy (IVM) allows longitudinal noninvasive observation of tumour angiogenesis in the living animal. In this study we studied the effects of the LMWH nadroparin on tumour-associated angiogenesis, using a dorsal skinfold window chamber model in the Syrian golden hamster.

3.1.3 Methods
The experimental protocol was approved by the animal experimental ethical committee of the Ghent University, Ghent, Belgium.

Animals and tumour model
Male syrian gold hamsters (Harlan, Horst, The Netherlands) weighing 80–100g were housed separately in plastic cages with free access to tap water and standard pellet food.
AMel-3 (Fortner's amelanotic hamster melanoma; 50% of the animals) or HaP-T1 (nitrosamine-induced pancreatic cancer in hamsters; 50% of the animals) cancer cell lines were cultured and 1 million cells suspended in 0.1ml of saline were injected subcutaneously in the proximal hind leg of donor hamsters. When tumours reached a size of 10mm^3 (usually after 2–3 weeks), four tumour fragments (±0.5–1mm^2) were implanted in the window chamber of acceptor animals at 24h after dorsal skinfold window chamber implantation.

Dorsal skinfold window chamber implantation
Hamsters were anaesthetised with intraperitoneal injection of ketamine (Ketalar, Pfizer, Elsene, Belgium) and xylazin (Rompun, Bayer, Diegem, Belgium) and placed on a heating pad. The procedure is described in detail by Endrich *et al* (1980) and Menger *et al* (2002).

In brief, a titanium frame is surgically fixed onto a dorsal skinfold of the animal (Figure 3.1). On one side of the skinfold, a circular area of dermis and subcutis is surgically removed (15mm diameter) and covered by a circular cover glass. Animal were housed separately and were allowed to recover for 24h from surgery and anaesthesia before tumour fragment implantation. Window chambers were inspected daily for the presence of air bubbles, inflammation, infection, or vascular thrombosis.

FIGURE 3.1 Dorsal skinfold window chamber

Experimental therapy

Animals (N=23 per group) were treated with daily subcutaneous injections of either 0.07ml of saline or 200IU aXa of nadroparin (Fraxiparine, GSK, Genval, Belgium) dissolved in 0.07ml of saline. Injections started the day before tumour implantation.

Intravital microscopy

In vivo fluorescence microscopy was performed on days 0 (day of tumour implantation), 3, 6, and 9. Unconscious animals (ketamine/xylazin anaesthesia) received an i.v. bolus of 0.1ml of fluorescein isothiocyanate (FITC)–labelled dextran (20mgml^{-1}) (Sigma-Aldrich NV, Bornem, Belgium) and were placed on the stage of a modified Olympus BX51WI microscope (Olympus NV, Aartselaar, Belgium). Fluorescence microscopy was performed using an HBO 50W mercury lamp (Osram, Zaventem, Belgium) and a FITC filter set (excitation filter 460–490nm) for detecting epifluorescent intravascular plasma. Static and dynamic images of the microcirculation were obtained in four different regions in each chamber. Digital images were captured real time on the hard disc of a computer using a high sensitivity digital camera (model C8484-05, Hamamatsu Photonics, Hamamatsu, Japan). Quantitative microcirculatory analysis was performed using a software package (CapImage, H Zeintl Engineering, Heidelberg, Germany). The following parameters were calculated: microvessel length per area (LA; cm^{-2}), number of microvessels per high-power field (NA; n/HPF × 20), vascular area fraction (AF; %), and microvessel diameter (*D*; μm). In addition, centreline red blood cell velocity (*V*; mm s^{-1}) was measured by analysing 10 microvessels per region of interest, randomly chosen among those that crossed a vertical line drawn over the centre of the computer screen, as described by Laschke *et al* (2005). Volumetric blood flow (VQ; pl s^{-1}) was calculated from *V* and *D* as VQ=π × (*D*/2)^2 × *V/K*, in which *K* (=1.3) represents the Baker–Wayland factor (Baker and Wayland, 1974), and considers the parabolic velocity profile of blood in microvessels. Functional capillary density was not calculated as angiogenic sprouts and buds contain red blood cells without a measurable perfusion and therefore this parameter does not accurately reflect tumour angiogenesis (Torres *et al*, 1995).

On day 9 after implantation of the tumour fragments, animals were killed and the tissue inside the observation chambers was excised for histology. Tissue fragments were fixed

in 10% formalin, embedded in paraffin, and 4μm thick sections were cut and mounted for immunohistochemistry.

Immunohistochemistry

Factor VIII (von Willebrand factor, FVIII) immunostaining was used to visualise tumour microvessels and calculate microvessel density (MVD), whereas α-smooth muscle actin (αSMA) was used to identify pericytes and calculate the pericyte coverage index (PCI) as a measure of microvessel maturation. Serial tissue sections were deparaffinised in xylene, hydrated by serial immersion in ethanol, and subsequently incubated in Proteinase K (Dako, Heverlee, Belgium) for antigen retrieval. Endogenous peroxidase activity was blocked with 3% H_2O_2 in methanol. Slides were washed in Tris-buffered saline (TBS)–Tween and treated with UltraSens Block RTU (ImmunoLogic, Duiven, The Netherlands) to inhibit nonspecific antibody binding. Sections were incubated with mouse monoclonal antibodies against FVIII (Dako) or αSMA (Abcam, Cambridge, UK) at room temperature for 1h, rinsed in TBS–Tween, and incubated with secondary antibodies (UltraSens Biotinylated Goat Anti-polyvalent RTU; ImmunoLogic) followed by streptavidin peroxidase (UltraSens Streptavidin Peroxidase RTU; ImmunoLogic) for 10min each. Visualisation of the immunoprecipitate was performed by adding 3,3'-diaminobenzidine (Biogenex, San Ramon, CA, USA) and counterstaining with haematoxylin. Positive and negative controls were processed simultaneously.

Serial FVIII and αSMA-stained sections of dorsal skinfold tissue were entirely scanned for tumour regions (magnification × 20) and digitised. Microvessel density was calculated by digital image analysis using the NIH ImageJ software (version 1.39s, available from http://rsb.info.nih.gov/ij). Using the threshold colour plugin, FVIII- and αSMA-positive cells were isolated from background staining and the resulting images converted to binary. Microvessel density was calculated using the ratio of black pixels over the total number of pixels in the binary image, whereas the PCI was calculated as the ratio of αSMA-positive pixels vs FVIII-positive pixels. The fractal dimension of the microvessel bed was calculated using the ImageJ FracLac plugin. The fractal dimension is a rational number between 1 and 2 (the dimensions of a line and plane, respectively), and has been shown to correlate with the degree of branching, tortuosity, and irregularity of the tumour-associated microvascular network (Dey, 2005).

Statistical analysis

Data are expressed as mean±s.d. or median (interquartile range). Differences were analysed using Student's *t*-test or Mann–Whitney rank-sum test where appropriate. Results were considered statistically significant when the probability of a type I error was ≤5%. Statistical analysis was performed with SigmaStat 11.0 (Systat Software, Richmond, CA, USA).

3.1.4 Results

All animals (N=46) developed 2–4 macroscopically visible tumours in the observation window, indicating appropriate angiogenesis and viability (Figure 3.2). As both the dynamic *in vivo* microscopic results and histology parameters with the exception of the

PCI did not differ between the HaP-T1 cell line and the AMel-3 cell line (data not shown), statistical analyses were performed on the combined group. Five animals were excluded on the first day of observation because of insufficient optical quality of the window chamber. In all other animals (*N*=41), the skinfold chamber provided excellent image quality and resolution over the duration of the experiment (9 days).
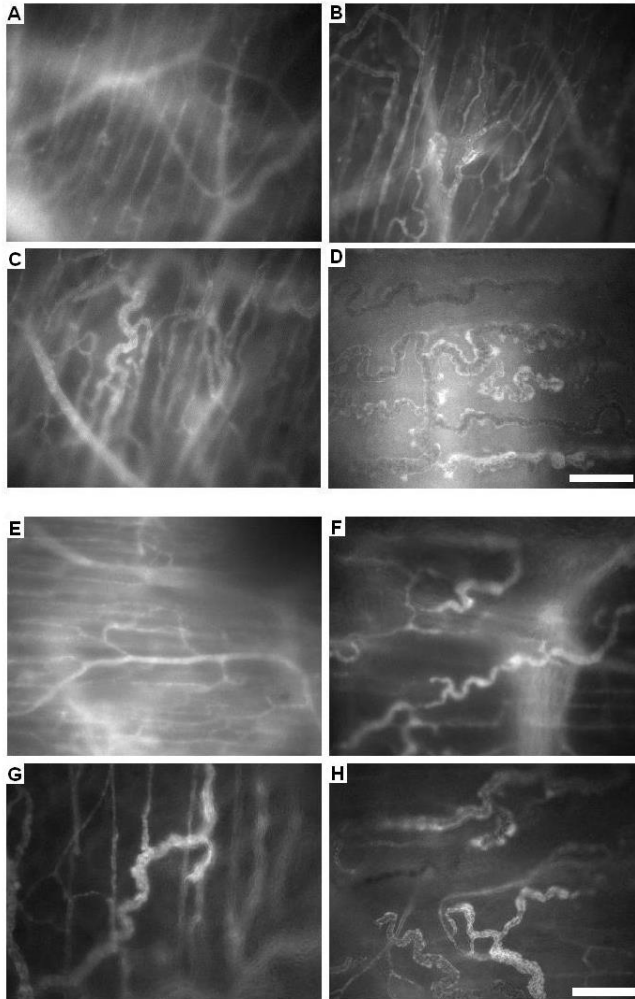
FIGURE 3.2 Representative tumour growth and angiogenesis observed for 9 days in a control animal **(A–D)** and a nadroparin-treated animal **(E–H)**. The difference in microvessel density is clearly visible, as is the higher number of neovascular buds and sprouts in the control animal (image D). Scale bar=100 µm.

Effects of nadroparin on tumour-induced angiogenesis

The microvascular parameters derived from *in vivo* microscopic observations are summarised in Figure 3.3 and Table 3.1. In control animals (*N*=20), the number of microvessels and the vascular area fraction increased significantly whereas a nonsignificant increase in vessel length was observed. In nadroparin-treated animals (*N*=21), however, vessel length and number of microvessels did not change significantly over time whereas a significant decrease in vascular area fraction was noted.
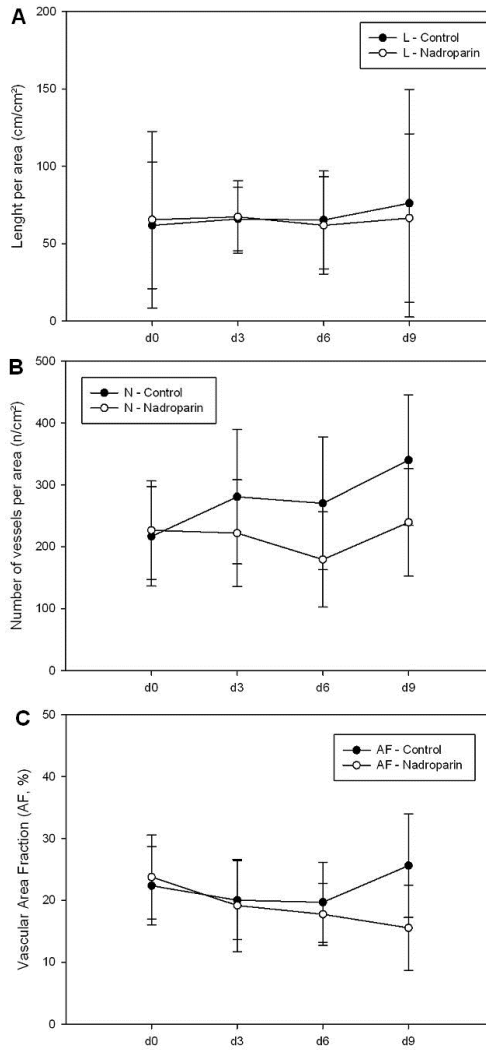
FIGURE 3.3 Vessel length **(A)**, number of microvessels per area **(B)**, and vascular area fraction **(C)** in control and nadroparin-treated animals for 9 days. Data represent mean ±SD.

TABLE 3.1. Evolution of microvessel length, number, and area fraction over time.

Control (N = 20)	Day 0	Day 3	Day 6	Day 9
L (cm/cm²)	61.8 ± 41	65.9 ± 21	65.2 ± 32	76.0 ± 74
N (n/cm²)	216.8 ± 80	280.8 ± 108*	270.3 ± 107*	340.2 ± 105°
VAF (%)	22.4 ± 6.3	20 ± 6.4*	19.7 ± 6.5*	25.6 ± 8.4°
Nadroparin (N = 21)	**Day 0**	**Day 3**	**Day 6**	**Day 9**
L (cm/cm²)	65.4 ± 57	67.2 ± 23	61.8 ± 31	66.5 ± 54
N (n/cm²)	226.8 ± 80	222.2 ± 86[a]	179.4 ± 77*[a]	238.9 ± 87[a]
VAF (%)	23.8 ± 6.7	19.2 ± 7.4*	17.8 ± 5.0*[a]	15.6 ± 6.9°[a]

L, microvessel length; N, number of microvessels; VAF, vascular area fraction; *$P < 0.05$ vs day 0; °$P < 0.05$ vs day 0, 3 and 6; [a]$P < 0.05$ vs untreated animals at corresponding time points. Data represent mean ± SD.
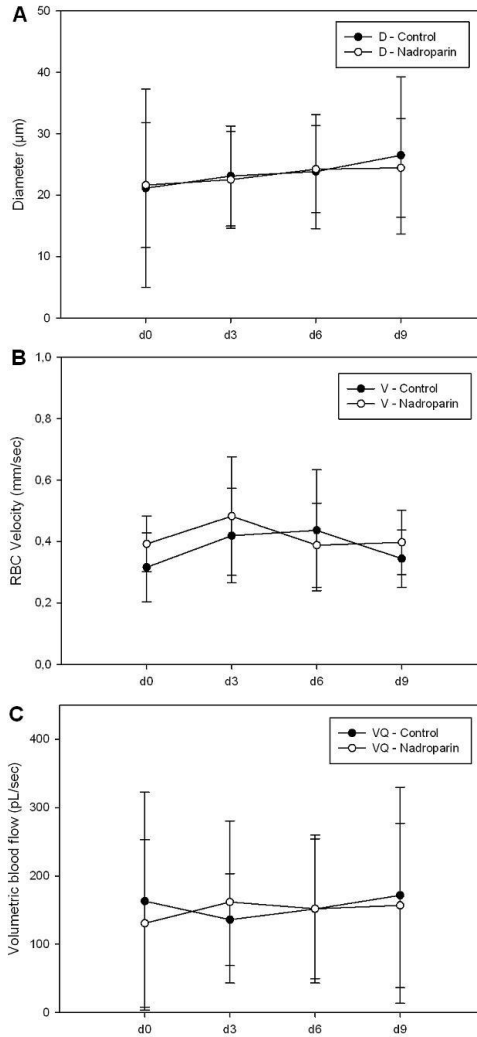
FIGURE 3.4 Microvessel diameter **(A)**, red blood cell velocity **(B)**, and volumetric blood flow **(C)** in control and nadroparin-treated animals for 9 days. Data represent mean ± SD.

TABLE 3.2. Evolution of microvessel diameter, red blood cell velocity, and volumetric blood flow over time.

Control (N = 20)	Day 0	Day 3	Day 6	Day 9
D (μm)	21.2 ± 16.1	23.1 ± 8.1	23.8 ± 9.3	26.5 ± 12.8*
V (mm/sec)	0.3 ± 0.1	0.4 ± 0.1*	0.4 ± 0.2*	0.3 ± 0.1[#]
VQ (pL/sec)	163.1 ± 159	135.8 ± 67*	151.6 ± 108*	171.5 ± 158*
Nadroparin (N = 21)	**Day 0**	**Day 3**	**Day 6**	**Day 9**
D (μm)	21.6 ± 10.1	22.5 ± 7.9	24.2 ± 7.1*	24.4 ± 8.0*
V (mm/sec)	0.4 ± 0.1[a]	0.5 ± 0.2	0.4 ± 0.1	0.4 ± 0.1[a]
VQ (pL/sec)	130.4 ± 122[a]	161.7 ± 118	151.9 ± 102	156.8 ± 120*

D, microvessel diameter; V, red blood cell velocity; VQ, volumetric blood flow; *P < 0.05 vs day 0; [#]P < 0.05 vs day 3 and 6; [a]P < 0.05 vs untreated animals at corresponding time points. Data represent mean ± SD.
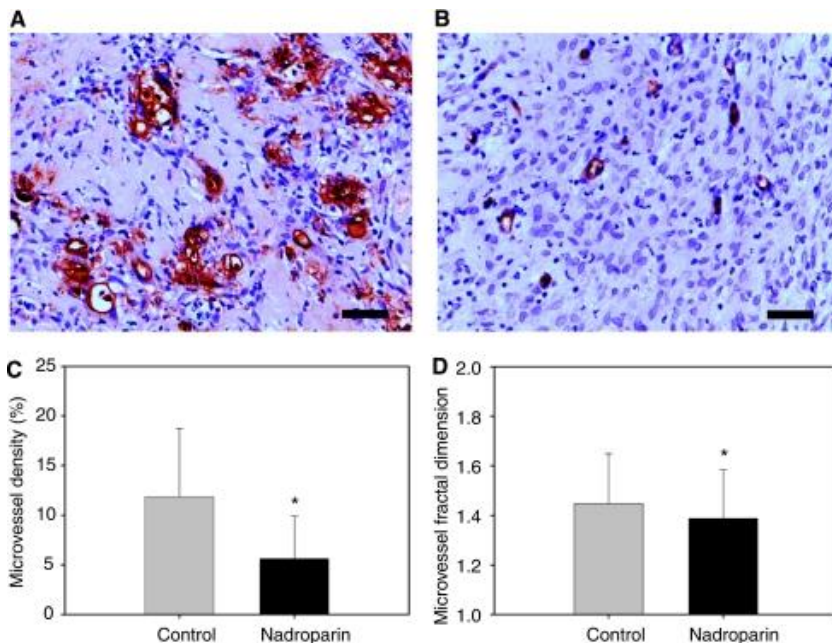
FIGURE 3.5 Microvessel density (FVIII staining) and fractal dimension in control and nadroparin-treated animals. (**A, B**) Examples of FVIII-stained microvessels of control and nadroparin-treated animals, respectively. Scale bar=25 µm. (**C**) Microvessel density. Columns= mean; Bars= s.d.; *$P<0.001$. (**D**) Microvessel fractal dimension. Columns=mean; Bars= s.d.; *$P=0.029$.
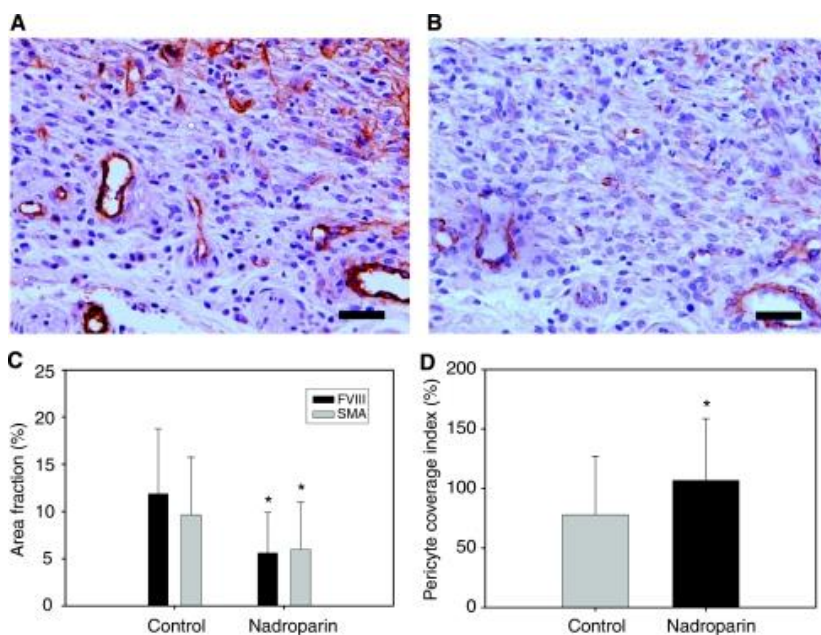
FIGURE 3.6 Microvessel maturity (pericyte coverage index) in control and nadroparin-treated animals. (**A, B**) Serial sections of FVIII- and αSMA-stained microvessels, respectively, in control hamsters. Weak αSMA staining is present around tumour microvessels, illustrating deficient pericyte coverage. Scale bar=25 µm. (**C**) Area fraction (percentage of stained pixels vs total number of pixels in binary images) of FVIII- and αSMA-stained cells. Columns=mean; Bars=s.d.; *$P<0.001$. (**D**) Microvessel pericyte coverage index. Columns=mean; Bars=s.d.; *$P=0.012$.

Effects of nadroparin on the dynamic properties of the tumour vascular bed

The results of microcirculatory calculations are summarised in Figure 3.4 and Table 3.2. In both groups, microvessel diameter increased significantly over time, although in the nadroparin group the increase in diameter between days 6 and 9 was less pronounced. The evolution of microvessel RBC velocity is depicted in Figure 3.3B. In the control group, velocity increased progressively until day 6, followed by a significant decline at day 9. In the experimental group, however, RBC velocity peaked earlier (day 3) and subsequently stabilised at a lower value. Volumetric blood flow increased significantly over time in control animals, whereas nadroparin-treated animals show an early peak on day 3, followed by stable readings until the end of the experiment.

Immunohistochemical analysis

Histological examination of the dissected dorsal skinfolds on day 9 after tumour fragment implantation showed macroscopically vital tumour tissue in all animals. Microvessel quantitative and morphology data are illustrated in Figure 3.5. The microvessel density (FVIII staining) was 11.1% (6.2–18.1) in the control group and 4.5% (1.8–9.1) in the nadroparin-treated group ($P<0.001$, Mann–Whitney U-test). Fractal dimension was significantly higher in control animals than in nadroparin-treated animals (1.5 (1.3–1.6) and 1.4 (1.3–1.5), respectively, $P=0.029$, Mann–Whitney U-test).

Data concerning microvessel maturation are depicted in Figure 3.6. The PCI was 73.6% (39.1–108.5) in untreated animals and 96.8% (74.3–126.1) in nadroparin-treated animals ($P=0.012$, Mann–Whitney U-test). The difference in PCI between control and nadroparin-treated animals was more pronounced when the HaPT-1 cell line was used (Table 3.3).

TABLE 3.3. Immunohistochemistry results.

Amel 3	Control (N = 10)	Nadroparin (N = 10)	P-value
FVIII	9.4 (5.2-15.1)	3.8 (1.4-6.6)	< 0.001
SMA	5.1 (3.8-8.0)	1.7 (1.4-7.9)	0.020
PCI (%)	95.7 (54.5-117.9)	111.8 (63.3-134.3)	NS
HaP-T1	Control (N = 10)	Nadroparin (N = 11)	P-value
FVIII	11.7 (6.9-19.9)	5.8 (2.4-10.7)	< 0.001
SMA	10.9 (7.4-17.2)	5.8 (2.6-10.4)	< 0.001
PCI (%)	76.5 (39.7-111.7)	108.3 (80.2-157.8)	0.003

FVIII, factor VIII staining; SMA, smooth muscle antigen staining; PCI, pericyte coverage index. Data represent median (interquartile range).

3.1.5 Discussion

The results from recent clinical studies in advanced cancer patients have led to increasing interest in the effects of heparins on tumour growth. Klerk *et al* (2005) randomised advanced or metastatic cancer patients to either 6 weeks of nadroparin or placebo, and found a significant overall survival benefit in favour of nadroparin therapy (hazard ratio of mortality 0.75; 95% CI 0.59–0.96).

The underlying mechanisms by which heparins inhibit tumour progression are incompletely understood, and may include inhibition of selectin-mediated cellular adhesion, inhibition of tumour invasion, and induction of cancer cell apoptosis (Smorenburg and Noorden, 2001; Niers *et al*, 2007; Lee, 2007).

One of the causal pathways under scrutiny is the inhibition of tumour-associated angiogenesis. Most *in vivo* angiogenesis assays, such as the mouse cremaster muscle or rat mesenteric window model, allow to observe the microcirculation only once after therapy (Norrby, 2000; Wan *et al*, 2001). The dorsal skinfold chamber model allows noninvasive detailed and repetitive analysis of tumour microvascular properties (Torres *et al*, 1995). Our study is the first to use repetitive observation in a dorsal skinfold window chamber model to assess the effects of an LMWH on tumour-associated angiogenesis in an immunocompetent animal model.

Our results suggest that nadroparin exerts an antiangiogenic effect *in vivo*, as evidenced by a significantly lower vascular area fraction and MVD when compared with control animals. Moreover, nadroparin-treated tumours showed signs of microvessel normalisation, including a smaller increase in diameter, a higher PCI, and less vessel tortuosity (smaller fractional dimension). Vessel normalisation is a well-characterised early phenotypic effect of antiangiogenic therapy (Fukumura and Jain, 2008). The difference in vessel diameter and tortuosity may explain the decrease in vascular area fraction over time in nadroparin-treated animals despite the fact that both vessel length and vessel number did not change appreciably over time in this group.

Most of the published studies examining the antiangiogenic effects of LMWHs have used physiological angiogenesis models such as the rat mesentery or matrigel plug assays. Mousa and Mohamed (2004) showed that the LMWH tinzaparin inhibits angiogenesis in the chick chorioallantoic membrane model by upregulation of the tissue factor pathway inhibitor. Tissue factor, which is the initiator of the extrinsic coagulation pathway, is expressed by many cancer types and was shown to promote tumour angiogenesis through protease-activated receptor 2 (PAR-2) signalling (Belting *et al*, 2004). Similarly, Marchetti *et al* (2008) showed that the LMWHs, enoxaparin and dalteparin, but not unfractionated heparin, significantly inhibited capillary tube formation in a Matrigel assay. Interestingly, the antiangiogenic potential of LMWHs seems to be depending on the size of the molecule and number of saccharide units. Khorana *et al* (2003) showed that molecules with a weight in the range of 3–6kDa or >8 saccharide units maximally inhibited angiogenesis in a Matrigel assay. Similar findings were reported by Norrby (2000), who showed that 2.5–5kDa heparin fragments maximally suppressed VEGF-induced angiogenesis in a rat mesenteric window assay. As the molecular weight of nadroparin is approximately 4.5kDa, our data confirm the antiangiogenic potential of heparin fragments within the above-mentioned range.

The basic mechanisms underlying the anti-angiogenic effect of the LMWHs remain to be elucidated. Several potential pathways have been proposed. First, LMWHs suppress TF gene expression and enhance the release of TF pathway inhibitor (Mousa and Mohamed, 2000; Schultz *et al*, 2001). Second, heparin fragments smaller than 18 saccharide units were shown to interfere with the binding of VEGF to its cellular receptor (Soker *et al*, 1994). In addition, heparins inhibit the release of heparanase by malignant tissue (Parish

et al, 1999, 2001). Heparanase not only creates a pro-angiogenic environment through the release of heparin-bound growth factors (VEGF, bFGF) from the interstitial matrix and upregulation of TF and VEGF expression, but is also a key enzyme in the degradation of this matrix, which renders it 'permissive' for neovascular outgrowth (El-Assal et al, 2001; Wood *et al*, 2005). Indeed, Collen *et al* (2000) found that structural alterations of the fibrin matrix induced by LMWH reduced the invasion of capillary-forming ECs. Nadroparin may exert a similar effect on ECM properties, as Barner *et al* (1987) found that *in vitro*, LMWH with a mean weight of 4.5kDa inhibited 99% of heparanase activity. In addition to a decrease in the number of microvessels, several other structural effects were found to result from nadroparin administration in this study. It is noteworthy that microvascular diameter at day 9 was significantly smaller compared with control animals. Theoretically, this may be explained by the inhibition bFGF and PDFG activity, which both exert a vasodilatory activity (Pukac *et al*, 1997; Takase *et al*, 1999; Millette *et al*, 2005).

The higher PCI and more efficient perfusion that we found in nadroparin-treated animals suggest a normalising effect of this LMWH on the tumour's vascular bed. As a consequence, there may be a role for LMWH to enhance drug delivery of concurrently administered cytotoxic therapy. In patients with pancreatic cancer and small cell lung cancer, administration of LMWH enhanced the efficacy of combined chemotherapy (Icli *et al*, 2002; Altinbas *et al,* 2004).

Several limitations apply to the interpretation of the current results. First, although it may be assumed that inhibition of tumour angiogenesis in this model translates into inhibition of tumour growth, this could not be assessed because of the short time frame used (9 days). Second, implantation of window chambers invariably induces a certain degree of inflammation that might confound the findings related to tumour angiogenesis. Finally, it is unclear to what extent findings in a heterotopic animal tumour model will translate into relevant clinical effects in patients.

In addition to the uncertain basic mechanisms by which heparins interfere with tumour angiogenesis, several other questions remain open. It is unclear whether the antiangiogenic effects of LMWHs depend only on their molecular weight and number of saccharide units, or also on other physicochemical properties such as manufacturing process and degree of sulphation. In addition, although most of the mechanisms shown thus far suggest a rather generic mode of action, preclinical studies suggest that the antitumour effects of heparins depend on the cancer cell type (Niers *et al*, 2009). Finally, the LMWH dose and duration in the clinical setting remain to be determined.

In conclusion, nadroparin inhibits tumour-associated angiogenesis and normalises microvessel structure in this immunocompetent tumour model using the dorsal skinfold chamber. Further study is required to determine whether direct effects on EC proliferation and modelling, changes in the structure of the extracellular matrix, or both explain our observations.

3.1.6 References

- Altinbas M, Coskun HS, Er O, Ozkan M, Eser B, Unal A, Cetin M, Soyuer S. A randomized clinical trial of combination chemotherapy with and without low-molecular-weight heparin in small cell lung cancer. *J Thromb Haemost.* 2004;2:1266–1271.
- Baker M, Wayland H. On-line volume flow rate and velocity profile measurements for blood in microvessels. *Microvasc Res.* 1974;7:131–143.
- Barner M, Eldor A, Wasserman L, Matzner Y, Cohen IR, Fuks Z, Vlodavsky I. Inhibition of heparanase-mediated degradation of extracellular-matrix heparan-sulfate by non-anticoagulant heparin species. *Blood.* 1987; 70: 551–557.
- Belting M, Dorrell MI, Sandgren S, Aguilar E, Ahamed J, Dorfleutner A, Carmeliet P, Mueller BM, Friedlander M, Ruf W. Regulation of angiogenesis by tissue factor cytoplasmic domain signaling. *Nature Med.* 2004;10:502–509.
- Carrier M, Agnes YY. Prophylactic and therapeutic anticoagulation for thrombosis-major issues in oncology. *Nat Clin Pract Oncol.* 2009;6:74–84.
- Collen A, Smorenburg SM, Peters E, Lupu F, Koolwijk P, Van Noorden C, van Hinsbergh VWM. Unfractionated and low molecular weight heparin affect fibrin structure and angiogenesis *in vitro*. *Cancer Res.* 2000; 60: 6196–6200.
- Dey P. Basic principles and applications of fractal geometry in pathology. *Anal Quant Cytol Histol*. 2005;27:284–290.
- El-Assal ON, Yamanoi A, Ono T, Kohno H, Nagasue N. The clinicopathological significance of heparanase and basic fibroblast growth factor expressions in hepatocellular carcinoma. *Clin Cancer Res.* 2001;7:1299–1305.
- Endrich B, Asaishi K, Gotz A, Messmer K. Technical report – a new chamber technique for microvascular studies in unanesthetized hamsters. *Res Exp Med.* 1980;177:125–134.
- Folkman J, Weisz PB, Joullie MM, Li WW, Ewing WR. Control of angiogenesis with synthetic heparin substitutes. *Science.* 1989; 243: 1490–1493.
- Fukumura D, Jain R. Imaging angiogenesis and the microenvironment. *APMIS.* 2008;116:695–715.
- Kakkar AK, Levine MN, Kadziola Z, Lemoine NR, Low V, Patel HK, Rustin G, Thomas M, Quigley M, Williamson RCN. Low molecular weight heparin, therapy with dalteparin, and survival in advanced cancer: the fragmin advanced malignancy outcome study (FAMOUS) *J Clin Oncol.* 2004; 22: 1944–1948.
- Khorana AA, Sahni A, Altland OD, Francis CW. Heparin inhibition of endothelial cell proliferation and organization is dependent on molecular weight. *Arteriosclers Thromb Vasc Biol.* 2003;23:2110–2115.
- Klerk CPW, Smorenburg SM, Otten HM, Lensing AWA, Prins MH, Piovella F, Prandoni P, Bos MMEM, Richel DJ, van Tienhoven G, Buller HR. The effect of low molecular weight heparin on survival in patients with advanced malignancy. *J Clin Oncol.* 2005;23:2130–2135.
- Laschke MW, Elitzsch A, Vollmar B, Menger MD. *In vivo* analysis of angiogenesis in endometriosis-like lesions by intravital fluorescence microscopy. *Fertil Steril.* 2005;84:1199–1209.
- Lee A. The effects of low molecular weight heparins on venous thromboembolism and survival in patients with cancer. *Thromb Res.* 2007;120:S121–S127.
- Marchetti M, Vignoli A, Russo L, Balducci D, Pagnoncelli M, Barbui T, Falanga A. Endothelial capillary tube formation and cell proliferation induced by tumor cells are affected by low molecular weight heparins and unfractionated heparin. *Thromb Res.* 2008;121:637–645.
- Menger M, Laschke M, Vollmar B. Viewing the microcirculation through the window: some twenty years experience with the hamster dorsal skinfold chamber. *Eur Surg Res.* 2002;34:83–91.
- Millette E, Rauch BH, Defawe O, Kenagy RD, Daum G, Clowes AW. Platelet-derived growth Factor-BB-induced human smooth muscle cell proliferation depends on basic FGF release and FGFR-1 activation. *Circ Res.* 2005;96:172–179.
- Mousa S. Low-molecular-weight heparin in thrombosis and cancer. *Semin Thromb Hemost.* 2004;30:25–30.
- Mousa SA, Mohamed S. Anti-angiogenic efficacy & mechanism of the low molecular weight heparin (LMWH), Tinzaparin and tissue factor pathway inhibitor (TFPI): potential anti-cancer link and benefits. *Blood*. 2000; 96: 182b.

- Mousa SA, Mohamed S. Inhibition of endothelial cell tube formation by the low molecular weight heparin, tinzaparin, is mediated by tissue factor pathway inhibitor. *Thromb Haemos.* 2004;92:627–633.
- Niers TMH, Bruggemann LW, Klerk CPW, Muller FJM, Buckle T, Reitsma PH, Richel DJ, Spek CA, Van Tellingen O, Van Noorden CJF. Differential effects of anticoagulants on tumor development of mouse cancer cell lines B16, K1735 and CT26 in lung. *Clin Exp Metastasis.*2009;26:171–178.
- Niers TMH, Klerk CPW, DiNisio M, Van Noorden CJF, Buller HR, Reitsma PH, Richel DJ. Mechanisms of heparin induced anti-cancer activity in experimental cancer models. *Crit Rev Oncol Hematol.* 2007;61:195–207.
- Norrby K. Heparin and angiogenesis: a low-molecular-weight fraction inhibits and a high-molecular-weight fraction stimulates angiogenesis systemically. *Haemostasis.* 1993;23:141–149.
- Norrby K. 2.5 and 5.0kDa heparin fragments specifically inhibit microvessel sprouting and network formation in VEGF(165)-mediated mammalian angiogenesis. *Int J Exp Pathol.* 2000;81:191–198.
- Norrby K, Ostergaard P. Basic-fibroblast-growth-factor-mediated de novo angiogenesis is more effectively suppressed by low-molecular-weight than by high-molecular-weight heparin. *Int J Microcirc Clin Exp.* 1996;16:8–15.
- Norrby K, Ostergaard P. A 5.0kDa heparin fraction systemically suppresses VEGF (165)-mediated angiogenesis. *Int J Microcirc Clin Expl.* 1997;17:314–321.
- Parish CR, Freeman C, Brown KJ, Francis DJ, Cowden WB. Identification of sulfated oligosaccharide-based inhibitors of tumor growth and metastasis using novel *in vitro* assays for angiogenesis and heparanase activity. *Cancer Research.* 1999;59:3433–3441.
- Parish CR, Freeman C, Hulett MD. Heparanase: a key enzyme involved in cell invasion. *Biochimica Et Biophysica Acta-Reviews on Cancer.* 2001; 1471:M99–M108.
- Pukac LA, Carter JE, Ottlinger ME, Karnovsky MJ. Mechanisms of inhibition by heparin of PDGF stimulated MAP kinase activation in vascular smooth muscle cells. *J Cell Physiol.* 1997;172:69–78.
- Schultz C, Ma Q, Fu S, Ahmad S, Hoppensteadt DA, Fareed J. Differential anticoagulant effects of three different low-molecular-weight heparins: assay-dependence and release of tissue factor pathway inhibitor. *Clin Chem.* 2001;47:A169.
- Smorenburg SM, Van Noorden CJF. The complex effects of heparins on cancer progression and metastasis in experimental studies. *Pharmacol Rev.* 2001;53:93–105.
- Soker S, Goldstaub D, Svahn CM, Vlodavsky I, Levi BZ, Neufeld G. Variations in the size and sulfation of heparin modulate the effect of heparin on the binding of Vegf(165) to its receptors. *Biochem Biophys Res Comm.* 1994;203:1339–1347.
- Takase H, Oemar BS, Pech M, Luscher TF. Platelet-derived growth factor-induced vasodilatation in mesenteric resistance arteries by nitric oxide: blunted response in spontaneous hypertension. *J Cardiovasc Pharmacol.* 1999;33:223–228.
- Torres IP, Hartleyasp B, Borgstrom P. Quantitative angiogenesis in a syngeneic tumor spheroid model. *Microvasc Res.* 1995;49:212–226.
- Icli F, Akbulut H. 38th Annual Meeting of the American Society of Clinical Oncology. Fl: Wiley-Liss; 2002. Low molecular weight heparin (LMWH) increases the efficacy of cisplatinum plus gemcitabine combination in advanced pancreatic cancer; pp. 507–512.
- Wan MX, Zhang XW, Torkvist L, Thorlacius H. Low molecular weight heparin inhibits tumor necrosis factor alpha-induced leukocyte rolling. *Inflammation Res.* 2001;50:581–584.
- Wood RJ, Parish CR, Hulett MD. The pro-inflammatory enzyme heparanase binds the CIMPR (CD222) in a M6P independent manner and promotes cell invasion by degrading the ECM. *Tissue Antigens.* 2005; 66:592.
- Zacharski LR, Lee AYY. Heparin as an anticancer therapeutic. *Expert Opin Investig Drugs.* 2008;17:1029–1037.

Chapter 3.2: Intravital microscopy to study the microvascular effects of nadroparin versus enoxaparin in colorectal tumour angiogenesis

I Debergh,[1] N Rosseel,[1] P Pattyn,[1] and WP Ceelen[1]

[1]Department of Surgical Oncology, University Hospital, B-9000 Ghent, Belgium
Submitted

3.2.1 Abstract

Background: Heparin or LMWH might improve survival in subgroups of cancer patients with better prognosis, independent of their anticoagulant effect. The specific anticancer mechanism of LMWH is not completely understood. Different pathways are influenced, e.g. influencing tumour cell proliferation, invasion, angiogenesis and metastasis. In our study, we try to elucidate the microcirculatory antiangiogenic effect of nadroparin and enoxaparin on colorectal angiogenesis in a mouse xenograft dorsal window chamber model using IVM studies and immunohistochemistry.

Methods: HT29 human colorectal cancers were implanted in a dorsal skinfold window chamber in athymic mice. Animals (N=8 per group) were treated with 200 IU of nadroparin, enoxaparin or saline for 8 days. Repeated intravital fluorescence microscopy was performed to calculate functional microcirculatory parameters: number (N) and length (L) of microvessels, vascular area fraction (AF), and red blood cell velocity (V). Microvessel density (MVD), fractal dimension, and pericyte coverage were assessed histologically.

Results: Active angiogenesis was observed in control animals, resulting in a significant increase in N, L, and AF. In nadroparin- and enoxaparin-treated animals, however, AF did not change significantly over time and N and L remained significantly lower than untreated animals on day 7. Compared with control animals, nadroparin- and enoxaparin-treated animals showed a significantly lower MVD, but a higher PCI depicting a more mature microvessel network.

3.2.2 Introduction

Cancer patients are at risk of venous thromboembolic events (VTE) induced by the hypercoagulable state associated with malignancy (Mousa S., 2004). There is therefore a clear rationale for prophylactic administration of unfractionated heparin (UFH) or low molecular weight heparin (LMWH) in these patients (Carrier & Agnes, 2009). Both UFH and LMWH exert their anticoagulant effect by activating antithrombin (AT), which neutralizes a number of serine proteases in the clotting cascade, notably thrombin and factor X. Current international guidelines recommend LMWH as gold standard anticoagulant prophylaxis (Lyman, *et al.*, 2013).

Recent clinical studies have suggested that, independent from its effects on the incidence of VTE, heparin therapy might alter survival in cancer patients (Kakkar, *et al.*, 2004; Klerk, *et al.*, 2005). In the FAMOUS trial, 385 patients with advanced malignancy where randomized to receive either dalteparin (Fragmin, mean mol weight 5 kDa) 5000 IU once daily or placebo. Overall survival after 1, 2 or 3 years did not differ between two

groups. In a post hoc subgroup analysis of patients with a better prognosis, however, survival was significantly improved in dalteparin treated patients (55% versus 36% after 3 years, p=0.03). Another recent trial randomized advanced cancer patients to either nadroparin (Fraxiparine, 5.5 kDa) 0.4-0.8 ml or placebo during 6 weeks. In a predefined subgroup of patients with better prognosis, the hazard ratio was 0.64 (95%CI: 0.45-0.9) in favour of the nadroparin group while the incidence of major bleeding did not differ significantly. Enoxaparin (Clexane, 4.5 kDa), the worldwide most used LMWH, may also have a positive effect on survival, for instant by prolonging the time to progression in patients with metastatic non-small cell lung cancer (Robert, Busby, Marques, Reynolds, & Carey, 2003).

The mechanisms through which LMWHs exert anticancer effects remain incompletely understood. Several aspects of cancer growth including tumor cell proliferation, invasion, angiogenesis and metastasis have been examined in relation to the effects of heparin (Niers, *et al.*, 2007; Mousa & Petersen, 2009).

Most experimental data thus far were generated from cell culture experiments. *In vivo* microscopy (IVM) allows to repeatedly and noninvasively examine tumour associated angiogenesis through an implanted glass covered observation window. A recent study shows favorable antiangiogenic results in melanoma and pancreatic carcinoma of nadroparin in a hamster model (Debergh, Van Damme, Pattyn, Peeters, & Ceelen, 2010). The aim of the present experiment is to study the effects of nadroparin and enoxaparin on colorectal angiogenesis in a mouse xenograft dorsal window chamber model using IVM studies and immunohistochemistry. The use of IVM in this setting represents a good approach to study the interactions of LMWHs with tumor microcirculatory events.

3.2.3 Methods

Animal and tumor model

Athymic mice (athymic nu/nu, Harlan, The Netherlands) weighing 25-30g were housed separately in plastic cages with free access to tap water and standard pellet food. HT29 human colon cancer cell lines were cultured in McCoy's 5A (Gibco life technologies, Invitrogen) and 1 million cells suspended in 0.05 mL of PBS (phosphate-buffered saline, Gibco life technologies, Invitrogen) were injected in the dorsal window chamber (on day 1 after implantation) as xenografts.

Dorsal skinfold chambers implantation

Mice were anaesthetised using isoflurane inhalation (1.5-2%) and placed on a heating pad. A titanium frame is surgically fixed onto a dorsal skinfold of the animal. On one side of the skinfold, a circular area of dermis and subcutis is surgically removed (10 mm diameter) and covered by a circular cover glass. Animals were housed separately and were allowed to recover for 24h from surgery and anaesthesia before tumour suspension was injected. Window chambers were inspected daily for the presence of air bubbles, inflammation, infection, or vascular thrombosis.

Drug therapy

Animals (N = 8 per group) were treated with daily intraperitoneal injections of either 0.05 mL of saline, 200 IU aXa of nadroparin dissolved in 0.1 mL of saline, or 200 IU aXa of enoxaparin dissolved in 0.1 mL of saline. Injections started the day before tumour implantation.

In vivo fluorescence microscopy was performed on days 1 (day of tumour injection), 3, 5, and 7. Unconscious animals (isoflurane inhalation) received an i.v. bolus of 0.03 mL of fluorescein isothiocyanate (FITC)-labelled dextran (20 mg/mL) (MW 150 000 Da; Sigma-Aldrich NV, Bornem, Belgium) and were placed on the stage of a modified Olympus BX51W1 microscope (Olympus NV, Aartselaar, Belgium). Fluorescence microscopy was performed using a HBO 50W mercury lamp (Osram, Zaventem, Belgium) and a FITC filter set (excitation filter 460-490 nm) for detecting epifluorescent intravascular plasma. Static and dynamic images of the microcirculation were obtained in 4 different regions in each chamber. Digital images were captured real time on the hard disc of a computer using a high sensitivity digital camera (model C8484-05, Hamamatsu Photonics, Hamamatsu, Japan). Quantitative microcirculatory analysis was performed using the Capimage software (H Zeintl Engineering, Heidelberg, Germany). The following parameters were calculated: microvessel length per area (L; cm/cm²), number of microvessels per high-power field (N; n/HPF x20), vascular area fraction (AF; %), and microvessel diameter (D; μm). In addition, centerline red blood cell velocity (V; mm/s) was measured by analyzing 10 microvessels per region of interest, randomly chosen among those that crossed a vertical line drawn over the centre of the computer screen, as described by Laschke *et al.* (2005). Volumetric blood flow (VQ; pL/s) was calculated from V and D as $VQ = \pi \times (D/2)^2 \times V/K$, in which K (= 1.3) represents the Baker-Wayland factor (Baker & Wayland, 1974), and considers the parabolic velocity profile of blood in microvessels.

On day 8 after skinfold chamber implantation, animals were killed and the tissue inside the observation window was excised for histology. Tissue fragments were fixed in 10% formalin, embedded in paraffin, and 4 μm thick sections were cut and mounted for immunohistochemistry.

Factor VIII (von Willebrand factor, FVIII) immunostaining was used to visualize tumour microvessels and calculate microvessel density (MVD), whereas α-smooth muscle actin (αSMA) was used to identify pericytes and calculate the pericyte coverage index (PCI) as a measure of microvessel maturation. Serial tissue sections were deparaffinised in xylene, hydrated by serial immersion in ethanol, and subsequently incubated in Proteinase K (Dako, Heverlee, Belgium) for antigen retrieval. Endogenous peroxidase activity was blocked with 3% H_2O_2 in methanol. Slides were washed in Tris-buffered saline (TBS) – Tween and treated with UltraSens Block RTU (ImmunoLogic, Duiven, The Netherlands) to inhibit nonspecific antibody binding. Sections were incubated with mouse monoclonal antibodies against FVIII (Dako) or αSMA (Abcam, Cambridge, UK) at room temperature for 1h, rised with TBS-Tween, and incubated with secondary antibodies (UltraSens Biotinylated Goat Anti-polyvalent RTU; ImmunoLogic) for 10 min each. Visualisation of the immunoprecipitate was performed by adding 3,3'-diaminobenzidine (Biogenex, San Ramon, CA, USA) and counterstaining with haematoxylin. Positive and negative controls were processed simultaneously.

Serial FVIII and αSMA- stained sections of dorsal skinfold tissue were entirely scanned for tumour regions (magnification x20) and digitized. Microvessel density was calculated by digital image analysis using the NIH ImageJ software (version 1.47, available from

http://rsbweb.nih.gov/ij). Using the threshold colour plugin, FVIII and αSM-positive cells were isolated from background staining and the resulting images converted to binary. Microvessel density was calculated using the ratio of black pixels over the total number of pixels in the binary image, whereas the PCI was calculated as the ratio of αSMA-positive pixels vs FVIII-positive pixels. The fractal dimension of the microvessel bed was calculated using the ImageJ FracLac plugin. The fractal dimension is a rational number between 1 and 2 (the dimensions of a line and plane, respectively), and has been shown to correlate with the degree of branching, tortuosity, and irregularity of the tumour-associated microvessel network (Dey, 2005).

STATISTICAL ANALYSIS
Data are expressed as median (interquartile range). As the distribution of all the variables may not be Gaussian, differences were analysed using Mann–Whitney rank-sum test or differences between more than two groups were analysed by ANOVA. Results were considered statistically significant when the probability of a type I error was ≤ 5%. Statistical analysis was performed with SigmaPlot 11.0 (Systat Software, Richmond, CA, USA).

3.2.4 Results
All animals (n = 24) developed tumour-induced angiogenesis, microscopically visible in the observation window (Figure 3.7). Three animals were excluded on day 1 for further analysis because of insufficient optical quality of the window chamber. In all other animals (N=21), the skinfold chamber provided excellent image quality and resolution over the duration of the experiment (7 days).

Effects of nadroparin and enoxaparin on tumour-induced angiogenesis
The microvascular parameters derived from *in vivo* microscopic observations are summarised in Figure 3.8A-C and Table 3.4A. In control animals (N=7), the number and the length of microvessels and the vascular area fraction increased significantly. In nadroparin- and enoxaparin-treated animals (N=7 each), however, vascular area fraction did not change significantly over time. A significant increase in the number and the length of microvessels was also noted in the LMWH-treated groups, but the result at day 7 remained significantly lower than untreated animals.

Effects of nadroparin and enoxaparin on the dynamic properties of the tumour vascular bed
The results of microcirculatory calculations are summarised in Figure 3.8D-F and Table 3.4B. In treated groups, microvessel diameter did not change significantly over the course of 7 days of tumour evolution, compared to untreated animals. In the nadroparin group, a further significant decrease of diameter was observed on day 7 when compared to diameters of the enoxaparin-treated group.
In the control group, velocity and volumetric blood flow increased progressively until day 5, followed by a decline at day 7. In the enoxaparin-treated group, RBC velocity has the same tendency, whereas volumetric blood flow peaked earlier.
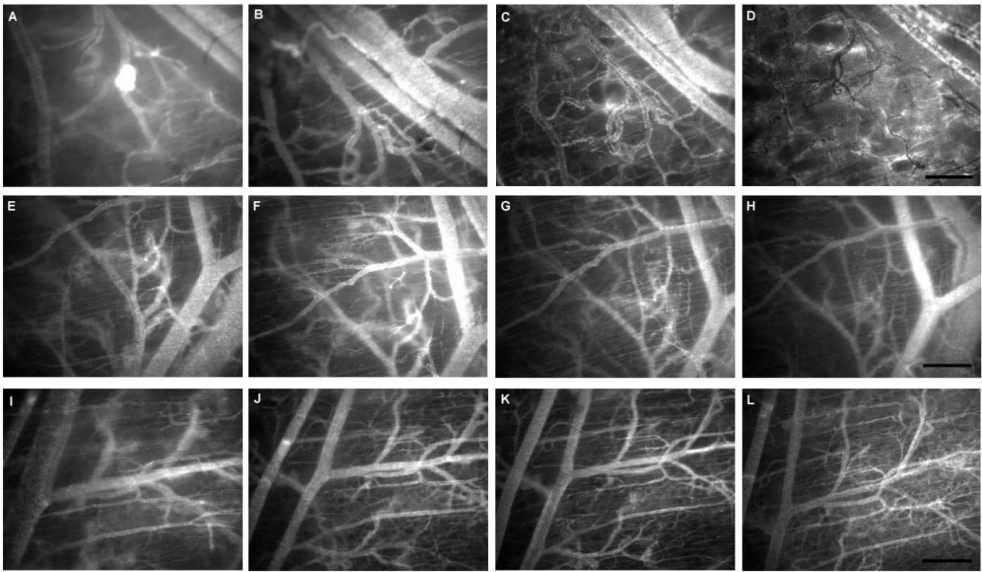
FIGURE 3.7 Representative tumour growth and angiogenesis observed for 7 days in a control animal (**A-D**), a nadroparin-(**E-H**) and an enoxaparin-treated animal (**I-L**). IVM evaluation was done on day 1 (**A,E,I**), day 3 (**B,F,J**), day 5 (**C,G,K**), and day 7 (**D,H,L**). Scale bar = 200μm.

In nadroparin-treated animals dynamic properties of red blood cell are completely different. A significant higher RBC velocity and volumetric blood flow compared to enoxaparin treated animals was measured at day 1, with a statistically significant drop in velocity and flow at day 3 compared to both other groups. At day 5 and 7 no differences in velocity or volumetric blood flow between the groups are observed.

Immunohistochemical analysis
Histological examination of the dissected dorsal skinfolds on day 8 after tumour fragment implantation showed macroscopically vital tumour tissue in all animals. Microvessel quantitative and morphology data are illustrated in Figure 3.9A-D. The microvessel density (FVIII staining) was 7.6% (4.4-10.8) in the control group, 5.5% (3.5-7.4) in the nadroparin-treated group, and 3.9% (2.1-8.1) in the enoxaparin-treated group ($P < 0.05$, ANOVA on ranks) (Table 2).

Data concerning microvessel maturation are depicted in Figure 3.9E. The PCI was 77.9% (50.0-118.1) in untreated animals, 112.2% (60.2-179.0) in nadroparin-treated animals and 106.5% (43.6-216.2) in enoxaparin-treated animals ($P = 0.005$ and $P = 0.034$, respectively; Mann–Whitney U-test) (Table 3.5).
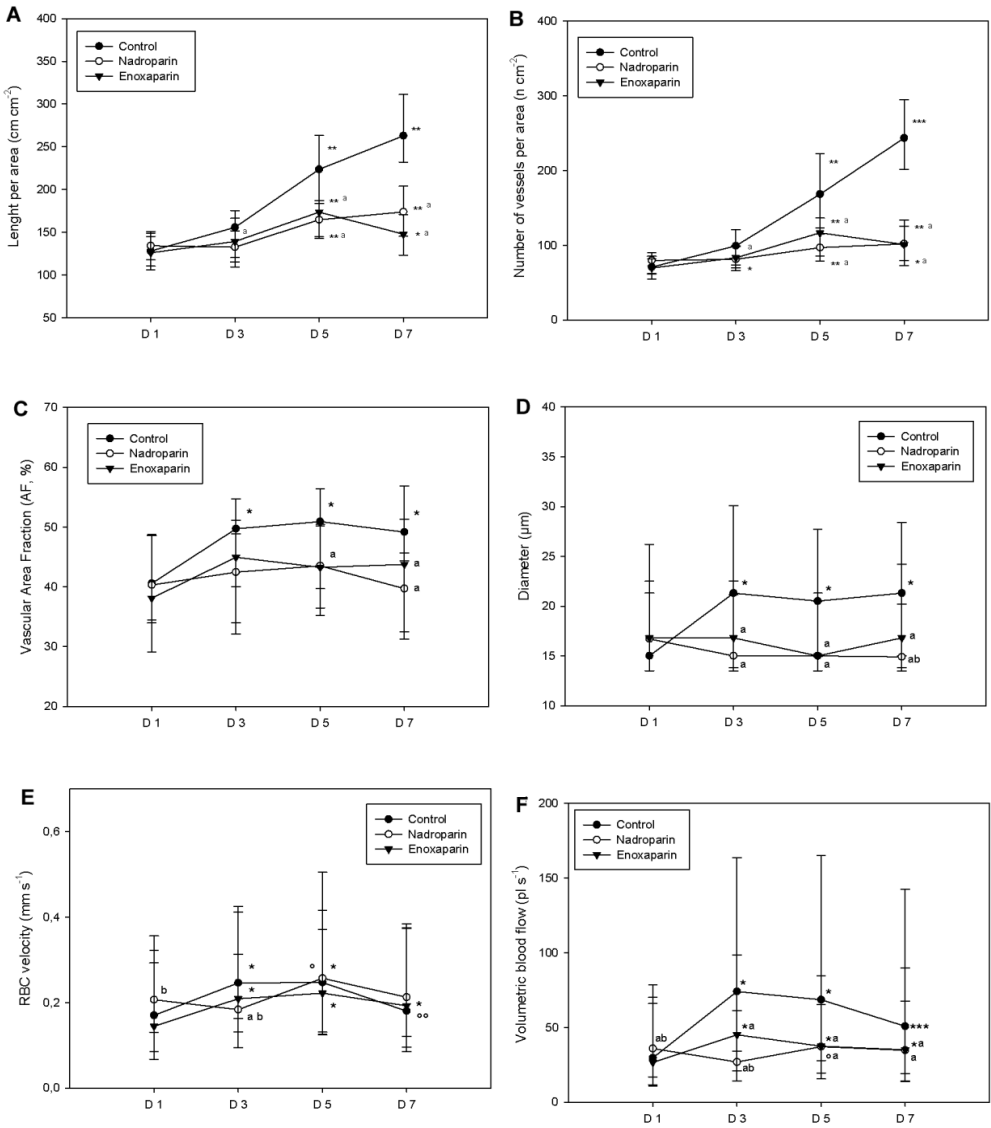
FIGURE 3.8 Vessel length (**A**), number of microvessels per area (**B**), vascular area fraction (**C**), microvessel diameter (**D**), red blood cell velocity (**E**), and volumetric blood flow (**F**) in control, nadroparin- and enoxaparin-treated animals for 7 days.

*P<0.05 vs day 1; **P<0.05 vs day 1 and 3; ***P<0.05 vs day 1, 3 and 5; °P<0.05 vs day 3; °°P<0.05 vs day 3 and 5; [a]P<0.05 vs untreated animals; [b]P<0.05 vs treatment with enoxaparin.

TABLE 3.4 (A) Evolution of microvessel length, number, and area fraction over time. (**B**) Evolution of microvessel diameter, red blood cell velocity, and volumetric blood flow over time.

A	Day 1	Day 3	Day 5	Day 7
Control (n = 7)				
L (cm cm⁻²)	127,9 (110,7-148,8)	155,5 (121,1-174,6)	223,5 (186,4-262,5)**	262,8 (233,5-310,1)**
N (n cm⁻²)	70,7 (61,8-85,2)	99,2 (74,8-120,3)	168,3 (124,7-220,1)**	243,5 (203,6-293,8)***
VAF (%)	40,6 (29,2-48,5)	49,7 (41,0-54,6)*	50,9 (40,1-56,1)*	49,2 (44,9-56,7)*
Fractal Dimension	1,67 (1,63-1,72)	1,69 (1,65-1,76)	1,70 (1,66-1,74)	1,69 (1,66-1,74)
Nadroparin (n = 7)				
L (cm cm⁻²)	133,9 (118,1-150,5)	132,4 (110,9-151,5)[a]	164,4 (144,6-183,5)[a]**	173,7 (145,7-203,6) [a]**
N (n cm⁻²)	79,7 (63,1-90,2)	81,2 (66,2-99,2)[a]	96,8 (79,4-114,1)[a]**	101,7 (80,0-134,0)[a]**
VAF (%)	40,3 (34,0-48,5)	42,4 (32,6-48,9)	43,5 (36,8-50,1)	39,7 (32,5-45,2)[a]
Fractal Dimension	1,69 (1,64-1,73)	1,70 (1,64-1,75)	1,68 (1,64-1,73)	1,72 (1,67-1,76)
Enoxaparin (n = 7)				
L (cm cm⁻²)	125,8 (106,2-144,8)	139,0 (116,3-165,4)	173,5 (142,9-186,7)[a]**	147,7 (123,7-169,8)[a]*
N (n cm⁻²)	69,5 (54,6-81,9)	83,1 (69,5-98,0)*	116,6 (86,2-136,5)[a]**	101,0 (73,5-125,3)[a]*
VAF (%)	38,1 (34,5-47,9)	44,9 (35,4-50,7)	43,3 (35,2-50,2)[a]	43,8 (31,6-51,0)[a]
Fractal Dimension	1,68 (1,62-1,74)	1,70 (1,66-1,74)	1,70 (1,65-1,75)	1,71 (1,65-1,75)

B	Day 1	Day 3	Day 5	Day 7
Control (n = 7)				
D (µm)	15,0 (13,5-24,1)	21,3 (15,0-30,1)*	20,5 (14,9-27,7)*	21,3 (15,0-28,4)*
V (µm / s)	170,2 (67,4-354,0)	246,1 (163,5-410,8)*	247,0 (131,2-505,4)*	180,7 (85,6-365,1)°°
VQ (pL / s)	29,6 (10,7-70,1)	74,0 (34,2-163,5)*	69,6 (27,8-165,1)*	50,7 (19,2-141,1)***
Nadroparin (n = 7)				
D (µm)	16,7 (13,5-21,3)	15,0 (13,5-21,1) a	15,0 (13,5-20,5) a	14,9 (13,5-20,2)[ab]
V (µm / s)	206,5 (132,0-321,6)[b]	184,7 (96,1-313,5)[ab]	257,4 (126,2-370,9)°	212,6 (96,2-384,5)
VQ (pL / s)	35,9 (16,9-77,8)[ab]	26,9 (14,1-61,0)[ab]	37,1 (19,7-65,1)[°a]	34,7 (13,9-67,2)[a]
Enoxaparin (n = 7)				
D (µm)	16,8 (13,5-22,5)	16,8 (13,8-22,5)[a]	15,0 (13,5-21,3)[a]	16,8 (13,8-24,2)[a]
V (µm / s)	144,0 (85,3-293,3)	209,1 (132,6-424,8)*	222,4 (126,0-415,9)*	193,3 (122,5-373,3)*
VQ (pL / s)	26,5 (11,6-65,6)	45,1 (20,8-97,3)[*a]	37,5 (15,6-84,4)[*a]	35,0 (14,3-89,2)[*a]

Abbreviations: L = microvessel length; N = number of microvessels; VAF = vascular area fraction. D = microvessel diameter; V = red blood cell velocity; VQ = volumetric blood flow.
*P<0,05 vs day 1; **P<0,05 vs day 1 and 3; ***P<0,05 vs day 1, 3 and 5; °P<0,05 vs day 3; °°P<0,05 vs day 3 and 5; [a]P<0,05 vs untreated animals and [b]P<0.05 vs enoxaparin-treated animals at corresponding time points. Data represent median (interquartile range).

TABLE 3.5 Immunohistochemistry results

	Control (n = 7)	**Nadroparin (n = 7)**	**Enoxaparin (n = 7)**
FVIII (%)	7,6 (4,4-10,8)	5,5 (3,5-7,4)[a]	3,9 (2,1-8,1)[a]
αSMA (%)	5,2 (3,8-6,9)	5,6 (3,4-7,7)[b]	4,0 (2,8-6,0)
PCI (%)	77,9 (50,0-118,1)	112,2 (60,2-179,0)[a]	106,5 (43,6-216,2)[a]

Abbreviations: FVIII = factor VIII staining; αSMA = α-smooth muscle actin staining; PCI = pericyte coverage index. Data represent median (interquartile range). [a]P<0,05 vs untreated animals and [b]P<0.05 vs enoxaparin-treated animals.
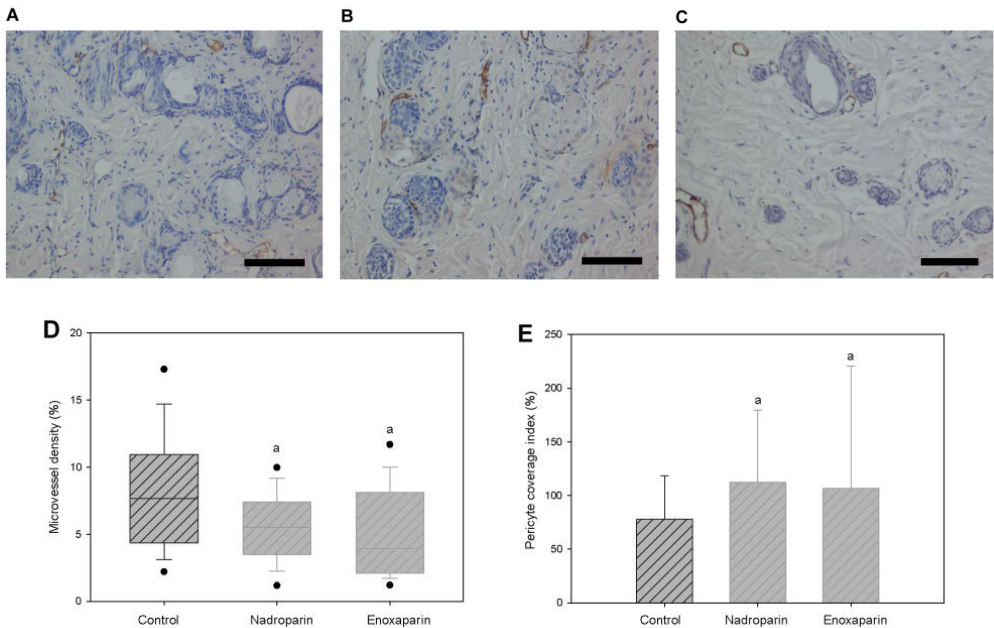
FIGURE 3.9 Examples of FVIII-stained microvessels of control (**A**), enoxaparin- (**B**) and nadroparin-treated (**C**) animals. Scale bar = 100µm.

Microvessel density (FVIII-staining) (**D**) in the three experimental groups. Box plot shows median values and interquartile ranges, with dots expressing 5th-95th percentiles.

Microvessel maturity (pericyte coverage index) (**E**) in the three experimental groups. Columns = median; Bars = interquartile range. [a]$P<0.05$ vs untreated animals.

3.2.5 Discussion

Anticancer properties of heparins and LMWHs are the topic of intensive experimental research for several decades. Important variation in study design, animal models, and tumour type makes interpretation and comparison difficult. Variations include the type of heparin or LMWH used, heparin dose and duration of treatment, interval between heparin administration and cancer cell inoculation and route of administration (subcutaneous (s.c.), intraperitoneal (i.p.) or intravenous (i.v.)).

The effect on primary tumour growth was investigated in s.c. tumour models, where only high doses of heparins (i.p. or s.c.) demonstrated significant antitumour activity (Back & Steger, 1976; Niers, *et al.*, 2007). In several studies, heparin administration into the peritoneal cavity reduced the peritoneal tumour deposits. These findings suggest that high heparin concentrations around the tumour cells could excert a local effect. Other studies reveal that (even lower doses of) heparin and LMWH induce a significant reduction in the number of metastases. Also, not only heparins but modified heparins with limited or no anticoagulant activity were used, and showed to have tumour growth reducing or anti-metastatic properties, which proves that the effect is not only dependent on the inhibition of coagulation (Niers, *et al.*, 2007).

The topic of our study is the effect of LMWH on tumour-associated angiogenesis alone, which has a pivotal role in successful growth of tumour and spreaded metastases. Our results suggest that both nadroparin and enoxaparin exert an antiangiogenic effect

in a human colorectal tumour mouse model, as evidenced by a significantly lower vascular area fraction, microvessel density, length and number of microvessels when compared with control animals (Figure 3.8A-C and 3.9D). Indeed, Marchetti *et al.* (2008) demostrated that the LMWHs, enoxaparin and dalteparin, significantly inhibited capillary tube formation in a Matrigel assay. A former study, with a dorsal chamber skinfold model in hamsters, inoculated with pancreatic carcinoma or melanoma, and treated with 200 IU s.c. nadroparin only proved to provoke lower vascular area fraction and MVD than control animals, but had no effect on length and number of microvessels (Debergh, Van Damme, Pattyn, Peeters, & Ceelen, 2010). The current antiangiogenic effect on L and N, can possibly be explained by the relatively higher dosages of LMWHs in mice (200 IU) and not by different route of administration (i.p. vs s.c.).

Angiogenesis is a critical process in malignant growth regulated by a number of heparin binding angiogenic growth factors such as vascular endothelial growth factor (VEGF) and basic fibroblast growth factor (bFGF). These angiogenic growth factors bind to heparane sulphate proteoglycans (HSPGs) present on both the endothelial cells (ECs) and the extracellular matrix (ECM). Soluble heparins have been shown to compete with growth factors for ECM binding sites, and therapeutic dosages of UFH cause an increase in plasma levels of certain growth factors (Colin, *et al.*, 1999; Folkman, Weisz, Joullie, Li, & Ewing, 1989). In contrast to UFH, LMWH has been shown to inhibit binding of angiogenic growth factors to their endothelial receptors, an effect that is depending on the number of sulphated polysaccharide glycosaminoglycan chains in the heterogenous mixture of LMWH (Norrby, 1993). In a Matrigel assay, endothelial cell proliferation and tube formation was inhibited maximally by LMWH with a chain length of >8 polysaccharides and a molecular weight of 6 kDa while no inhibition was observed with UFH, tetrasaccharide, pentasaccharide, or octasaccharide (Khorana, Sahni, Altland, & Francis, 2003). Also *in vitro*, heparin fragments of less than 18 saccharides reduce the activity of VEGF (Soker, Goldstaub, Svahn, Vlodavsky, Levi, & Neufeld, 1994) and fragments of less than 10 saccharide residues inhibit the activity of bFGF (Lepri, *et al.*, 1994). *In vivo*, the same effect of small heparin fractions on bFGF activity has been described (Jayson & Gallagher, 1997; Norrby & Ostergaard, 1996). Similar findings were reported by Norrby (2000), who showed that 2.5–5kDa heparin fragments maximally suppressed VEGF-induced angiogenesis in a rat mesenteric window assay.

So, the antiangiogenic potential of LMWHs seems to be depending on the molecular weight and number of saccharide units. In our experiment, we compared the *in vivo* effect of commercially available nadroparin (4.3 kDa) and enoxaparin (4.5 kDa) on tumour angiogenensis with similar molecular weights. Small differences in results can be explained by different polysaccharide mixtures, e.g. enoxaparin is composed of 70-80% characterizable 2 to 12 saccharides (< 3600 Da). The 20-30% remaining mixture is incompletely known and contains 13 to 32 saccharides (> 3600 Da). As these LMWHs are polysaccharide mixtures, both bFGF and VEGF can be targeted in the antiangiogenic process, which is a plausible explanation of the positive short term results on tumour-associated angiogenesis. It is known that in patients receiving bevacizumab, a monoclonal anti-VEGF antibody, therapy resistance or disease progression can be expected due to the upregulation of placental growth factor (PlGF), platelet-derived growth factor (PDGF) and bFGF (Saif, 2013).

Another critical event in the process of cancer invasion, metastasis or tumoural angiogenesis is the degradation of various components of the ECM, including collagen, laminin, fibronectin and HSPGs. This can be obtained by heparanase, secreted by cancer cells. Heparanase expression is rare in normal tissue, but is evident in many human tumours where it significantly increases both the angiogenic and metastatic potential of cancer cells (Vlodavsky, Korner, Ishai-Michaeli, Bashkin, Bar-Shavit, & Fuks, 1990). *In vitro*, LMWH with a mean weight of 4.5kDa inhibited 99% of heparanase activity (Bar-Ner, *et al.*, 1987). Thus, nadroparin- and enoxaparin-induced blocking of heparanase could possibly make the ECM less permissive for tumoural neovasculature. Indeed, structural alterations of the fibrin matrix induced by LMWH reduced the invasion of capillary-forming endothelial cells (Collen, *et al.*, 2000).

Our study also describes a statistically significant increase in PCI, thus a better maturation of microvessels compared to tumoural vessels due to treatment with enoxaparin and nadroparin (figure 5). An angiogenic signal (f.i. VEGF or bFGF) coming from tumour cells, will detach pericytes from the vessel wall and make endothelial cells loosen their junctions; as a consequence this pathological vessel dilates. VEGF increases the permeability of the endothelial cell layer, causing plasma proteins to extravasate and to increase the interstitial pressure (Carmeliet & Jain, 2011). Currently, vessel normalization appeared to be able to open new therapeutic opportunities to slow down tumour invasiveness and dissemination, and increase tumour responses to chemotherapeutics and radiotherapy than anti-angiogenic therapy alone (Jain, 2002). Besides the increased PCI (Figure 3.9E), we also observed a normalized diameter after 7 days of treatment with nadroparin and enoxaparin in tumoural microvessels (Figure 3.8D). Unfortunately, our current study did not measure microvessel permeability nor its normalization after treatment, which however, can be easily done in the IVM model. Furthermore, this model has some limitations as measuring plasma and interstitial oncotic pressure, or hypoxia in the tumor is not technically feasible.

Tumoural microvessel hemodynamic properties change also during treatment with LMWHs. Red blood cell velocity tend to increase significantly from day 3-5 after tumour implantation, to satisfy the high demands of early tumour formation (Lin, *et al.*, 2010). On day 7, a significant decrease in velocity is observed (Figure 3.8E), probably due to increased interstitial pressure in the leaking vascular bed. Hence, volumetric blood flow follows the same pattern. Enoxaparin-treated tumoural microvessels, have also a significant increase of blood flow between 3-5 days, but tend to decrease on day 7 (Figure 3.8F). As microvessel diameter is normalized in these animals, volumetric blood flow is significantly lower on day 5 and 7 compared to control animals and tends to normalize again. Nadroparin treatment reveals other hemodynamic properties with a high red blood cell velocity on day 1 and a significant lower velocity on day 3 compared to both other groups. From day 5 on, red blood cell velocity follows more or less the pattern of both other groups. Whether a nadroparin-inflicted effect on the interstitial pressure during day 1 and 3 is the cause of this aberrant velocity pattern, and concomitant volumetric blood flow pattern, must be elaborated in future studies. At day 5 and 7, volumetric blood flow in nadroparin treated groups has a tendency to normalize, with significant lower values than control animals at corresponding time points.

Several limitations can be found in our study. Besides exploring the effect of LMWHs

on microvessel normalization more thoroughly, we must examine dose-response effect of LMWHs and duration of treatment not only in animal models, but also in the clinical setting. For future experiments, it would be useful to quantify vascular normalization properties of LMWH in a similar *in vivo* tumour model, with additional measurements of permeability of the microvasculature, tissue oxygen pressure and interstitial fluid pressure.

Encouraging however, is that the antitumour effects of heparins with vascular normalization, which are depending on the cancer cell type, could be validated in a hamster model with melanoma and pancreatic carcinoma, and now in a mouse xenograft model with human colorectal cancer.

In conclusion, nadroparin and enoxaparin inhibit tumour-associated angiogenesis and normalizes microvessel structure in this mouse xenograft model using the dorsal skinfold chamber. Further study is required to determine whether direct effects on EC proliferation and modelling, changes in the structure of the extracellular matrix, or both explain our observations.

3.2.6 References

Back, N., & Steger, R. (1976). Effect of aprotinin, EACA and heparin on growth and vasopeptide system of Murphy-Sturm lymphosarcoma. *Eur J Pharmacol* (38), 313–9.

Baker, M., & Wayland, H. (1974). On-line volume flow rate and velocity profile measurement for blood in microvessels. *Microvasc Res.,* 1 (7), 131-43.

Bar-Ner, M., Eldor, A., Wasserman, L., Matzner, Y., Cohen, I., Fuks, Z., *et al.* (1987). Inhibition of heparanase-mediated degradation of extracellular matrix heparan sulfate by non-anticoagulant heparin species. *Blood,* 2 (70), 551-7.

Carmeliet, P., & Jain, R. (2011). Molecular mechanisms and clinical applications of angiogenesis. *Nature,* 473, 298-307.

Carrier, M., & Agnes, Y. (2009). Prophylactic and therapeutic anticoagulation for thrombosis-major issues in oncology. *Nat Clin Pract Oncol,* 6, 74-84.

Colin, S., Jeanny, J., Mascarelli, F., Vienet, R., Al-Mahmood, S., Courtois, Y., *et al.* (1999). *In vivo* involvement of heparan sulfate proteoglycan in the bioavailability, internalization, and catabolism of exogenous basic fibroblast growth factor. *Mol Pharmacol* (55), 74–82.

Collen, A., Smorenburg, S., Peters, E., Lupu, F., Koolwijk, P., Van Noorden, C., *et al.* (2000). Unfractionated and low molecular weight heparin affect fibrin structure and angiogenesis *in vitro*. *Cancer Res* (60), 6196–6200.

Debergh, I., Van Damme, N., Pattyn, P., Peeters, M., & Ceelen, W. (2010). The low-molecular-weight heparin, nadroparin, inhibits tumour angiogenesis in a rodent dorsal skinfold chamber model. *Br J Cancer,* 5 (102), 837-843.

Dey, P. (2005). Basic principles and applications of fractal geometry in pathology: a review. *Anal Quant Cytol Histol,* 5 (27), 284-90.

Folkman, J., Weisz, P., Joullie, M., Li, W., & Ewing, W. (1989). Control of angiogenesis with synthetic heparin substitutes. *Science* (243), 1490–3.

Jain, R. K. (2002). Normalization of tumor vasculature: an emerging concept in antiangiogenic therapy. *Science.* 5706 (307), 58-62.

Jayson, G., & Gallagher, J. (1997). Heparin oligosaccharides: inhibitors ofthe biological activity of bFGF on Caco-2 cells. *Br J Cancer* (75), 9-16.

Kakkar, A., Levine, M., Kadziola, Z., Lemoine, N., Low, V., Patel, H., *et al.* (2004). Low molecular weight heparin, therapy with dalteparin, and survival in advanced cancer: the fragmin advanced malignancy outcome study (FAMOUS). *J Clin Oncol.,* 10, 1944-8.

Khorana, A., Sahni, A., Altland, O., & Francis, C. (2003). Heparin inhibition of endothelial cell proliferation

and organization is dependent on molecular weight. l. 2003;. [PubMed]. *Arteriosclers Thromb Vasc Biol,* 25, 2110–2115.

Klerk, C., Smorenburg, S., Otten, H., Lensing, A., Prin, M., Piovella, F., *et al.* (2005). The effect of low molecular weight heparin on survival in patients with advanced malignancy. *J Clin Oncol,* 10, 2130-5.

Laschke, M., Elitzsch, A., Vollmar, B., & Menger, M. (2005). *In vivo* analysis of angiogenesis in endometriosis-like lesions by intravital fluorescence microscopy. *Fertil Steril, Suppl 2* (84), 1199-209.

Lepri, A., Benelli, U., Bernardini, N., Bianchi, F., Lupetti, M., Danesi, R., *et al.* (1994). Effect of low molecular weight heparan sulphate on angiogenesis in the rat cornea after chemical cauterization. *J Ocul Pharmacol.,* 1 (10), 273-80.

Lin, W., Chih-Chieh, W., Tzung-Chi, H., Wen-Chi, L., Bill Yuan-Chi, C., Ren-Shyan, L., *et al.* (2010). Red Blood Cell Velocity Measurement in Rodent Tumor Model: An *in vivo* Microscopic Study. *Journal of Medical and Biological Engineering,* 2 (32), 97-102.

Lyman, G., Khorana, A., Kuderer, N., Lee, A., Arcelus, J., Balaban, E., *et al.* (2013). Venous thromboembolism prophylaxis and treatment in patients with cancer: american society of clinical oncology clinical practice guideline update. *J Clin Onco,* 17 (31), 2189-204.

Marchetti, M., Vignoli, A., Russo, L., Balducci, D., Pagnoncelli, M., Barbui, T., *et al.* (2008). Marchetti M, Vignoli A, Russo L, Balducci D, Pagnoncelli M, Barbui T, Falanga A. Endothelial capillary tube formation and cell proliferation induced by tumor cells are affected by low molecular weight heparins and unfractionated heparin. *Thromb Res* (121), 637–645.

Mousa, S. (2004). Low-molecular-weight heparin in thrombosis and cancer. *Semin Thromb Hemost*, 30, 25-30.

Mousa, S., & Petersen, L. (2009). Anti-cancer properties of low-molecular-weight heparin: Preclinical evidence. *Thromb Haemost* (102), 258-267.

Niers, T., Klerk, C., DiNisio, M., Van Noorden, C., Büller, H., Reitsma, P., *et al.* (2007). Mechanisms of heparin induced anti-cancer activity in experimental cancer models. *Crit Rev Oncol Hematol,* 3 (61), 195-207.

Norrby, K. (2000). 2.5 and 5.0kDa heparin fragments specifically inhibit microvessel sprouting and network formation in VEGF(165)-mediated mammalian angiogenesis. *Int J Exp Pathol* (81), 191–198.

Norrby, K. (1993). Heparin and angiogenesis: a low-molecular-weight fraction inhibits and a high-molecular-weight fraction stimulates angiogenesis systemically. *Haemostasis* (23), 141–149.

Norrby, K., & Ostergaard, P. (1997). A 5.0kDa heparin fraction systemically suppresses VEGF (165)-mediated angiogenesis. *Int J Microcirc Clin Expl* (17), 314-321.

Norrby, K., & Ostergaard, P. (1996). Basic-fibroblast-growth-factor-mediated de novo angiogenesis is more effectively suppressed by low-molecular-weight than by high-molecular-weight heparin. *Int J Microcirc Clin Exp* (16), 8–15.

Robert, F., Busby, E., Marques, M., Reynolds, R., & Carey, D. (2003). Phase II study of docetaxel plus enoxaparin in chemotherapy-naive patients with metastatic non-small cell lung cancer: preliminary results. *Lung Cancer,* 2 (42), 237-45.

Saif, M. (2013). Anti-VEGF agents in metastatic colorectal cancer (mCRC): are they all alike? *Cancer Manag Res* (3), 103-115.

Soker, S., Goldstaub, D., Svahn, C., Vlodavsky, I., Levi, B., & Neufeld, G. (1994). Variations in the size and sulfation of heparin modulate the effect of heparin on the binding of VEGF165 to its receptors. *Biochem Biophys Res Commun,* 2 (203), 1339-47.

Vlodavsky, I., Korner, G., Ishai-Michaeli, R., Bashkin, P., Bar-Shavit, R., & Fuks, Z. (1990). Extracellular matrix-resident growth factors and enzymes: possible involvement in tumor metastasis and angiogenesis. *Cancer Metastasis Rev,* 3 (9), 203-26.

Vlodavsky, I., Mohsen, M., Lider, O., Svahn, C., Ekre, H., Vigoda, M., *et al.* (1994). Inhibition of tumor metastasis by heparanase inhibiting species of heparin. *Invasion Metastasis*, 1-6 (14), 290-302.

Functional imaging of cancer

CHAPTER 4: Functional imaging of cancer

Chapter 4.1: Innovation in cancer imaging

Debergh I[a], Vanhove C[b], Ceelen W[a]

[a]Department of Surgery, Ghent University Hospital, and [b]Department of Electronics and Information Systems, Medical Image and Signal Processing (MEDISIP) Research Group, Ghent University and IbiTech – IBBT, Ghent, Belgium

4.1.1 Abstract

Cancer is rapidly becoming the worldwide leading cause of premature death. Iconographic techniques have traditionally provided information on tumor anatomy. The recent introduction of functional and molecular imaging techniques allows probing tumor physiology and biology in addition to mere anatomical description. In addition to the research implications, these novel imaging techniques offer early response assessment and target visualization which, in the era of personalized medicine, may offer significant advances in cancer therapy. Here, we provide an overview of the most important developments in cancer imaging, with a focus on the clinical applications.

4.1.2 Introduction

Cancer is a leading cause of death worldwide, accounting for well over 7 million deaths in 2008 [1]. Since most solid cancers are not readily amenable for palpation and inspection, accurate imaging has traditionally been one of the cornerstones of cancer therapy. Indeed, imaging allows for correct anatomical delineation and staging of the malignant process, which have a direct impact on the therapeutic strategy as well as the patient's prognosis. Until the beginning of the 21st century, medical iconography was primarily focused on anatomical imaging, with computed tomography (CT) and magnetic resonance imaging (MRI) being the most important imaging technologies. These structural imaging modalities can offer images with exquisite spatial resolution within seconds or minutes, but they share the limitation of not being able to detect lesions until the structural changes in the tissue (e.g. tumor growth) are large enough to be detected by these imaging technologies [2].

Recent advances in molecular and functional imaging have had a significant impact on modern oncology practice. First, nuclear techniques such as positron emission tomography (PET) and single-photon emission CT (SPECT) offer the potential of detecting cellular or molecular changes which precede structural abnormalities. Obviously, these techniques, when combined with novel molecular tracers, also hold considerable promise in early drug development. Secondly, functional and molecular imaging allow for rapid assessment of therapy response, which allows disease biology to gauged well before any change in tumor dimension occurs as measured by the traditional RECIST criteria [3]. The use of imaging as a biomarker of response allows tailoring the therapeutic strategy and limiting the cost and side effects of ineffective regimens. Here, we review

the currently available functional and molecular imaging modalities and briefly highlight some promising preclinical developments.

4.1.3 Diffusion Imaging

By incorporating diffusion-sensitizing gradients in a T2-weighted spin echo sequence, diffusion-weighted MRI enables quantifying the microscopic mobility of water in biological tissues [4,5]. Images are acquired at multiple diffusion sensitivities, allowing the calculation of the apparent diffusion coefficient (ADC, in μm2/s) in each image element. In general, the cellular proliferation associated with cancer growth results in restricted water mobility (low ADC), while apoptosis and necrosis caused by anticancer therapy results in increased water mobility and thus in increased ADC values [6]. Historically, the application of diffusion-weighted MRI in gastrointestinal cancer has been limited due to physiological organ motility. Several authors have examined its use in rectal cancer, esophageal cancer, and gastrointestinal stromal tumors (table 4.1). Although the reported findings are not entirely consistent, taken together these studies suggest that pretreatment ADC values and the extent of ADC changes during therapy may serve as imaging biomarkers of response.

TABLE 4.1. Clinical results of diffusion-weighted MRI in gastrointestinal cancer

Tumor type	Therapy	n	Findings
Rectal cancer [83]	chemotherapy, CRT	14	negative correlation between pretreatment ADC and tumor size change after chemotherapy (r = –0.67, p = 0.01) and CRT (r = –0.83, p = 0.001)
Rectal cancer [84]	CRT	34	pretreatment ADC significantly lower in pathologic responders (p < 0.001, ANOVA)
Rectal cancer [85]	CRT	9	significant decrease of ADC in the 2nd (p = 0.028), 3rd (p = 0.012), and 4th (p = 0.008) weeks of treatment
Rectal cancer [86]	CRT	76	percentage change between pre- and posttreatment ADC significantly higher in complete pathological responders (p < 0.0001). Post-CRT but not pre-CRT ADC were significantly different between complete and noncomplete responders
Rectal cancer [87]	CRT	50	post-CRT but not pre-CRT accurate in predicting complete response
Rectal cancer [88]	CRT	37	early increase of ADC and low pre-CRT ADC correlate with good response to CRT
GIST [89]	imatinib	32	low pretherapy ADC and ADC increase at 1 week after therapy is associated with good response to imatinib
Esophageal cancer [90]	CRT	80	high pre-CRT ADC values predicted response; better survival in high ADC patients
Esophageal cancer [91]	–	123	negative correlation between ADC and tumor diameter/clinical stage

CRT = Chemoradiation.

4.1.4 Perfusion Imaging

Since an adequate blood supply is a prerequisite for developing tumors, perfusion imaging may be used to differentiate tumors, assess response to therapy, and aid in prognostication. Dynamic contrast-enhanced (DCE) MRI has been applied to the study of tumor perfusion. DCE-MRI encompasses the dynamic study of tissue enhancement over time after intravascular injection of a paramagnetic contrast agent (CA) [7]. The acquired images provide insight into tumor tissue properties such as blood volume, perfusion, and vascular permeability, all of which have been shown to represent adequate markers of therapy response [8]. The images acquired may be processed to generate semiquantitative (heuristic) parameters such as area under the curve, time to peak enhancement, peak intensity, and CA washout rate. Alternatively, when tissue

enhancement is combined with simultaneous measurement of CA concentration in a feeding vessel, pharmacokinetic compartmental modeling becomes possible, which yields parametric maps of parameters such as the endothelial transfer constant K^{trans} [9]. The physiological interpretation of the calculated parameters critically depends on the properties of the CA [10]. When using a small molecule such as gadopentetate dimeglumine, extravasation is 'perfusion limited' and mainly reflects tissue perfusion, while the use of larger (preclinical) molecules, which do not readily diffuse across the endothelial lining, allows probing vessel permeability (fig. 4.1). Table 4.2 lists clinical trials in digestive cancer using DCE-MRI, all of which have shown that a decrease in CA exchange between the vascular and the tumor interstitial compartment represents a valid biomarker of therapy response. Since the imaging endpoints of a DCE study reflect blood supply in the first place, this technique is ideally suited to study the effects of antiangiogenic therapy in early-phase clinical trials [11].

TABLE 4.2. Clinical results with DCE-MRI in cancer patients

Tumor type	Therapy	n	Findings
Rectal cancer [92]	CRT	31	responsive tumors showed a marked reduction in permeability at the end of treatment
Rectal cancer [93]	RT	10	RT reduced magnitude and intratumor heterogeneity of the endothelial transfer constant K_{PS} ($p = 0.01$)
Pancreatic cancer [94]	chemotherapy + antiangiogenic therapy	11	K^{trans}, v(e), C_{peak}, slope, and AUC(60) decrease significantly after therapy; pretreatment K^{trans} measurement in pancreatic tumors predicts response to antiangiogenic therapy
Esophageal cancer [95]	CRT	5	K^{trans} decreased 11.4-fold after CRT
Esophageal cancer [96]	CRT	48	CRT led to a significant decrease of the contrast agent exchange rate (k_{21})

RT = Radiotherapy; CRT = chemoradiation; AUC = area under the curve.
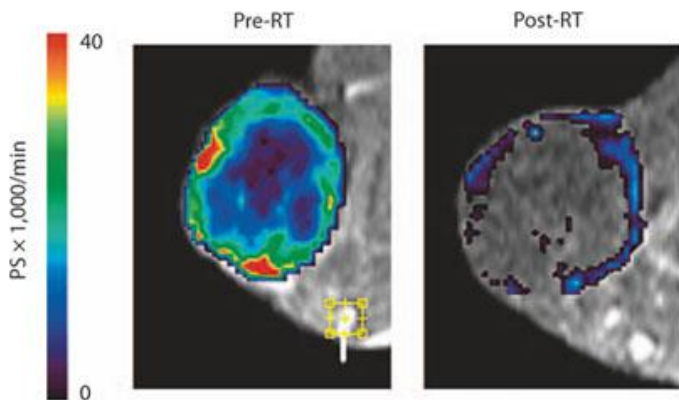
FIGURE 4.1. Example of kinetic modeling based on DCE-MRI. Serial imaging was performed (500 images, temporal resolution 1.1 s) after intravenous injection of the macromolecular contrast agent gadomelitol (P792). Parametric map of microvascular permeability before and 1 week after 5 × 5 Gy of radiotherapy in a rat colorectal tumor implanted in the hind leg. The arrow points to vessel used as the arterial input function. PS = Permeability surface product; RT = radiotherapy.

Using similar kinetic modeling methods, dynamic CT may provide insight into tumor perfusion [12]. DCE-CT has been used to monitor the effects of anticancer therapy in

lung cancer, rectal cancer, and hepatocellular carcinoma [13,14]. An attractive perfusion imaging modality is DCE ultrasound using intravenous injection of gas 'microbubbles' surrounded by a polymer shell [15,16]. Obviously, ultrasound-based technology is cheap, portable, and minimally invasive. Contrast-enhanced ultrasound has been used to predict response in liver, renal, and stromal tumors [17,18]. In addition to the diagnostic information gained by DCE-ultrasound, the combination of microbubbles carrying a drug payload and focused ultrasound bursts allow targeted drug delivery under ultrasound guidance [19,20].

4.1.5 Functional Lymph Node Imaging
Nodal spread is one of the most important prognostic variables in solid cancer, and nodal status may significantly impact the therapeutic strategy as well as the patient's prognosis. Since morphological criteria have proven insufficiently accurate in the detection of nodal cancer spread, functional imaging techniques that would facilitate nodal staging are under scrutiny.

4.1.5.1 ULTRASMALL SUPERPARAMAGNETIC IRON OXIDE
Nodal involvement represents one of the most powerful prognosticators in digestive cancer, and considerable efforts have been invested in techniques allowing accurate detection of lymph node spread. After intravenous injection, ultrasmall superparamagnetic iron oxide (USPIO) will be taken up by nodal tissue, which will darken uniformly and homogeneously on T_2- and T_2^*- weighted MRI. In rectal cancer, several authors have attempted to diagnose mesorectal nodal involvement. Koh et al. [21] compared nodal enhancement patterns after USPIO injection with histological analysis and found that eccentric and uniform high signal intensity were observed in lymph nodes that contained metastases larger than 1 mm in diameter. The same authors found that compared to standard MRI, USPIO-enhanced imaging improved specificity (93 vs. 75%), although sensitivity was similar (65%) when compared to histological analysis [22]. Beets et al. [23] examined the accuracy of USPIO-enhanced MRI in nodal staging of rectal cancer, and found sensitivity, specificity, PPV, and NPV of 97, 94, 66, and 99%, respectively, after node-by-node analysis. Unfortunately, the CA used in these studies (ferumoxtran-10, Sinerem, Combidex) never received FDA approval and production was discontinued several years ago.

4.1.5.2 GADOLINIUM-BASED BLOOD POOL AGENTS
Using large CAs with a prolonged plasma half-life facilitates measurement of neovascular permeability as well as lymphangiography and nodal staging. Many of these compounds are in preclinical development, but at present only MS-325 (gadofosveset), a gadolinium chelate that is chemically modified causing it to bind strongly but reversibly to plasma albumin, is available for clinical use [24]. Lambregts et al. [25] reported on the use of gadofosveset-enhanced MRI for nodal staging in rectal cancer. When comparing it to histology as the standard, they found that sensitivity and specificity improved from 76 and 82% to 80 and 97%, respectively, when using gadofosveset (p < 0.001). Other macromolecular CAs composed of albumin, polylysine, polysaccharides, poly(ethylene glycol), copolymers of cystamine and cystine with GD-DTPA, and dendritic structures based on polyamidoamine and polylysine (Gadomers) seem very promising, but are presently unavailable for clinical use [26].

4.1.6 Metabolic Imaging

The cornerstone of imaging tumor metabolism is PET using radiolabeled glucose. The use of glucose-based PET imaging is based on the Warburg effect, i.e. the phenomenon that under aerobic conditions, tumor tissues metabolize approximately tenfold more glucose to lactate in a given time than normal tissues, notwithstanding preserved mitochondrial respiration [27]. With the exception of prostate cancer, the uptake of ^{18}F-fluorodeoxyglucose (FDG) is increased in most cancer types and correlates with the proliferation and number of malignant cells [28]. Since changes in metabolic activity are an early manifestation of a drug's anticancer effect, there is considerable interest in the use of FDG-PET to measure tumor response. One of the drawbacks associated with FDG-PET is the variability in methods to measure FDG uptake, which renders comparison between studies difficult. Tracer uptake is usually measured semiquantitatively by calculating the standardized uptake value, defined as the tumor radiotracer concentration (in MBq/ml) × body weight (in kg) divided by the injected activity (in MBq). Alternatively, kinetic modeling (Patlak plot) may be used to derive the metabolic rate for glucose using measurements of the time course of radioactivity in tissue and in serial arterial blood samples [29]. A recent systematic review of the accuracy of FDG-PET in the prediction of response to neoadjuvant therapy in esophageal cancer showed a pooled sensitivity of 67% and specificity of 68% [30]. There was significant heterogeneity between included studies, which led the author to conclude that the results of FDG-PET should not be used to guide therapy in this patient population. In rectal cancer patients treated with neoadjuvant CRT, several small studies have demonstrated that FDG-PET uptake predicts the pathological response of the tumor [31,32,33]. On the other hand, FDG-PET was shown to be insufficiently accurate in predicting nodal involvement [34].

4.1.7 Hypoxia Imaging

Tissue oxygenation has been recognized as a central microenvironmental parameter in solid tumors for at least 100 years [35]. Areas of varying degrees of hypoxia (defined as O_2 partial pressure <2.5 mm Hg) are present in most tumors as a consequence of limited oxygen diffusion, increased utilization by vessel-proximal cells, and perfusion deficiencies resulting from a structurally and functionally abnormal microvascular bed. Hypoxia represents an adverse predictive and prognostic factor, and has been implicated in mechanisms as diverse as chemoresistance, radioresistance, angiogenesis, vasculogenesis, invasiveness, metastasis, and genomic instability [36]. Several PET tracers have been designed for hypoxia imaging [37]. These include the 2-nitroimidazole derivatives ^{18}F-fluoromisonidazole and ^{18}F-azomycin arabinoside, and ^{64}Cu-methyl-thiosemicarbazone [38,39,40]. In the absence of molecular oxygen, the 2-nitroimidazole compounds are reduced to a highly reactive hydroxylamine, which attaches to cellular proteins. In head and neck cancer, cervical cancer, and NSCLC, hypoxia PET imaging was successfully used to predict response to radiation or chemoradiation [41,42]. Dietz *et al.* [43] reported a pilot study using Cu-64-ATSM in rectal cancer patients undergoing neoadjuvant CRT. They found that a higher tumor tissue uptake correlated with worse overall and progression free survival. In esophageal cancer patients, Yue *et al.* [44] used hypoxia PET imaging with ^{18}F-fluoroerythronitroimidazole. They found that tracer uptake

predicted response to CRT, while a high standardized uptake value was associated with poor clinical response.

4.1.8 Proliferation Imaging

Cellular proliferation is one of the hallmarks of cancer. [18]F-3'-fluoro-3'deoxythymidine (FLT)-PET is incorporated by proliferating cells in the pyrimidine salvage pathway during the S-phase. The tracer is then phosphorylated by thymidine kinase 1, after which it accumulates in the cells [45]. In preclinical models, however, tracer avidity was significantly inversely correlated with tumor thymidine level and, as a consequence, did not always reflect tumor cell proliferation [46]. Several clinical studies have aimed to use FLT-PET to monitor the response to antiproliferative therapy. In breast cancer, FLT-PET enabled early response prediction, i.e. after one course of chemotherapy [47,48]. Similarly, FLT avidity changes reflected early therapy response in head and neck cancer patients, whereas discrimination between malignant and reactive lymph nodes turned out to be impossible due to due to reactive B-lymphocyte proliferation [49,50]. Wieder *et al.* [51] used sequential FLT-PET before and after neoadjuvant CRT in rectal cancer patients. Although a significant decrease in standardized uptake value was observed, the degree of change in FLT uptake did not correlate with histological tumor regression. Along the same line, Muijs *et al.* [52] compared CT and FLT-PET in the primary staging of rectal cancer and found that compared to CT, FLT-PET performed poorly in delineation of the tumor as well as in malignant node detection. A comparison of FDG-PET with FLT-PET in colorectal cancer patients was reported by Yamamato *et al.* [53]. They found that FLT uptake was significantly lower than FDG uptake, and that neither imaging modality correlated with the Ki67 proliferation index. More favorable results were noted in gastric cancer patients. Herrmann *et al.* [97] compared FLT-PET with FDG-PET and found FLT uptake in all 45 patients, whereas 14 gastric tumors were not FDG avid.

4.1.9 Apoptosis Imaging

Induction of apoptosis is assumed to be the most important mechanism by which anticancer drugs exert their effect. One of the discriminating features of the apoptotic cell is the rapid redistribution of phosphatidylserine from the inner to the outer layer of the plasma membrane. Phosphatidylserine-binding agents therefore represent attractive targets for apoptosis imaging. The first radiolabeled tracer with a nanomolar affinity for membrane-bound phosphatidylserine was ^{99m}Tc-annexin V, the activity of which is imaged using SPECT. Kartachova *et al.* [54] used sequential annexin V imaging in lung cancer patients treated with platinum-based chemotherapy, and found a significant correlation between annexin V uptake and treatment response. Similar results were obtained by Rottey *et al.* [55], who showed that sequential annexin V scintigraphy using a 25% change threshold allowed discrimination of nonresponders with 94% accuracy after 3 days of chemotherapy initiation in solid tumor patients (fig. 4.2). Compared with SPECT, the use of PET offers the advantages of higher count rate, quantitative imaging, and improved resolution. Efforts have therefore been invested in the synthesis of annexin V-based PET tracers. Examples in preclinical development include labeling of annexin V with gallium-68 or N-succinimidyl 4- [18F] fluorobenzoate, and labeling of the annexin V-128 with N- [4- [(4- [18F] fluorobenzylidene)aminooxy] butyl] maleimide ([F-

18], FBABM) [56,57,58]. Other apoptosis tracer targets include synaptotagmin, caspase inhibitors, and hydrophobic cations. Recently, Hoglund *et al.* [59] reported on a study in healthy volunteers with 18F-labeled 2-(5-fluoropentyl)-2-methyl malonic acid [(18) F-ML-10], a PET apoptosis tracer. In addition to a favorable pharmacokinetic and safety profile, the authors observed tracer binding to apoptotic cells in testicular tissue, where these occur in normal circumstances.
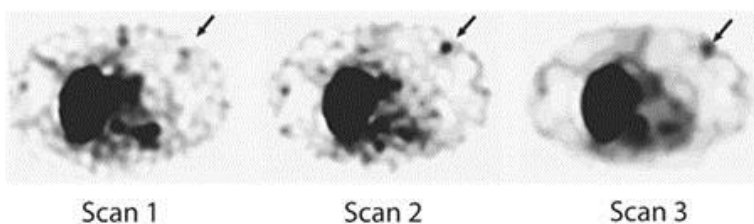

FIGURE 4.2. Example of sequential ^{99m}Tc-hydrazinonicotinamide-annexin V imaging for predicting response to chemotherapy. A significant increase in tracer uptake is noted over time in a primary breast tumor (arrows). Reproduced with permission from Rottey *et al.* [55].

Another feature of the apoptotic process is the sudden halt in protein synthesis, including that of choline and choline-containing molecules. Decreases in choline synthesis may be detected using ^{1}H magnetic resonance spectroscopy. Thus, several authors have demonstrated that reduction of tumor choline content represents a valid biomarker of chemotherapy response in breast cancer patients [60,61]. In prostate cancer, the maximal choline + creatine to citrate ratio and choline to creatine ratio as measured by magnetic resonance spectroscopy were shown to separate low-grade from higher-grade tumors [62]. An exciting development is the use of hyperpolarization techniques to dramatically (more than 10,000-fold) increase the sensitivity of magnetic resonance spectroscopy tracers based on stable isotopes such as ^{13}C and ^{15}N, which hold significant promise in probing the biochemical pathways associated with cancer [63].

4.1.10 Optical Imaging

Optical imaging is a rapidly emerging field, with widespread applications ranging from clinical diagnosis to molecular biology. In the clinic, the endoscope has served as an optical imaging tool since the 17th century. Compared to cross-sectional imaging modalities, endoscopy can provide real-time images with high spatial resolution, enabling the detection of very small anatomic changes, and offers immediate intervention, such as biopsy of neoplastic lesions. With the introduction of fluorescent CA, the functions of traditional endoscopy are further extended. Chromoendoscopy involves the application of spraying a fluorescent CA onto the mucosa using a spray catheter passed through a standard endoscope. It has been shown that in large human studies, chromoendoscopy improves earlier diagnosis of adenomas and colorectal cancers [64]. Another study showed that chromoendoscopy permits more accurate diagnosis of the extent and the severity of neoplastic lesions [65]. Despite these positive preliminary results, some studies have shown that the fluorescent CA used during chromoendoscopy (methylene blue) might induce DNA damage, and consequently accelerate carcinogenesis [66]. Such

risks need to be carefully balanced against the possible benefits of improved earlier disease detection.

Indocyanine green has been heavily tested for adverse reactions and is a fluorescent CA that rapidly binds to blood proteins after intravenous injection [67]. It can be used to provide information of the vasculature of the digestive tract that cannot be obtained by conventional endoscopy [68]. Kimura *et al.* [69] evaluated the effectiveness of fluorescent endoscopy for the preoperative evaluation of tumor invasion in patients with superficial gastric tumors, and concluded that submucosal invasion has a higher correlation with fluorescence than macroscopic morphology of tumors and histopathologic tumor differentiation. Indocyanine green has also been used for the detection of metastases to a sentinel lymph node in melanoma, gastric cancer, and lung cancer patients [70,71,72]. Recently, more sophisticated optical probes have been developed that target or interact with biological processes on a molecular level after being exogenously delivered. Most of these probes are completing preclinical validation in mouse models and the design of such probes involves the attachment of a fluorophore to a targeting moiety, such as a peptide, an antibody or a fragment of an antibody, small molecules, and nanoparticles [73,74,75]. Another class of optical agents changes their fluorescent properties after target interaction, rather than targeting surface receptors and proteins.

These smart probes are initially optically silent and become fluorescent as a result of enzymatic cleavage of fluorophores from a delivery backbone in the presence of protease [76]. This technique has been proven to be very successful in combination with endoscopic applications [77].

4.1.11 Multimodality Imaging

In previous paragraphs, various structural, functional, and molecular imaging technologies were introduced. Table 4.3 lists some performance parameters of different imaging modalities available. Since the properties of anatomical (CT, MRI) and functional (PET, SPECT) imaging modalities are rather complementary, integrating the information obtained from these modalities into one platform takes 'the best of both worlds'. Multimodality platforms – such as PET/CT, SPECT/CT, PET/MRI, and SPECT/MRI – with each modality having its unique strengths and limitations play an increasingly important role in the diagnosis and staging of human disease [78]. The major technological advances in PET instrumentation before the advent of CT, excellently documented by Muehllehner and Karp [79], culminated in the introduction of a hybrid PET/CT system in 1998 [80]. This was undeniably a very important step to use PET as a viable clinical tool, with PET/CT being the most widely used multimodality platform today. Among multimodality platforms, PET/MRI may ultimately provide the greatest yield of scientific information, combining the impressive technological developments of PET with the excellent anatomic resolution and soft-tissue contrast provided by MRI [81]. An important advantage of PET/MRI over the other multimodality platforms is that PET and MRI data can be acquired simultaneously, rather than sequentially. A clinical PET/MRI device that allows the simultaneous acquisition of whole-body PET and MRI images became commercially available in 2011 (Biograph™ mMR, Siemens).

TABLE 4.3. Performance parameters of different imaging modalities

Modality	EM spectrum	Spatial resolution		Image contrast		Sensitivity to contrast agent
		clinical	preclinical		intrinsic	
SPECT	gamma rays	10 mm	<1 mm	+++	none	10^{-9} molar
PET	gamma rays	5 mm	1–2 mm	+++	none	10^{-12} molar
CT	X-rays	1–2 mm	<200 μm	+		10^{-3} molar
MRI	radio waves	1 mm	<100 μm	++		10^{-6} molar
Fluorescence	visible light or NIR	<5 mm	<5 mm	++	autofluorescence	10^{-12} molar

Preclinically, there is a trend to combine optical imaging and radionuclide (PET/SPECT) imaging. Besides the large difference in the energy of the emitted photons (1–2 eV vs. 10^5 eV), optical and radionuclide imaging are quite similar. Both are based on the detection of photons emitted from a source inside the body, and both use highly sensitive photon detectors positioned outside the body to detect the signals. In addition, for both the measured signal is directly proportional to the biological process under examination. Due to these similarities, and because optical imaging suffers from poor tissue penetration, it is natural to consider the development of combined optical/radionuclide imaging devices and dual-modality probes that can be used in a similar fashion to produce optical signals when used in small animals, or yield PET/SPECT signals to facilitate the translation to the clinic. In the clinic, these dual-modality probes can provide, next to radionuclide images, additional information when combined with surgical techniques, where the excited tissue can be visualized optically [82].

4.1.12 Conclusion

Cancer imaging has evolved from a mere morphological investigation to a physiology-based in-depth analysis of tumor biology. In the era of personalized medicine, functional and molecular imaging will allow us to tailor treatment according to predictive and prognostic imaging-based biomarkers. Standardization and clinical validation of novel imaging modalities should be a priority in clinical cancer therapy and incorporated in interventional cancer trials.

4.1.13 References

1   World Health Organization: Cancer Facts. http://www.who.int/mediacentre/factsheets/fs297/en/index.html (accessed February 10, 2012).

2   Weissleder R, Pittet MJ: Imaging in the era of molecular oncology. *Nature* 2008; 452: 580–589.

3   Response Evaluation Criteria in Solid Tumors. http://www.recist.com (accessed March 2, 2012).

4   Padhani AR, Koh DM, Collins DJ: Wholebody diffusion-weighted MR imaging in cancer: current status and research directions. *Radiology* 2011; 261: 700–718.

5   Lambregts DMJ, Maas M, Cappendijk VC, Prompers LM, Mottaghy FM, Beets GL, Beets-Tan RGH: Whole-body diffusionweighted magnetic resonance imaging: current evidence in oncology and potential role in colorectal cancer staging. *Eur J Cancer* 2011; 47: 2107–2116.

6   Harry VN, Semple SI, Parkin DE, Gilbert FJ: Use of new imaging techniques to predict tumour response to therapy. *Lancet Oncology* 2010; 11: 92–102.

7   Hylton N: Dynamic contrast-enhanced magnetic resonance imaging as an imaging biomarker. *J Clin Oncol* 2006; 24: 3293–3298.

8   Ceelen W, Smeets P, Backes W, Van Damme N, Boterberg T, Demetter P, Bouckenooghe I, De Visschere M, Peeters M, Pattyn P: Noninvasive monitoring of radiotherapy-induced microvascular changes using

dynamic contrast enhanced magnetic resonance imaging (DCE-MRI) in a colorectal tumor model. *Int J Radiat Oncol Biol Phys* 2006; 64: 1188–1196.

9   Sourbron SP, Buckley DL: Tracer kinetic modelling in MRI: estimating perfusion and capillary permeability. *Phys Med Biol* 2012; 57:R1–R33.

10   Delrue LJ, Casneuf V, Van Damme N, Blanckaert P, Peeters M, Ceelen WP, Duyck PCO: Assessment of neovascular permeability in a pancreatic tumor model using dynamic contrast-enhanced (DCE) MRI with contrast agents of different molecular weights. *MAGMA* 2011; 24: 225–232.

11   Liu G, Rugo HS, Wilding G, McShane TM, Evelhoch JL, Ng C, Jackson E, Kelcz F, Yeh BM, Lee FT, Charnsangavej C, Park JW, Ashton EA, Steinfeldt HM, Pithavala YK, Reich SD, Herbst RS: Dynamic contrast-enhanced magnetic resonance imaging as a pharmacodynamic measure of response after acute dosing of AG-013736, an oral angiogenesis inhibitor, in patients with advanced solid tumors: results from a phase I study. *J Clin Oncol* 2005; 23: 5464–5473.

12   Bellomi M, Viotti S, Preda L, D'Andrea G, Bonello L, Petralia G: Perfusion CT in solid body-tumours part II. Clinical applications and future development. *Radiologia Medica* 2010; 115: 858–874.

13   Curvo-Semedo L, Portilha MA, Ruivo C, Borrego M, Leite JS, Caseiro-Alves F: Usefulness of perfusion CT to assess response to neoadjuvant combined chemoradiotherapy in patients with locally advanced rectal cancer. *Acad Radiol* 2012; 19: 203–213.

14   Jiang T, Kambadakone A, Kulkarni NM, Zhu AX, Sahani DV: monitoring response to antiangiogenic treatment and predicting outcomes in advanced hepatocellular carcinoma using image biomarkers, CT perfusion, tumor density, and tumor size (RECIST). *Invest Radiol* 2012; 47: 11–17.

15   Lassau N, Chebil M, Chami L, Bidault S, Girard E, Roche A: Dynamic contrast-enhanced ultrasonography (DCE-US): a new tool for the early evaluation of antiangiogenic treatment. *Target Oncol* 2010; 5: 53–58.

16   Cosgrove D, Lassau N: Imaging of perfusion using ultrasound. *Eur J Nucl Med Mol Imaging* 2010; 37:S65–S85.

17   De Giorgi U, Aliberti C, Benea G, Conti M, Marangolo M: Effect of angiosonography to monitor response during imatinib treatment in patients with metastatic gastrointestinal stromal tumors. *Clin Cancer Res* 2005; 11: 6171–6176.

18   Williams R, Hudson JM, Lloyd BA, Sureshkumar AR, Lueck G, Milot L, Atri M, Bjarnason GA, Burns PN: Dynamic microbubble contrast-enhanced US to measure tumor response to targeted therapy: a proposed clinical protocol with results from renal cell carcinoma patients receiving antiangiogenic therapy. *Radiology* 2011; 260: 581–590.

19   Suzuki R, Oda Y, Utoguchi N, Maruyama K: Progress in the development of ultrasoundmediated gene delivery systems utilizing nano- and microbubbles. *J Control Release* 2011; 149: 36–41.

20   Rapoport N, Nam KH, Gupta R, Gao ZG, Mohan P, Payne A, Todd N, Liu X, Kim T, Shea J, Scaife C, Parker DL, Jeong EK, Kennedy AM: Ultrasound-mediated tumor imaging and nanotherapy using drug loaded, block copolymer stabilized perfluorocarbon nanoemulsions. *J Control Release* 2011; 153: 4–15.

21   Koh DM, Brown G, Temple L, Raja A, Toomey P, Bett N, Norman AR, Husband JE: Rectal cancer: mesorectal lymph nodes at MR imaging with USPIO versus histopathologic findings – initial observations. *Radiology* 2004; 231: 91–99.

22   Koh DM, George C, Temple L, Collins DJ, Toomey P, Raja A, Bett N, Farhat S, Husband JE, Brown G: Diagnostic accuracy of nodal enhancement pattern of rectal cancer at MRI enhanced with ultrasmall superparamagnetic iron oxide: findings in pathologically matched mesorectal lymph nodes. *Am J Roentgenol* 2010; 194:W505–W513.

23   Beets GL, Lahaye M, Engelen SME, de Bruine AP, von Meyenfeldt MF, van Engelshoven JMA, van de Velde CJH, Beets-Tan RGH: Can we predict the nodal status in primary rectal cancer accurately with USPIO MRI? *EJC Suppl* 2007; 5: 236–236.

24   Goyen M: Gadofosveset: the first intravascular contrast agent EU-approved for use with magnetic resonance angiography. *Future Cardiol* 2007; 3: 19–26.

25   Lambregts DM, Beets GL, Maas M, Kessels AG, Bakers FC, Cappendijk VC, Engelen SM, Lahaye MJ, de Bruine AP, Lammering G, Leiner T, Verwoerd JL, Wildberger JE, BeetsTan RG: Accuracy of gadofosveset-enhanced MRI for nodal staging and restaging in rectal cancer. *Ann Surg* 2011; 253: 539–545.

26 Bumb A, Brechbiel MW, Choyke P: Macromolecular and dendrimer-based magnetic resonance contrast agents. *Acta Radiologica* 2010; 51: 751–767.

27 Koppenol WH, Bounds PL, Dang CV: Otto Warburg's contributions to current concepts of cancer metabolism. *Nat Rev Cancer* 2011; 11: 325–337.

28 Juweid ME, Cheson BD: Current concepts – positron-emission tomography and assessment of cancer therapy. *N Engl J Med* 2006; 354: 496–507.

29 Young H, Baum R, Cremerius U, Herholz K, Hoekstra O, Lammertsma AA, Pruim J, Price P: Measurement of clinical and subclinical tumour response using [F-18]-fluorodeoxyglucose and positron emission tomography: review and 1999 EORTC recommendations. *Eur J Cancer* 1999; 35: 1773–1782.

30 Kwee RM: Prediction of tumor response to neoadjuvant therapy in patients with esophageal cancer with use of (18)F FDG PET: a systematic review. *Radiology* 2010; 254: 707–717.

31 Janssen MHM, Ollers MC, van Stiphout R, Riedl RG, van den Bogaard J, Buijsen J, Lambin P, Lammering G: PET-based treatment response evaluation in rectal cancer: prediction and validation. *Int J Radiat Oncol Biol Phys* 2012; 82: 871–876.

32 Everaert H, Hoorens A, Vanhove C, Sermeus A, Ceulemans G, Engels B, Vermeersch M, Verellen D, Urbain D, Storme G, De Ridder M: Prediction of response to neoadjuvant radiotherapy in patients with locally advanced rectal cancer by means of sequential 18FDGPET. *Int J Radiat Oncol Biol Phys* 2011; 80: 91–96.

33 Yeung JMC, Kalff V, Hicks RJ, Drummond E, Link E, Taouk Y, Michael M, Ngan S, Lynch AC, Heriot AG: Metabolic response of rectal cancer assessed by 18-FDG PET following chemoradiotherapy is prognostic for patient outcome. *Dis Colon Rectum* 2011; 54: 518–525.

34 Denecke T, Rau B, Hoffmann KT, Hildebrandt B, Ruf J, Gutberlet M, Hunerbein M, Felix R, Wust P, Amthauer H: Comparison of CT, MRI and FDG-PET in response prediction of patients with locally advanced rectal cancer after multimodal preoperative therapy: is there a benefit in using functional imaging? *Eur Radiol* 2005; 15: 1658–1666.

35 Overgaard J: Hypoxic radiosensitization: adored and ignored. *J Clin Oncol* 2007; 25: 4066–4074.

36 Wilson WR, Hay MP: Targeting hypoxia in cancer therapy. *Nat Rev Cancer* 2011; 11: 393–410.

37 Mees G, Dierckx R, Vangestel C, Van de Wiele C: Molecular imaging of hypoxia with radiolabelled agents. *Eur J Nucl Med Mol Imaging* 2009; 36: 1674–1686.

38 Bussink J, Kaanders JHAM, van der Graaf WTA, Oyen WJG: PET-CT for radiotherapy treatment planning and response monitoring in solid tumors. *Nat Rev Clin Oncol* 2011; 8: 233–242.

39 Evans CE, Mattock K, Humphries J, Saha P, Ahmad A, Waltham M, Patel A, Modarai B, Porter L, Premaratne S, Smith A: Techniques of assessing hypoxia at the bench and bedside. *Angiogenesis* 2011; 14: 119–124.

40 Gambino D: Potential therapeutic applications of metal compounds directed towards hypoxic tissues. **Curr Med Chem** 2010; 17: 3616–3631.

41 Thorwarth D, Eschmann SM, Holzner F, Paulsen F, Alber M: Combined uptake of [(18)F]FDG and [(18)F]FMISO correlates with radiation therapy outcome in headand-neck cancer patients. *Radiother Oncol* 2006; 80: 151–156.

42 Koh WJ, Bergman KS, Rasey JS, Peterson LM, Evans ML, Graham MM, Grierson JR, Lindsley KL, Lewellen TK, Krohn KA, Griffin TW: Evaluation of oxygenation status during fractionated radiotherapy in human nonsmall cell lung cancers using [F-18] fluoromisonidazole positron emission tomography. *Int J Radiat Oncol Biol Phys* 1995; 33: 391–398.

43 Dietz DW, Dehdashti F, Grigsby PW, Malyapa RS, Myerson RJ, Picus J, Ritter J, Lewis JS, Welch MJ, Siegel BA: Tumor hypoxia detected by positron emission tomography with Cu-60-ATSM as a predictor of response and survival in patients undergoing neoadjuvant chemoradiotherapy for rectal carcinoma: a pilot study. *Dis Colon Rectum* 2008; 51: 1641–1648.

44 Yue J, Yang Y, Cabrera AR, Sun X, Zhao S, Xie P, Zheng J, Ma L, Fu Z, Yu J: Measuring tumor hypoxia with 18 F-FETNIM PET in esophageal squamous cell carcinoma: a pilot clinical study. *Dis Esophagus* 2012; 25: 54–61.

45 Alexander S, Varaha ST, John G, Vesselle H: FLT: measuring tumor cell proliferation *in vivo* with positron emission tomography and 3-deoxy-3-F-18 fluorothymidine. *Semin Nucl Med* 2007; 37: 429–439.

46 Zhang CC, Yan Z, Li W, Kuszpit K, Painter CL, Zhang Q, Lappin P, Nichols T, Lira ME, Affolter T, Fahey N, Cullinane C, Spilker ME, Zasadny K, O'Brien PJ, Buckman D, Wong A, Christensen JG: [18F]FLT-PET imaging does not always 'light up' proliferating tumor cells. *Clin Cancer Res* 2012; 18: 1303–1312.

47 Contractor KB, Kenny LM, Stebbing J, Rosso L, Ahmad R, Jacob J, Challapalli A, Turkheimer F, Al-Nahhas A, Sharma R, Coombes RC, Aboagye EO: [(18)F]-3-Deoxy-3-fluorothymidine positron emission tomography and breast cancer response to docetaxel. *Clin Cancer Res* 2011; 17: 7664–7672.

48 Kenny L, Coombes RC, Vigushin DM, AlNahhas A, Shousha S, Aboagye EO: Imaging early changes in proliferation at 1 week post chemotherapy: a pilot study in breast cancer patients with 3-deoxy-3-[F-18]fluorothymidine positron emission tomography. *Eur J Nucl Med Mol Imaging* 2007; 34: 1339–1347.

49 de Langen AJ, Klabbers B, Lubberink M, Boellaard R, Spreeuwenberg MD, Slotman BJ, de Bree R, Smit EF, Hoekstra OS, Lammertsma A: Reproducibility of quantitative (18)F-3-deoxy-3-fluorothymidine measurements using positron emission tomography. *Eur J Nucl Med Mol Imaging* 2009; 36: 389–395.

50 Troost EGC, Vogel WV, Merkx MAW, Slootweg PJ, Marres HAM, Peeters WJM, Bussink J, van der Kogel AJ, Oyen WJG, Kaanders JHAM: F-18-FLT PET does not discriminate between reactive and metastatic lymph nodes in primary head and neck cancer patients. *J Nucl Med* 2007; 48: 726–735.

51 Wieder HA, Geinitz H, Rosenberg R, Lordick F, Becker K, Stahl A, Rummeny E, Siewert JR, Schwaiger M, Stollfuss J: PET imaging with F-18 3-deoxy-3-fluorothymidine for prediction of response to neoadjuvant treatment in patients with rectal cancer. *Eur J Nucl Med Mol Imaging* 2007; 34: 878–883.

52 Muijs CT, Beukema JC, Widder J, van den Bergh ACM, Havenga K, Pruim J, Langendijk JA: (18)F-FLT-PET for detection of rectal cancer. *Radiother Oncol* 2011; 98: 357–359.

53 Yamamoto Y, Kameyama R, Izuishi K, Takebayashi R, Hagiike M, Asakura M, Haba R, Nishiyama Y: Detection of colorectal cancer using (18)F-FLT PET: comparison with (18)F-FDG PET. *Nucl Med Commun* 2009; 30: 841–845.

54 Kartachova M, van Zandwijk N, Burgers S, van Tinteren H, Verheij M, Olmos RAV: Prognostic significance of Tc-99m Hynicrh-annexin V scintigraphy during platinumbased chemotherapy in advanced lung cancer. *J Clin Oncol* 2007; 25: 2534–2539.

55 Rottey S, Slegers G, Van Belle S, Goethals I, Van de Wiele C: Sequential Tc-99m-hydrazinonicotinamide-annexin V imaging for predicting response to chemotherapy. *J Nucl Med* 2006; 47: 1813–1818.

56 Bauwens M, De Saint-Hubert M, Devos E, Deckers N, Reutelingsperger C, Mortelmans L, Himmelreich U, Mottaghy FM, Verbruggen A: Site-specific (68)Ga-labeled Annexin A5 as a PET imaging agent for apoptosis. *Nucl Med Biol* 2011; 38: 381–392.

57 Murakami Y, Takamatsu H, Taki J, Tatsumi M, Noda A, Ichise R, Tait JF, Nishimura S: F-18-labelled annexin V: a PET tracer forapoptosis imaging. *Eur J Nucl Med Mol Imaging* 2004; 31: 469–474.

58 Li XH, Link JM, Stekhova S, Yagle KJ, Smito C, Krohn KA, Tait JF: Site-specific labeling of annexin V with F-18 for apoptosis imaging. *Bioconjug Chem* 2008; 19: 1684–1688.

59 Hoglund J, Shirvan A, Antoni G, Gustavsson SA, Langstrom B, Ringheim A, Sorensen J, Ben-Ami M, Ziv I: (18)F-ML-10, a PET tracer for apoptosis: first human study. *J Nucl Med* 2011; 52: 720–725.

60 Danishad KK, Sharma U, Sah RG, Seenu V, Parshad R, Jagannathan NR: Assessment of therapeutic response of locally advanced breast cancer (LABC) patients undergoing neoadjuvant chemotherapy (NACT) monitored using sequential magnetic resonance spectroscopic imaging (MRSI). *NMR Biomed* 2010; 23: 233–241.

61 Sharma U, Baek HM, Su MY, Jagannathan NR: *In vivo* (1)H MRS in the assessment of the therapeutic response of breast cancer patients. *NMR Biomed* 2011; 24: 700–711.

62 Kobus T, Hambrock T, Hulsbergen-van de Kaa CA, Wright AJ, Barentsz JO, Heerschap A, Scheenen TWJ: *In vivo* assessment of prostate cancer aggressiveness using magnetic resonance spectroscopic imaging at 3 T with an endorectal coil. *Eur Urol* 2011; 60: 1074–1080.

63 Kurhanewicz J, Vigneron DB, Brindle K, Chekmenev EY, Comment A, Cunningham CH, DeBerardinis RJ, Green GG, Leach MO, Rajan SS, Rizi RR, Ross BD, Warren WS, Malloy CR: Analysis of cancer metabolism by imaging hyperpolarized nuclei: prospects for translation to clinical research. *Neoplasia* 2011; 13: 81–97.

64 Rembacken BJ, Fujii T, Cairns A, Dixon MF, Yoshida S, Chalmers DM, Axon ATR: Flat and depressed

colonic neoplasms: a prospective study of 1000 colonoscopies in the UK. *Lancet* 2000; 355: 1211–1214.

65 Kiesslich R, Fritsch J, Holtmann M, Koehler HH, Stolte M, Kanzler S, Nafe B, Jung M, Galle PR, Neurath MF: Methylene blue-aided chromoendoscopy for the detection of intraepithelial neoplasia and colon cancer in ulcerative colitis. *Gastroenterology* 2003; 124: 880–888.

66 Olliver JR, Wild CP, Sahay P, Dexter S, Hardie LJ: Chromoendoscopy with methylene blue and associated DNA damage in Barrett's oesophagus. *Lancet* 2003; 362: 373–374.

67 Hopeross M, Yannuzzi LA, Gragoudas ES, Guyer DR, Slakter JS, Sorenson JA, Krupsky S, Orlock DA, Puliafito CA: Adverse reactions due to indocyanine green. *Ophthalmology* 1994; 101: 529–533.

68 Okamoto K, Muguruma N, Kimura T, Yano H, Imoto Y, Takagawa M, Kaji M, Aoki R, Sato Y, Okamura S, Kusaka Y, Ito S: A novel diagnostic method for evaluation of vascular lesions in the digestive tract using infrared fluorescence endoscopy. *Endoscopy* 2005; 37: 52–57.

69 Kimura T, Muguruma N, Ito S, Okamura S, Imoto Y, Miyamoto H, Kaji M, Kudo E: Infrared fluorescence endoscopy for the diagnosis of superficial gastric tumors. *Gastrointest Endosc* 2007; 66: 37–43.

70 Morton DL, Wen DR, Wong JH, Economou JS, Cagle LA, Storm FK, Foshag LJ, Cochran AJ: Technical details of intraoperative lymphatic mapping for early stage melanoma. *Arch Surg* 1992; 127: 392–399.

71 Ishikawa K, Yasuda K, Shiromizu A, Etoh T, Shiraishi N, Kitano S: Laparoscopic sentinel node navigation achieved by infrared ray electronic endoscopy system in patients with gastric cancer. *Surg Endosc* 2007; 21: 1131–1134.

72 Ito N, Fukuta M, Tokushima T, Nakai K, Ohgi S: Sentinel node navigation surgery using indocyanine green in patients with lung cancer. *Surg Today* 2004; 34: 581–585.

73 Kelly K, Alencar H, Funovics M, Mahmood U, Weissleder R: Detection of invasive colon cancer using a novel, targeted, library-derived fluorescent peptide. *Cancer Res* 2004; 64: 6247–6251.

74 Gee MS, Upadhyay R, Bergquist H, Weissleder R, Josephson L, Mahmood U: Multiparameter noninvasive assessment of treatment susceptibility, drug target inhibition and tumor response guides cancer treatment. *Int J Cancer* 2007; 121: 2492–2500.

75 Weissleder R, Kelly K, Sun EY, Shtatland T, Josephson L: Cell-specific targeting of nanoparticles by multivalent attachment of small molecules. *Nat Biotechnol* 2005; 23: 1418–1423.

76 Weissleder R, Tung CH, Mahmood U, Bogdanov A: *In vivo* imaging of tumors with protease-activated near-infrared fluorescent probes. *Nat Biotechnol* 1999; 17: 375–378.

77 Funovics MA, Alencar H, Montet X, Weissleder R, Mahmood U: Simultaneous fluorescence imaging of protease expression and vascularity during murine colonoscopy for colonic lesion characterization. *Gastrointest Endosc* 2006; 64: 589–597.

78 Townsend DW: Multimodality imaging of structure and function. *Phys Med Biol* 2008; 53:R1–R39.

79 Muehllehner G, Karp JS: Positron emission tomography. *Phys Med Biol* 2006; 51:R117–R137.

80 Beyer T, Townsend DW, Brun T, Kinahan PE, Charron M, Roddy R, Jerin J, Young J, Byars L, Nutt R: A combined PET/CT scanner for clinical oncology. *J Nucl Med* 2000; 41: 1369–1379.

81 Wehrl HF, Sauter AW, Judenhofer MS, Pichler BJ: Combined PET/MR imaging – technology and applications. *Technol Cancer Res Treat* 2010; 9: 5–20.

82 Cai WB, Chen K, Li ZB, Gambhir SS, Chen XY: Dual-function probe for PET and nearinfrared fluorescence imaging of tumor vasculature. *J Nucl Med* 2007; 48: 1862–1870.

83 Dzik-Jurasz A, Domenig C, George M, Wolber J, Padhani A, Brown G, Doran S: Diffusion MRI for prediction of response of rectal cancer to chemoradiation. *Lancet* 2002; 360: 307–308.

84 DeVries AF, Kremser C, Hein PA, Griebel J, Krezcy A, Ofner D, Pfeiffer KP, Lukas P, Judmaier W: Tumor microcirculation and diffusion predict therapy outcome for primary rectal carcinoma. *Int J Radiat Oncol Biol Phys* 2003; 56: 958–965.

85 Hein PA, Kremser C, Judmaier W, Griebel J, Pfeiffer KP, Kreczy A, Hug EB, Lukas P, DeVries AF: Diffusion-weighted magnetic resonance imaging for monitoring diffusion changes in rectal carcinoma during combined, preoperative chemoradiation: preliminary results of a prospective study. *Eur J Radiol* 2003; 45: 214–222.

86 Kim SH, Lee JY, Lee JM, Han JK, Choi BI: Apparent diffusion coefficient for evaluating tumour response

to neoadjuvant chemoradiation therapy for locally advanced rectal cancer. *Eur Radiol* 2011; 21: 987–995.

87 Curvo-Semedo L, Lambregts DMJ, Maas M, Thywissen T, Mehsen RT, Lammering G, Beets GL, Caseiro-Alves F, Beets-Tan RGH: Rectal cancer: assessment of complete response to preoperative combined radiation therapy with chemotherapy-conventional MR volumetry versus diffusion-weighted MR imaging. *Radiology* 2011; 260: 734–743.

88 Sun YS, Zhang XP, Tang L, Ji JF, Gu J, Cai Y, Zhang XY: Locally advanced rectal carcinoma treated with preoperative chemotherapy and radiation therapy: preliminary analysis of diffusion-weighted MR imaging for early detection of tumor histopathologic downstaging. *Radiology* 2010; 254: 170–178.

89 Tang L, Zhang XP, Sun YS, Shen L, Li JA, Qi LP, Cui Y: Gastrointestinal stromal tumors treated with imatinib mesylate: apparent diffusion coefficient in the evaluation of therapy response in patients. *Radiology* 2011; 258: 729–738.

90 Aoyagi T, Shuto K, Okazumi S, Shimada H, Kazama T, Matsubara H: Apparent diffusion coefficient values measured by diffusion weighted imaging predict chemoradiotherapeutic effect for advanced esophageal cancer. *Dig Surg* 2011; 28: 252–257.

91 Aoyagi T, Shuto K, Okazumi S, Shimada H, Nabeya Y, Kazama T, Matsubara H: Evaluation of the clinical staging of esophageal cancer by using diffusion-weighted imaging. *Exp Ther Med* 2010; 1: 847–851.

92 George ML, Dzik-Jurasz ASK, Padhani AR, Brown G, Tait DM, Eccles SA, Swift RI: Noninvasive methods of assessing angiogenesis and their value in predicting response to treatment in colorectal cancer. *Br J Surg* 2001; 88: 1628–1636.

93 De Lussanet QG, Backes WH, Griffioen AW, Padhani AR, Baeten CI, Van Baardwijk A, Lambin P, Beets GL, Van Engelshoven JMA, Beets-Tan RGH: Dynamic contrast-enhanced magnetic resonance imaging of radiation therapy-induced microcirculation changes in rectal cancer. *Int J Radiat Oncol Biol Phys* 2005; 63: 1309–1315.

94 Akisik MF, Sandrasegaran K, Bu GX, Lin C, Hutchins GD, Chiorean EG: Pancreatic cancer: utility of dynamic contrast-enhanced MR imaging in assessment of antiangiogenic therapy. *Radiology* 2010; 256: 441–449.

95 Chang EY, Li X, Jerosch-Herold M, Priest RA, Enestvedt CK, Xu J, Springer CS, Jobe BA: The evaluation of esophageal adenocarcinoma using dynamic contrast-enhanced magnetic resonance imaging. *J Gastrointest Surg* 2008; 12: 166–175.

96 Oberholzer K, Pohlmann A, Schreiber W, Mildenberger P, Kunz P, Schmidberger H, Junginger T, Duber C: Assessment of tumor microcirculation with dynamic contrastenhanced MRI in patients with esophageal cancer: initial experience. *J Magn Reson Imaging* 2008; 27: 1296–1301.

97 Herrmann K, Erkan M, Dobritz M, Schuster T, Siveke JT, Beer AJ, Wester HJ, Schmid RM, Friess H, Schwaiger M, Kleeff J, Buck AK: Comparison of 3′-deoxy-3′-[(18)F]fluorothymidine positron emission tomography (FLT PET) and FDG PET/CT for the detection and characterization of pancreatic tumours. *Eur J Nucl Med Mol Imaging* 2012, E-pub ahead of print.

Chapter 4.2: Molecular imaging of tumour associated angiogenesis using a novel MRI contrast agent targeting AlphaVBeta3 integrin

Running title: molecular MRI in a colorectal xenograft model

Isabelle Debergh, MD (1), Nancy Van Damme, PhD (1), Dieter De Naeyer, PhD (2), Peter Smeets, MD (3), Pieter Demetter, MD, PhD (4), Philippe Robert (5), Sabin Carme (5), Piet Pattyn, MD, PhD (1), Wim Ceelen, MD, PhD (1)

(1) Department of Surgery, University Hospital, Ghent, Belgium; (2) Department of Biomedical Engineering, IBITECH, Ghent University, Belgium; (3) Department of Medical Imaging, Ghent University Hospital, Belgium; (4) Department of Pathology, ULB Erasme, Brussels, Belgium; (5) Guerbet Research, Paris, France

Synopsis
Molecular MRI enhances tumour associated angiogenesis in a colorectal xenograft model, using a monogadolinated tracer targeting $\alpha_v\beta_3$ integrin.

4.2.1 Abstract
Background: The recent introduction of biological anticancer therapy has renewed the interest in functional imaging of tumour associated angiogenesis (TAA) as a tool to monitor early therapy response. The present study evaluated imaging of TAA using P1227, a novel small molecular MRI probe targeting $\alpha_v\beta_3$ integrin.
Methods: HT29 human colorectal cancers were grown in athymic mice. Dynamic MR imaging was performed using a 3D VIBE sequence up to 110 minutes after injection of P1227 or gadolinium-tetraazacyclododecane tetraacetic acid (Gd-DOTA). Specificity was assessed by using P1227 one hour after IV administration of the $\alpha_v\beta_3$ inhibitor cilengitide. Regions of interest were drawn encompassing the tumour rim and normal muscle. Imaging data were compared with microvessel density (MVD) and $\alpha_v\beta_3$ expression.
Results: Using P1227, specific enhancement of the angiogenic tumour rim, but not of normal muscle was observed whereas Gd-DOTA enhanced tumour and normal muscle. After administering cilengitide, enhancement with P1227, but not with DOTA was significantly suppressed during the first 20 minutes. When using P1227, a significant correlation was observed between normalized enhancement of the tumour rim and immunohistochemical $\alpha_v\beta_3$ integrin expression.
Conclusions: molecular MR imaging using a small monogadolinated tracer targeting $\alpha_v\beta_3$ integrin and moderate magnetic field strength holds promise in assessing colorectal TAA.

4.2.2 Introduction
Early assessment of response to cytotoxic therapy is an area of intense investigation. Indeed, the ability to demonstrate activity early in the course of therapy not only allows to predict an individual patient's prognosis but also to tailor the therapeutic strategy by timely discontinuation of inactive regimens. Moreover, early imaging of tumour response is a valuable tool in preclinical and early phase clinical drug development.

Changes in the physical dimension of a solid tumour, which underly the traditional RECIST criteria, often occur late in the course of therapy[1]. Also, as exemplified by molecular therapy of gastrointestinal stromal tumours, significant tumour response can occur without any accompanying change in tumour dimension[2]. Early iconographic assessment of tumour response is not (only) based upon morphological, but on functional properties of the neoplastic tissue. Research for other valuable early imaging biomarkers is currently ongoing. Since the introduction of agents targeting tumour angiogenesis, increasing efforts have been invested in functional imaging of the neoplastic vascular bed. Importantly, it has been shown that the earliest functional change in response to anti-angiogenic therapy is 'microvessel normalization', id est, the return from a grossly distorted anatomy and function to more physiological microvascular properties[3]. One of the hallmarks of this process is a decrease in microvascular permeability. We recently showed that dynamic contrast enhanced (DCE) magnetic resonance imaging incorporating mathematical modelling allows to quantify these early changes in microvessel permeability as well as tumour perfusion[4].

Although of interest, these parameters remain indirect estimators of tumour angiogenesis. Direct, specific imaging requires probes directed against moieties expressed on the proliferating endothelial cell (EC) surface. A potential targets is $\alpha_v\beta_3$ integrin, which is selectively expressed on activated EC during migration through the basement membrane in the angiogenic process[6-7]. This protein is not upregulated on quiescent EC[8]. Here, we studied a novel $\alpha_v\beta_3$ integrin directed molecular MRI tracer (P1227) as a tool to visualise tumour angiogenesis in a colorectal xenograft model.

4.2.3 Methods

Animals and tumour model
Colorectal cancer xenografts (HT29) were subcutaneously grown in the hind leg of nude mice (athymic nu/nu, Harlan, The Netherlands). Animals were housed separately in plastic cages with free access to tap water and standard pellet food. When tumours reached a size of 0.2-0.3 cm³ (after 8-10 days), MRI imaging was performed. The protocol was approved by the local Animal Research institutional review board.

MR imaging protocol
Dynamic MR image acquisition was performed on a MAGNETOM Symphony 1.5 T clinical scanner (Siemens Healthcare, Brussels, Belgium) using a wrist coil (diameter 10 cm). Imaging was performed using a T1 weighted 3D VIBE sequence (FOV 180x80, matrix size 384x384, voxel dimension 0.5x0.5x2 mm, TR/TE 6.78/2.78 ms, flip angle 12°, 60 slices, total duration per scan 9 min 25 sec). Images were acquired at baseline (before contrast injection) and at regular intervals up to 225 minutes post injection. At each time point 60 images were acquired.

Signal intensity was measured in blinded, manually drawn regions of interest (ROIs) encompassing the tumour rim (outer third of the tumour volume) and normal tissue (contralateral paravertebral muscle). Normalized Enhancement Ratio (NER) was calculated as the ratio of enhancement in the tumour rim over enhancement in normal muscle tissue.

The contrast agent (P1227, Guerbet Research, Paris, France) is a tetraazacyclododecane tetraacetic acid (DOTA) – gadolinium (Gd) chelate linked to a cyclic RGD peptide (MW= 1297 Da). The purified protein used to determine binding IC50 of P1227 is vitronectin. The molecular weight of Gd-DOTA is 560 Da. The r1 relaxivities of P1227 and Gd-DOTA in plasma at 37°C and 1.5 T are 8.3 mM^{-1}s^{-1} and 3.8 mM^{-1}s^{-1} respectively. The binding IC50 of P1227 as tested with ELISA on purified protein is 3 nM.

Four experimental groups were studied. In the first group, imaging was performed before and after injection of P1227 (dose 50 µmol Gd/kg) (N=15), while in the second (control) group mice underwent imaging before and after injection of Gd-DOTA (Dotarem®, Guerbet, Paris, France; dose 100 µmol Gd/kg) (N=9). The choice of doubling the Gd-DOTA dose was based on the much higher relaxivity of P1227. In the third and fourth group imaging with P1227 (N=9) or Gd-DOTA (N=6), respectively, was performed one hour after IV administration of the $\alpha_v\beta_3$ inhibitor cilengitide (dose 1800 mg/m², Merck KGaA, Darmstadt, Germany). All products were injected as a rapid IV bolus through the tail vein.

On the day after MR imaging, tumours were excised and all mice were sacrificed using cervical dislocation. Half of the tumour tissue was fixed in 10% formalin, embedded in paraffin, and 4 µm thick sections were cut and mounted for immunohistochemistry. Factor VIII (von Willebrand factor, FVIII) immunostaining was used to visualise tumour microvessels and calculate microvessel density (MVD). FVIII staining procedure was adapted from Debergh et al.[9]. The other half of the tumour was snap frozen in liquid nitrogen, cut in 5 µm thick sections and mounted for immunohistochemistry with mouse anti-human integrin $\alpha_v\beta_3$ (US Biological – Immunosource), similar to the procedure of Schnell et al.

Quantification of $\alpha_v\beta_3$ integrin protein expression using Western Blot, was described by Schnell et al.[10]. Briefly, snap frozen tumour tissues were lysed in radioimmunoprecipitation assay buffer by sonication. Total protein content was determined with the Bio-Rad DC protein assay kit (Bio-Rad, Nazareth, Belgium). Fifty micrograms of protein per lane was mixed with LDS sample buffer (NuPAGE, Invitrogen, Merelbeke, Belgium). The proteins were denatured by heating at 70°C for 10 minutes, seperated with 170 V over 1 hour in running buffer (NuPAGE® MES, Invitrogen). After that, proteins were transferred to a nitrocellulose membrane (GE Healthcare, Buckinghamshire, United Kingdom) by a semidry blotting technique. Next, membranes were blocked over 1 hour at room temperature. The primary antibodies against integrin subunits (polyclonal rabbit anti-integrin αv subunit AB1930; dilution 1:5000 and polyclonal rabbit anti-integrin β_3 subunit AB1932; dilution 1:2000; Chemicon, Millipore, MA, USA) were incubated overnight at 4°C. Bound antibodies were labeled using a secondary antibody coupled to alkaline phosphatase (1:2000 goat anti-rabbit immunoglobulin/AP) for 1 hour. Visualisation was performed using chromogen nitroblue tetrazolium salt and 5-bromo-4-chloro-3-indolyl phosphate (BCIP/NBT substrate kit, Invitrogen). Blots were subsequently stripped and reprobed with monoclonal antibody against β-tubulin (Abcam, United Kingdom; dilution

1:5000) as an internal control for protein loading. All blots were digitized by scanning, mean intensity of each different chain was measured with NIH ImageJ software and the the overall relative intensity of the different chains of interest was calculated (mean intensity of chain of interest/mean intensity of tubulin).

STATISTICAL ANALYSIS

Data are expressed as mean ± SEM or median (interquartile range). Differences were analyzed using the student t or Mann-Whitney rank sum test where appropriate. Correlations between histology data and imaging parameters were assessed with Spearman rank correlation. Statistical analysis was performed with SigmaStat 11.0 (Systat Software, Richmond, USA). Results were considered statistically significant when the probability of a type I error was ≤ 5%.

4.2.4 Results

Signal enhancement in tumour and normal muscle after injection of P1227 versus Gd-DOTA

Typical enhancement patterns are illustrated in figure 4.3. It may be appreciated that, as illustrated by the signal intensity histograms, P1227 specifically enhanced the angiogenic tumour rim while Gd-DOTA was more homogeneously distributed towards the center of the tumour.
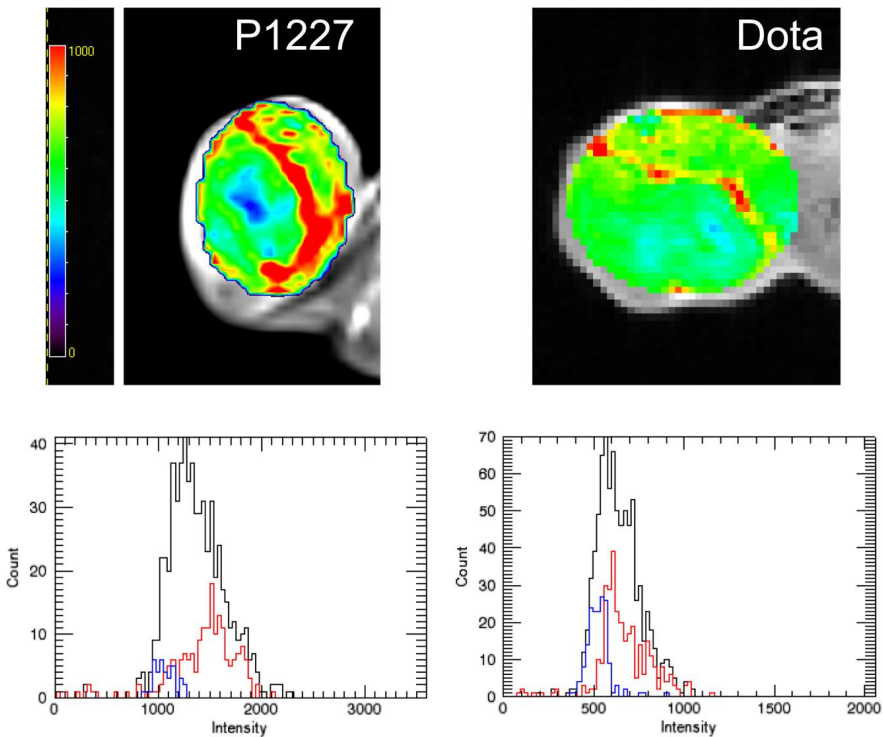
FIGURE 4.3 Enhancement pattern observed following administration of P1227 (upper left) or Gd-DOTA (upper right). The histograms (lower row) show frequency of signal intensities in the entire tumour (black), central (core) region (blue), and tumour rim (red).
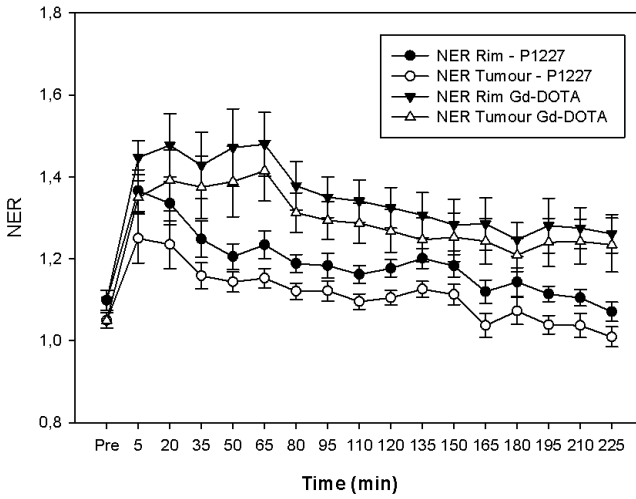
FIGURE 4.4 Normalized enhanced ratio (NER) over time in regions of interest encompassing the tumour rim and entire tumour following administration of P1227 (circles) or Gd-DOTA (triangles). NER, Normalized Enhanced Ratio, bars = s.e..

FIGURE 4.5 Normalized enhancement ratio (NER) of the tumour rim over time following administration of DOTA or P1227 with or without pretreatment with cilengitide (open circles). NER, Normalized Enhanced Ratio, bars = s.e.

Quantitative evaluation of the signal intensity changes observed in the tumour rim, entire tumour, and normal muscle is provided in figure 4.4, where NER are depicted. NER in the entire tumour appears to be lower than NER in the tumour rim at each 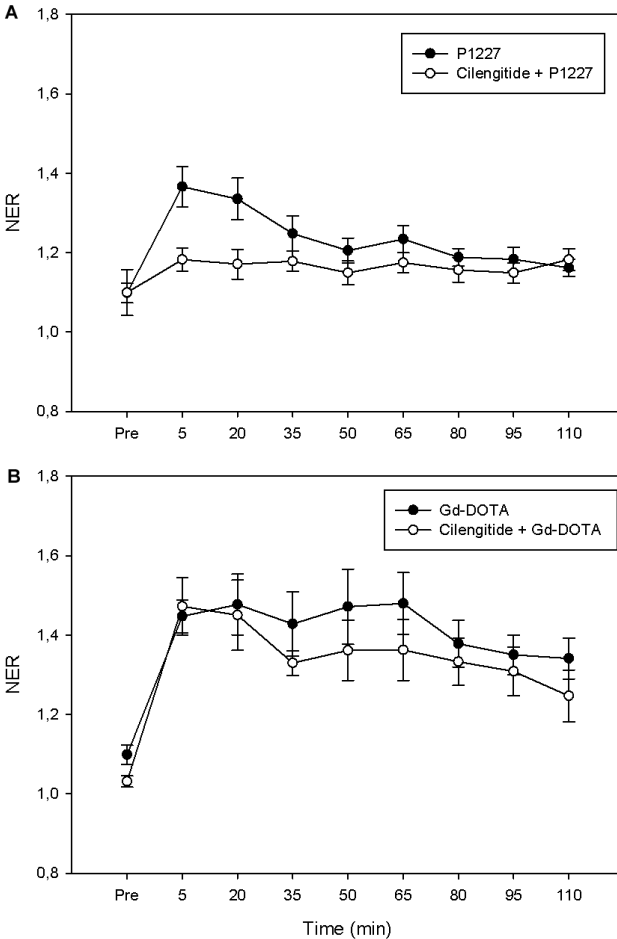time point. When using P1227, significant enhancement of signal intensity was observed of the tumour rim (569 ± 15 versus 472 ± 21, P=0.004, t test) but not of normal muscle. However, when using Gd-DOTA, significant enhancement of SI was noted in both tumour tissue and normal tissue (614 ± 24 versus 430 ± 17 in muscle tissue, P<0.001, t test). For both contrast agents, a peak in normalized enhancement was observed after 5 minutes. When using P1227 normalized enhancement after 225 minutes did return to baseline. When using Gd-DOTA, however, normalized enhancement at 225 minutes remained significantly elevated compared to baseline (precontrast) level (1,261 ± 0,0818 versus 1,098 ± 0,122; P=0.035, t-test).

Signal enhancement in the tumour rim with and without pretreatment with cilengitide
To verify whether P1227 binds the target integrin in a specific way, the inhibitor cilengitide was administered one hour before imaging with P1227 (n=9). The results, expressed as the ratio of enhancement in the tumour rim over enhancement in normal tissue, are illustrated in figure 4.5. Administration of cilengitide before P1227 resulted in a significantly lower normalized contrast enhancement of the tumour rim during the first 20 minutes (P=0.027, U test). Between 35 and 60 minutes NER was still higher in the P1227 group, but without showing statistically significant differences compared to the cilengitide pretreated group. After 80-90 minutes, however, no differences in SI were observed between both groups. When DOTA was used, however, pretreatment with cilengitide did not affect tumour rim enhancement.

Immunohistochemistry and Western blot
Microvessel density (vWF staining) in all tumours, expressed as the vascular area fraction, was significantly higher in the tumour rim compared to the entire tumour (11.25% (8.7-16.7) versus 8.4% (4.6-12.2), P<0.001, U test). Also, the percentage of $\alpha_v\beta_3$ integrin expressing endothelium was 12.8% (10.9-16.9) in the tumour rim versus 11.2% (7.9-14.6) in the entire tumour (P=0.002, U test; figure 4.6, panel B and C). The results of Western blotting confirmed that protein expression of the alpha v and beta 3 subunit was significantly higher in the vascular tumour rim (figure 4.6, panel A and D). Three different molecular masses can be found in alpha v subunits (at 137 kDa and to a much lesser extent at 27 and 25 kDa) and in beta 3 subunits (between 90-100 kDa and degradation products at 64 and 52 kDa)[10].

Correlation of MR imaging parameters with histology data
Correlation data are summarised in Table 4.4. When using Gd-DOTA, no correlation was observed between the NER in the tumour rim and either $\alpha_v\beta_3$ integrin expression or MVD. However, when using P1227, a statistically significant positive correlation was observed between $\alpha_v\beta_3$ integrin expression and the NER at 35, 50, and 65 minutes post contrast injection.
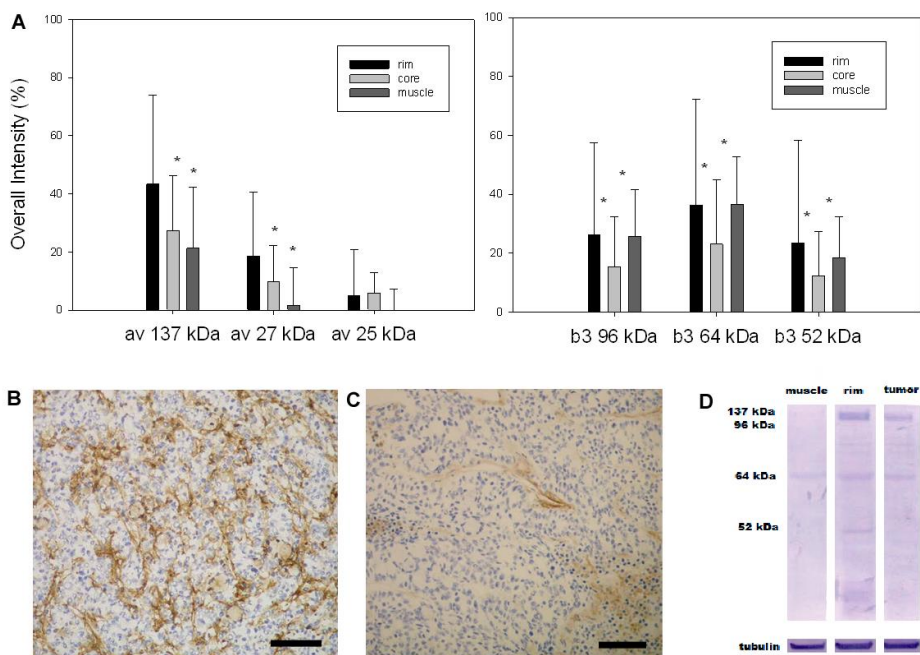
FIGURE 4.6 Protein expression measured by Western Blot of alphav chains and beta3 chains (A and D); bars = s.d., * P ≤ 0.05. Representative $\alpha_v\beta_3$ integrin immunohistology of the tumour rim (B) and tumour center (C). Scale bar = 100 µm.

TABLE 4.4 Correlation between histology and imaging parameters (normalized enhancement ratio of the tumour rim).

		5 min	20 min	35 min	50 min	65 min	80 min
$\alpha_v\beta_3$ integrin	DOTA	0.7	0.92	0.88	0.36	0.72	0.06
	P1227	0.43	0.39	0.019	0.0092	0.046	0.35
MVD	DOTA	0.52	0.63	0.99	0.9	0.59	0.86
	P1227	0.44	0.69	0.57	0.49	0.67	0.47

m, minutes ; numbers indicate P values from Pearson correlation analysis.

4.2.5 Discussion

We have studied the feasibility to probe tumour angiogenesis using a novel MR contrast agent targeting $\alpha_v\beta_3$ integrin.

The integrins are a group of evolutionary conserved heterodimeric cell surface receptors which are essential in cell-cell and cell-matrix interactions[11].

Some subtypes are highly overexpressed on cancer cells, e.g. $\alpha_v\beta_3$, $\alpha_v\beta_5$, $\alpha_5\beta_1$ (which play important role in mediating tumour angiogenesis), or $\alpha_v\beta_6$ and $\alpha_6\beta_4$ (with pivotal functions in cell migration and hence, metastasis)[12,13]. These interesting capacities of certain integrins, and the high level of expression on some tumour types, makes them ideal candidates for targeted therapy and imaging studies.

More specifically, integrin$\alpha_v\beta_3$ is not only overexpressed on some tumour cell types (lung cancer, ovarian cancer, breast cancer, glioblastoma multiforme,…), but also on

most tumour endothelial cells and not on normal blood vessels[13]. Targeting tumour angiogenesis and reducing side-effects on normal tissue is of major interest in the evoluting research of cancer treatment. In this way, site-specific delivery of drugs and imaging can show early effectiveness of therapy, and diminish chemo-resistance. The recognition sequence of the $\alpha_v\beta_3$ integrin is the RGD (Arg-Gly-Asp) peptide on the β3 domain, and its most abundant ligands are components of the extracellular matrix, f.i. fibronectin, vitronectin, and fibrinogen14. Its expression on endothelial cells is stimulated by angiogenic growth factors such as bFGF, TNFα and IL8 and is upregulated not only in neoplastic tissue but also during wound healing and inflammation8. The HT29 colorectal cancer cell line used in the present experiment was shown to express integrins $\alpha_v\beta_5$, $\alpha_v\beta_6$, and $\alpha_v\beta_8$[15,16]. The expression of human integrin $\alpha_v\beta_3$ is negligible on HT29 tumour cells, but tumours express murine integrin $\alpha_v\beta_3$, which is present on newborn tumour vasculature in this mouse model. Recently, several studies proved with the HT29 model the relation between RGD-based radiotracer uptake in tumours and the expression levels of both human integrin $\alpha_v\beta_3$ and murine integrin $\alpha_v\beta_3$[17,18]. In our study, the HT29 model allows us to focus directly on tumour associated angiogenesis via this novel $\alpha_v\beta_3$ integrin specific molecular tracer (P1227).

The utility of MRI based molecular imaging is hampered by its low sensitivity to visualize epitopes which are often present in the nanomolar range. Therefore, efforts have been directed towards the combination of the target-specific molecule with a large (super) paramagnetic payload. Several authors have used RGD-coupled liposomes containing Gd-DTPA to visualise tumour angiogenesis[19,20]. Others have used RGD-labeled ultra-small superparamagnetic iron oxide nanoparticles (USPIO) and T2 weighted imaging[21-23]. Several disadvantages are associated with the use of these large carriers. First, since they are exclusively limited to the vascular compartment, binding sites on the tumour cells and extracellular matrix will be out of reach[24]. Second, endocytosis of the Gd-labeled liposomes may lead to 'quenching' of the MRI signal. Third, concerns have risen regarding the safety and biological side effects of USPIOs in early clinical trials, although these were usually mild and reversible25. Finally, the pharmacokinetic properties of nano-sized tracers, including a plasma half live of several hours and retention by the reticulo-endothelial system better suit therapeutic than diagnostic purposes.

Here, we report for the first time the use of a low molecular weight tracer (1297 Da, diameter of 1-2 nm) consisting of a routinely used monogadolinated CA linked to a RGD peptide as a tool to image tumour associated angiogenesis. The results demonstrate that, compared to non-targeted DOTA (MW = 558 Da), P1227 better discriminates angiogenic tumour tissue from normal muscle. Gd-DOTA pools immediately in the blood, as both SI in tumour rim and muscle are high, whereas P1227 does not change SI in muscle. Furthermore, aspecific accumulation of Gd-DOTA in the well vascularised oedemateous tumour tissue leads to persistent high NERs, even after 225 minutes. At this point, SI in normal muscle tissue did return to baseline, indicating that the high SI of tumour rim is due to extravasated Gd-DOTA tracer. This may be explained by the higher molecular weight of P1227, which limits diffusion across normal and leaking tumoural microvessel linings. Retention of the tracer due to specific binding to the target integrin was demonstrated by the near complete disappearance of P1227-induced tumour enhancement after pretreatment with cilengitide. Cilengitide is a known inhibitor of

the integrins $\alpha_v\beta_3$, $\alpha_v\beta_5$, and $\alpha_5\beta_1$, but blocking the other integrins is not interfering with the imaging result of HT29 tumours as P1227 was designed to have only specificity for the RGD-sequence on the $\beta3$ domain of the $\alpha_v\beta_3$ integrin. Compared to nanoparticle imaging, the peak in signal enhancement after injecting P1227 occurs much earlier (after 5 minutes). Sipkins and coworkers[26], who used an $\alpha_v\beta_3$ targeting antibody conjugated paramagnetic liposome to image tumour angiogenesis in a rabbit model, noted specific enhancement of angiogenic areas after a time window of 24 hours. Similarly, Winter and coworkers[19], who used an integrin directed nanoparticle with a size of approximately 70 nm, observed steadily increasing signal intensity in the experimental tumour model until the completion of the imaging after 120 minutes. The relatively low accumulation of the tracer in the present model may be explained by the smaller size of the agent and by low internalisation by HT29 cells, as demonstrated *in vitro* by Bloch *et al.*[27]. This HT29 tumour cell line, is known to express little amounts of integrin $\alpha_v\beta_3$[15]. Radiolabeled cyclic RGD peptides specifically accumulate in $\alpha_v\beta_3$ expressing tumours by higher probe internalization, and increases when cyclic peptides are polymerized[28-29].

The specificity of the novel tracer for $\alpha_v\beta_3$ integrin was further demonstrated by the correlation between immunohistochemical staining and the observed MRI enhancement. No statistically significant correlation was noted with MVD, yet the the factor VIII staining method used does not allow to distinguish proliferating, active endothelial cells from resting microvessel linings.

Several limitations apply to the interpretation of the present results. First, although immunohistochemistry of integrin chain expression can be regarded as a valid surrogate marker of active angiogenesis, no golden standard is available at present. Correlation of MR imaging with *in vivo* microscopic imaging of fluorescently labelled tracers may hold promise in this regard[30].

Second, although expression of $\alpha_v\beta_3$ integrin is generally low in healthy tissue, it is known to be expressed by several other cell types (epithelial cells, fibroblasts, smooth muscle cells) and to be implicated in other conditions including arterial stenosis[31]. An additional tumour model with different integrin expression level to demonstrate the ability of the probe, would be interesting to discriminate tissues with different expression levels. Finally, it may be envisaged that compared to nanoparticles with a high Gd payload, the sensitivity of the current tracer for detecting small lesions will be limited.

In conclusion, we have shown that molecular MR imaging using a small monogadolinated tracer targeting $\alpha_v\beta_3$ integrin holds promise in safely and non-invasively assessing colorectal tumour angiogenesis. Future work will include assessment of antiangiogenic therapy effects using this novel tracer.

4.2.6 References

1. Desar IME, van Herpen CML, van Laarhoven HWM, Barentsz JO, Oyen WJG, van der Graaf WTA. Beyond RECIST: Molecular and functional imaging techniques for evaluation of response to targeted therapy. *Cancer Treat Rev.* 2009; 35: 309-321.
2. Kochhar R, Manoharan P, Leahy M, Taylor MB. Imaging in gastrointestinal stromal tumours: current status and future directions. *Clin Radiol.* 2010; 65: 584-592.
3. Jain RK. Normalization of tumor vasculature: An emerging concept in antiangiogenic therapy. *Science*. 2005; 307: 58-62.

4. Ceelen W, Smeets P, Van Damme N, *et al.* Noninvasive monitoring of radiotherapy-induced microvascular changes using dynamic contrast enhanced magnetic resonance imaging (DCE-MRI) in a colorectal tumor model *Int J Radiat Oncol Biol.* 2006; *Phys* 64: 1188-1196.

5. Ceelen W, Boterberg T, Smeets P, *et al.* Recombinant human erythropoietin alpha modulates the effects of radiotherapy on colorectal cancer microvessels. *Brit J Cancer.* 2007; 96: 692-700.

6. Meyer A, Auemheimer J, Modlinger A, Kessler H. Targeting RGD recognizing integrins: Drug development, biomaterial research, tumor imaging and targeting. *Current Pharm Design*. 2006; 12: 2723-2747.

7. Beer AJ, Schwaiger M. Imaging of integrin alpha v beta 3 expression. *Cancer Metastasis Rev*. 2008; 27: 631-644.

8. Brooks PC, Clark RAF, Cheresh DA. Requirement of Vascular Integrin Alpha(V)Beta(3) for Angiogenesis. *Science*. 1994; 264: 569-571.

9. Debergh I, Van Damme N, Pattyn P, Peeters M, Ceelen WP. The low-molecular-weight heparin, nadroparin, inhibits tumour angiogenesis in a rodent dorsal skinfold chamber model. *Br J Cancer.* 2010 Mar 2;102(5):837-43.

10. Schnell O, Krebs B, Wagner E, *et al.* Expression of integrin alphavbeta3 in gliomas correlates with tumor grade and is not restricted to tumor vasculature. *Brain Pathol.* 2008; 18(3):378-86.

11. Kiessling F, Morgenstern B, Zhang C. Contrast agents and applications to assess tumor angiogenesis *in vivo* by magnetic resonance imaging. *Curr Med Chem.* 2007; 14: 77-91.

12. Marelli UK, Rechenmacher F, Sobahi TRA, Mas-Moruno C, Kessler H. Tumor targeting via integrin ligands. *Front Oncol.* 2013; 3:222.

13. Hood J and Cheresh D. Role of integrins in cell invasion and migration. *Nature Reviews Cancer.* 2002; 2: 91-100.

14. Dunehoo A, Anderson M, Majumdar S, Kobayashi N, Berkland C, Siahaan TJ. Cell adhesion molecules for targeting drug delivery. *J Pharm Sci.* 2006; 95: 1856-1872.

15. Kemperman H, Wijnands YM, Roos E. alpha V integrins on HT-29 colon carcinoma cells: Adhesion to fibronectin is mediated solely by small amounts of alpha V beta 6, and alpha V beta 5 is codistributed with actin fibers. Exp Cell Res. 1997; 234: 156-164.

16. Haier J, Nasralla M, Nicolson GL. Different adhesion properties of highly and poorly metastatic HT-29 colon carcinoma cells with extracellular matrix components: role of integrin expression and cytoskeletal components. *Br J Cancer.* 1999; 80: 1867-1874.

17. Liu Z, Jia B, Shi J, *et al.* Tumor Uptake of the RGD Dimeric Probe (99m)Tc-G(3)-2P(4)-RGD2 is Correlated with Integrin alpha(v)beta(3) Expressed on both Tumor Cells and Neovasculature. *Bioconjug Chem.* 2010; 21 (3): 548–555.

18. Zhou Y, Kim YS, Chakraborty S, Shi J, Gao H, Liu S. 99mTc-labeled cyclic RGD peptides for noninvasive monitoring of tumor integrin $\alpha_v\beta_3$ expression. *Mol Imaging.* 2011; 10:386-397.

19. Winter PM, Caruthers SD, Kassner A, *et al.* Molecular Imaging of angiogenesis in nascent vx-2 rabbit tumors using a novel alpha(v)beta(3)-targeted nanoparticle and 1.5 tesla magnetic resonance imaging. *Cancer Res.* 2003; 63: 5838-5843.

20. Mulder WJM, Strijkers GJ, Habets JW, *et al.* MR molecular imaging and fluorescence microscopy for identification of activated tumor endothelium using a bimodal lipidic nanoparticle. *FASEB J.* 2005; 19: 2008-2010.

21. Zhang CF, Jugold M, Woenne EC, *et al.* Specific targeting of tumor angiogenesis by RGD-conjugated ultrasmall superparamagnetic iron oxide particles using a clinical 1.5-T magnetic resonance scanner. *Cancer Res.* 2007; 67: 1555-1562.

22. Jiang T, Zhang CF, Zheng X, Xu XF, Xie X, Liu HC, Liu SY. Noninvasively characterizing the different alpha v beta 3 expression patterns in lung cancers with RgD-USPIO using a clinical 3.0T MR scanner. *Int J Nanomed.* 2009; 4: 241-249.

23. Kiessling F, Huppert J, Zhang CF, *et al.* RGD-labeled USPIO Inhibits Adhesion and Endocytotic Activity of alpha(v)beta(3)-Integrin-expressing Glioma Cells and Only Accumulates in the Vascular Tumor Compartment. *Radiology.* 2009; 253: 462-469.

24. Wong C, Stylianopoulos T, Cui J, *et al.* Multistage nanoparticle delivery system for deep penetration into tumor tissue. *Proc Natl Acad Sci USA*. 2011; 108: 2426-2431.

25. Sharma R, Saini S, Ros PR, *et al.* Safety profile of ultrasmall superparamagnetic iron oxide ferumoxtran-10: Phase II clinical trial data. *J Magn Res Im.* 1999; 9: 291-294.

26. Sipkins DA, Cheresh DA, Kazemi MR, Nevin LM, Bednarski MD, Li KC. Detection of tumor angiogenesis *in vivo* by alphaVbeta3-targeted magnetic resonance imaging. *Nat Med.* 1998; 4: 623-626.

27. Bloch S, Xu B, Ye Y, Liang K, Achilefu S. Internalization of RGD peptide conjugates of near-infrared fluorescent probes in different cell lines occurs via different integrin receptor subtypes. *Proc SPIE*. 2006; 6097, 60970H.

28. Janssen ML, Oyen WJ, Dijkgraaf I, *et al.* Tumor targeting with radiolabeled alpha(v)beta(3) integrin binding peptides in a nude mouse model. *Cancer Res.* 2002; 62(21):6146-51.

29. Dijkgraaf I, Kruijtzer JA, Liu S, Soede AC, *et al.* Improved targeting of the alpha(v)beta (3) integrin by multimerisation of RGD peptides. *Eur J Nucl Med Mol Imaging.* 2007; 34(2):267-73.

30. Strijkers GJ, Kluza E, Van Tilborg GAF, van der Schaft DWJ, Griffioen AW, Mulder WJM, Nicolay K. Paramagnetic and fluorescent liposomes for target-specific imaging and therapy of tumor angiogenesis. *Angiogenesis*. 2010; 13: 161-173.

31. Avraamides CJ, Garmy-Susini B, Varner JA. Integrins in angiogenesis and lymphangiogenesis. *Nature Reviews Cancer*. 2008; 8: 604-617.

CHAPTER 5

General discussion and Conclusion

CHAPTER 5: General discussion and Conclusion

5.1 General discussion

Cancer incidence and mortality will most likely increase dramatically in the next decades, due to the growth and aging of the global population. Cancer prevention, early cancer diagnosis and patient-tailored treatment are important challenges for the near future, to improve survival rates and quality of life, and to avoid unnecessary side-effects for patients and reduce costs for the society. Currently, most patients are treated in a multimodality way, including surgery, chemotherapy, radiation and immunotherapy. Despite many efforts the underlying mechanisms of cancer development, cancer behaviour, response or resistance to treatment, metastasis, are not fully elucidated. The aim of our work was to unravel some basic aspects of targeting angiogenesis in tumours, as treatment option or imaging modality, and in this way to contribute to clinical solutions for the enigma of cancer.

Hypercoagulability is typically seen in cancer patients, due to the pro-coagulant effects of cancer cells (releasing TF) or to effects of chemotherapy, indwelling catheters, surgery, and immobility. For this reason, administration of LMWH is still the gold standard in the VTE prophylaxis of cancer patients [1]. LMWHs have been tested in various randomized controlled trials and clearly show a superiority to other anticoagulant treatments, due to predictable pharmacokinetic properties with rapid onset of action, fast clearance and easy dosage [2].

Coagulation can fuel tumour progression by forming tumour cell emboli with platelets and leukocytes, and seeding into the microcirculation. An essential role in the coagulation cascade is performed by the activation of thrombin, which promotes tumour cell adhesion and release of VEGF and bFGF from mast cells [3]. Results from several clinical studies suggested that heparin therapy might improve survival in cancer patients [4-6], independently of the anticoagulant effect. Heparins of various molecular weight, including LMWH, UF, and chemically modified non-anticoagulant heparins, have been shown to inhibit tumour growth and metastasis formation in animal studies [7-8]. The mechanisms through which LMWHs exert anticancer effects remain incompletely understood, but we highlighted the early antiangiogenic effect on tumour microcirculatory events using *in vivo* microscopy in an immunocompetent animal model.

In **chapter 3.1**, we studied tumoural angiogenesis via *in vivo* fluorescence microscopy in a dorsal skinfold chamber model using contrast agent that is tagged with a fluorescent marker (FITC–labelled dextran). This procedure in a hamster model is described in detail by Endrich *et al.* [9] and Menger *et al.* [10], and proved to be an excellent tool to visualize early microvascular changes by calculating static (microvessel length per area, number of microvessels per high-power field, vascular area fraction, and microvessel diameter) and dynamic (centreline red blood cell velocity and volumetric blood flow) parameters in a non-invasive, longitudinal way. Together with immunohistochemical data, Factor VIII (von Willebrand factor) immunostaining to calculate microvessel density (MVD) and fractal dimension, and α-smooth muscle actin (αSMA) staining to identify pericytes and calculate the pericyte coverage index (PCI), tumour microenvironment can be assessed. Other studies performed use cell culture experiments or other *in vivo* angiogenesis assays, such as the mouse cremaster muscle or rat mesenteric window

model, which allow to observe the microcirculation only once after therapy [11,12].

An orthotopic tumour model was studied (amelanotic melanoma) and an adenocarcinoma (pancreatic tumour). Our results suggest that nadroparin exerts an antiangiogenic effect *in vivo*, as evidenced by a significantly lower vascular area fraction and MVD when compared with control animals. Moreover, nadroparin-treated tumours showed signs of microvessel normalization, including a smaller increase in diameter, a higher PCI, and less vessel tortuosity (smaller fractal dimension). Vessel normalization is a well-characterised early phenotypic effect of antiangiogenic therapy [13]. The difference in vessel diameter and tortuosity may explain the decrease in vascular area fraction over time in nadroparin-treated animals despite the fact that both vessel length and vessel number did not change appreciably over time in this group. We extrapolated the study of tumour microvascular normalization using IVM to human cancer cells in a nude mouse model.

In **chapter 3.2,** we examined the effect of commercially available and widely used LMWHs nadroparin and enoxaparin, on human colorectal tumour in a mouse model. The results show that both nadroparin and enoxaparin have early antiangiogenic properties, as seen in IVM experimental data with significantly lower vascular area fraction, microvessel density, length and number of microvessels when compared with control animals.

Underlying mechanisms of the antiangiogenic properties of LMWHs, may include inhibition of binding of angiogenic growth factors to their endothelial receptors [14]. In a Matrigel assay, endothelial cell proliferation and tube formation was inhibited maximally by LMWH with a chain length of >8 polysaccharides and a molecular weight of 6 kDa while no inhibition was observed with UFH, tetrasaccharide, pentasaccharide, or octasaccharide [15]. Also *in vitro*, heparin fragments of less than 18 saccharides reduce the activity of VEGF [16] and fragments of less than 10 saccharide residues inhibits the activity of bFGF [17]. *In vivo*, the same effect of small heparin fractions on bFGF activity has been described [18,19]. Similar findings were reported by Norrby [11], who showed that 2.5–5kDa heparin fragments maximally suppressed VEGF-induced angiogenesis in a rat mesenteric window assay.

So, the antiangiogenic potential of LMWHs seems to be depending on the molecular weight and number of saccharide units. In our experiment, we compared the *in vivo* effect of commercially available nadroparin (4.3 kDa) and enoxaparin (4.5 kDa) on tumour angiogenensis with similar molecular weights. Small differences in results can be explained by different polysaccharide mixtures, but evidently, both bFGF and VEGF can be targeted in the antiangiogenic process, which is a plausible explanation of the positive short term results on tumour-associated angiogenesis. It is known that in patients receiving bevacizumab, a monoclonal anti-VEGF antibody, therapy resistance or disease progression can be expected due to "escape pathways", with upregulation of PlGF, PDGF, and bFGF [20]. Targeting multiple escape pathways is a tool to overcome adaptation of the tumour to treatment.

Another critical event in the process of cancer invasion, metastasis or tumoural angiogenesis is the degradation of various components of the ECM, including collagen, laminin, fibronectin and HSPGs. This can be accomplished by heparanase, secreted by cancer cells. Heparanase expression is rare in normal tissue, but is evident in many human tumours where it significantly increases both the angiogenic and metastatic

potential of cancer cells [21]. *In vitro,* LMWH with a mean weight of 4.5kDa inhibited 99% of heparanase activity [22]. Thus, nadroparin- and enoxaparin induced blocking of heparanase could possibly make the ECM less permissive for tumoural neovasculature. Indeed, structural alterations of the fibrin matrix induced by LMWH reduced the invasion of capillary-forming endothelial cells [23].

Our studies also describe a statistically significant increase in PCI, thus a better maturation of microvessels compared to tumoural vessels due to treatment with enoxaparin or nadroparin. An angiogenic signal (f.i. VEGF or bFGF) coming from tumour cells, will detach pericytes from the vessel wall and make endothelial cells loosen their junctions; as a consequence this pathological vessel dilates. VEGF increases the permeability of the endothelial cell layer, causing plasma proteins to extravasate and to increase the interstitial pressure [24]. We also observed a normalized diameter after treatment with nadroparin or enoxoparin in tumoural microvessels. In different reports, tumour vessel normalization appeared to be able to open new therapeutic opportunities to slow down tumour invasiveness and dissemination, and increase tumour responses to chemotherapeutics and radiotherapy than anti-angiogenic therapy alone [25] due to better perfusion of tumours and delivery of drugs.

Searching for early biomarkers of tumour response, different aspects of tumour physiology, rather than morphology, can be measured in a non-invasive way through various types of imaging modalities, as discussed in the overview given in **chapter 4.1**. A frequently used method of functional cancer imaging uses tumour metabolism of glucose: ^{18}F-fluorodeoxyglucose (FDG) PET or a multimodality scan combining PET and CT. Cancer cells often take up more glucose than normal cells, due to both increased and anaerobic metabolism (also known as the 'Warburg effect') [26]. In the prediction of reponse to neoadjuvant therapy, e.g. in esophageal cancer, this method proved to have a sensitivity of 67% and specificity of 68% [27], so FDG-PET should not be used to guide therapy in this clinical setting. More promising for this application are other types of PET tracers currently designed for tumour cell proliferation and apostosis, but wide clinical testing needs to be done yet. Also, for tumour hypoxia imaging [28], Yue *et al.* [29] used hypoxia PET imaging with ^{18}F-fluoroerythronitroimidazole. They found that tracer uptake predicted response to CRT, while a high standardized uptake value was associated with poor clinical response.

New developments in functional and molecular imaging have drawn attention on MR. Diffusion-weighted MRI enables quantifying the cellular proliferation index of cancer cells, as cancer growth results in restricted diffusion, while apoptosis and necrosis caused by anticancer therapy results in increased diffusion values [30]. Secondly, tumour perfusion-weighted imaging techniques are currently validated and include dynamic contrast enhanced (DCE)-MRI, but also DCE-CT or ultrasound, allowing the dynamic study of tissue enhancement over time after intravascular injection of a contrast agent (CA) [31]. The acquired images provide insight into tumour tissue properties such as blood volume, perfusion, and vascular permeability, all of which have been shown to represent adequate surrogate markers of therapy response [32]. Moreover, in DCE-MRI, when tissue enhancement is combined with simultaneous measurement of CA concentration in a feeding vessel, pharmacokinetic compartmental modeling is possible, which yields e.g. the endothelial transfer constant Ktrans [33], a parameter for

vascular permeability. Early response of tumour tissue to anti-angiogenic therapy, will lead to decreasing (normalizing) permeability of microvasculature. In **chapter 4.2,** we studied the feasibility of using a tumour angiogenesis specific probe for molecular MR imaging. We examined a human colorectal cancer cell line in a mouse model, known to express murine integrin $\alpha_v\beta_3$ on newborn tumour vasculature, but not on the tumour cells themselves [34-37]. The recognition sequence of the $\alpha_v\beta_3$ integrin is the RGD (Arg-Gly-Asp) peptide on the $\beta3$ domain [38], and the novel contrast agent tested in our experiment (P1227) consists of a routinely used monogadolinated CA linked to this RGD peptide as a tool to image tumour associated angiogenesis.

The utility of MRI based molecular imaging is hindered by its low sensitivity to visualize nanomolar epitopes. This is why target-specific molecules were developed in combination with a large (super)paramagnetic payload. Several authors have used RGD-coupled liposomes containing Gd-DTPA to visualize tumour angiogenesis [39,40]. Others have used RGD-labeled ultra-small superparamagnetic iron oxide nanoparticles (USPIO) and T2 weighted imaging [41-43], but several disadvantages are associated with the use of these particles. First, binding sites on the tumour cells and extracellular matrix can not be reached since these large carriers are limited to the intravascular compartment [44]. Also, concerns have risen regarding the safety and biological side effects of USPIOs in early clinical trials, although these were usually mild and reversible [45]. And finally, the pharmacokinetic properties of nano-sized tracers, including a plasma half live of several hours and retention by the reticulo-endothelial system better suit therapeutic than diagnostic purposes. Our results with the new low molecular weight tracer P1227 demonstrate that, compared to non-targeted DOTA, P1227 better discriminates angiogenic tumour tissue from normal muscle. Furthermore, aspecific accumulation of Gd-DOTA in the well vascularised oedemateous tumour tissue leads to persistently elevated signal intensities, even after several hours, due to contrast extravasation. Retention of the P1227 tracer due to specific binding to the target integrin was demonstrated by the near complete disappearance of P1227-induced tumour enhancement after pretreatment with cilengitide (a known inhibitor of the integrins $\alpha_v\beta_3$, $\alpha_v\beta_5$, and $\alpha_5\beta_5$). The specificity of the novel tracer for $\alpha_v\beta_3$ integrin was further demonstrated by the correlation between $\alpha_v\beta_3$ integrin immunohistochemical staining and the observed MRI enhancement.

5.2 Conclusion

Taken together, LMWHs act on several fronts of anticancer therapy, through anticoagulant-dependent mechanisms and direct antitumour effects. Although LMWHs significantly improved overall survival in cancer patients without venous thrombosis, the use of anticoagulants as antineoplastic therapy cannot be recommended until additional randomized controlled trials confirm these results [46]. The use of novel oral anticoagulants is not currently recommended for patients with malignancy and VTE, but trials are ongoing. In general, chariness is advised concerning the risk of bleeding during treatment with heparins. Therefore, non-anticoagulant low molecular weight heparins were developed for treating cancer patients because these products can be dosed higher, and can be administered in patients with bleeding risk. In this way, the antitumour or antimetastatic properties can be exploited completely [47]. Preclinically,

these non-anticoagulant LMWHs seem to be promising neoadjuvant therapies, as they distinctly increased tumour necrosis and enhanced chemoresponse in mouse breast, lung and pancreatic cancer models [48,49].

Developing new strategies in the war on cancer is crucial, but disrupting the cancer's capabilities is complex: multitargeting of the hallmarks of cancer is necessary [50,51], avoiding cumulative toxicities, and assuring correct timing and dosing of therapies to prevent adaptive or evasive resistance of the tumour [52-54]. Despite all efforts, vascular mimicry and mosaic vessel formation allow tumours to escape from antiangiogenic strategies. Other partners in the tumour ecosystem will have to be targeted too, such as carcinoma-associated fibroblasts, endothelial cells and immune cells (Fig.5.1) [55-58]. Another sobering issue is the great economic cost of cancer treatment, which poses serious cost-benefit dilemmas for patients and governments. Experimental work to deepen the knowledge of the mechanisms of angiogenesis is nonetheless necessary for treatment strategies in other fields of medicine, such as endometriosis, ocular diseases, cirrhosis, ischemic cardiac diseases, and tissue engineering [59].
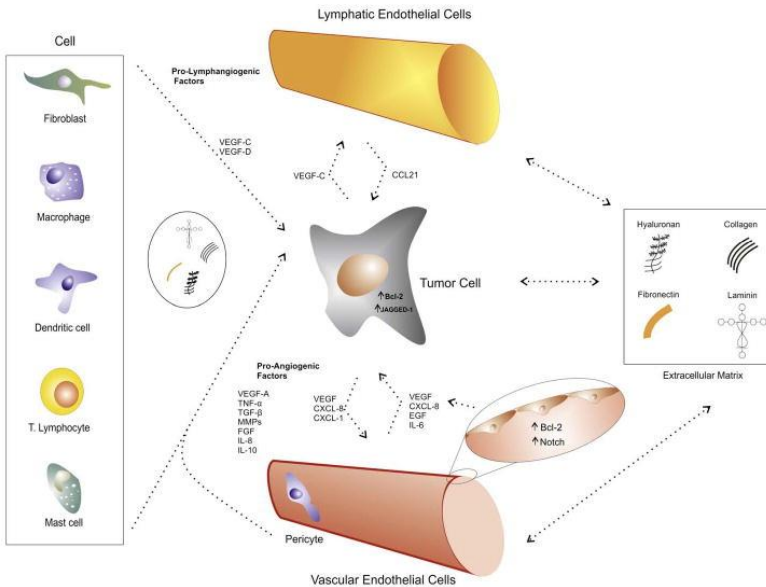

FIGURE 5.1 Tumour/endothelial crosstalk and cellular/microenvironmental signaling mechanisms. (Adapted from Gomes *et al.*, 2013 [57])

Searching performant biomarkers for evaluating anticancer therapy is another important topic of further experimental work. New preclinical and clinical studies will prove the efficacy of new imaging probes targeting tumour angiogenesis. In this way, site-specific imaging and delivery of drugs can show early effectiveness of therapy, diminish costs and chemo-resistance, and reduce side-effects on normal tissue, which is of major interest in the evolving research of cancer treatment. The development of these new imaging tools and contrast agents will be challenging, concerning selectivity for tumour tissue and avoidance of background noise, timing of administration of the product, bioavailability and safety for the patient [60].

Our group is currently studying the effects of VEGF-inhibitors on microvasculature in a peritoneal carcinomatosis model. Normalization of the tumour vasculature could lead to locally reduced IFP, and an increased diffusion/penetration of intraperitoneally delivered cytotoxic drugs.

Future work of our team will include the study of vascular normalization and treatment synergism in the combination of antiangiogenics. We will utilise *in vivo* fluorescence microscopy to study capillary permeability and its normalization after antiangiogenic regimens using fluorescently labelled tracers, and using tumour cells that express green fluorescent protein. Antiangiogenic regimens include radiotherapy (SARRP) with or without a pan-VEGF receptor tyrosine kinase inhibitor. Furthermore, comparison with concomitant in vivo tumour models (without dorsal skinfold chambers) are necessary to avoid some limitations of the IVM set up, and to have a detailed view on microvessel normalization with measurements of neovascular permeability (Ktrans in DCE-MRI), plasma and interstitial oncotic pressure (IFP), oxygenation (hyperspectral imaging filter) and erythrocyte flow (laser Doppler) in the tumour region.

Ultimately, these IVM findings can than be used as a gold standard for correlation with functional and molecular imaging of tumour neoangiogenesis and effects of multimodal treatment strategies.

5.3 References

1   Lyman GH, Khorana AA, Kuderer NM, Lee AY, Arcelus JI, Balaban EP, Clarke JM, Flowers CR, Francis CW, Gates LE, Kakkar AK, Key NS, Levine MN, Liebman HA, Tempero MA, Wong SL, Prestrud AA, Falanga A. Venous thromboembolism prophylaxis and treatment in patients with cancer: American Society of Clinical Oncology clinical practice guideline update. *J Clin Oncol.* 2013 Jun 10;31(17):2189-204.

2   Falanga A, Vignoli A, Diani E, Marchetti M. Comparative assessment of low-molecular-weight heparins in cancer from the perspective of patient outcomes and survival. *Patient Related Outcome Measures* 2011; 2: 175-188.

3   Norrby K. Low-molecular heparins and angiogenesis. *APMIS*. 2006; 114: 79-102.

4   Kakkar AK, Levine MN, Kadziola Z, Lemoine NR, Low V, Patel HK, Rustin G, Thomas M, Quigley M, Williamson RCN. Low molecular weight heparin, therapy with dalteparin, and survival in advanced cancer: the fragmin advanced malignancy outcome study (FAMOUS). *J Clin Oncol.* 2004; 22: 1944–1948.

5   Klerk CPW, Smorenburg SM, Otten HM, Lensing AWA, Prins MH, Piovella F, Prandoni P, Bos MMEM, Richel DJ, van Tienhoven G, Buller HR. The effect of low molecular weight heparin on survival in patients with advanced malignancy. *J Clin Oncol.* 2005; 23: 2130–2135.

6   Robert F, Busby E, Marques M, Reynolds R, Carey D. Phase II study of docetaxel plus enoxaparin in chemotherapy-naive patients with metastatic non-small cell lung cancer: preliminary results. *Lung Cancer.* 2003; 2 (42), 237-45.

7   Ono K, Ishihara M, Ishikawa K, *et al*. Periodate-treated non-anticoagulant heparin-carrying polystyrene (NAC-HCPS) affects angiogenesis and inhibits subcutaneous induced tumour growth and metastasis to the lung. *Br J Cancer.* 2002; 86: 1803-12.

8   Yoshitomi Y, Nakaniski H, Kusano Y, *et al*. Inhibition of experimental lung metastases of Lewis lung carcinoma cells by chemically modified heparin with reduced anti-coagulant activity. *Cancer Lett.* 2004; 207: 165-74.

9   Endrich B, Asaishi K, Gotz A, Messmer K. Technical report – a new chamber technique for microvascular studies in unanesthetized hamsters. *Res Exp Med.* 1980;177:125–134.

10 Menger M, Laschke M, Vollmar B. Viewing the microcirculation through the window: some twenty years experience with the hamster dorsal skinfold chamber. *Eur Surg Res.* 2002;34:83–91.

11 Norrby K. 2.5 and 5.0kDa heparin fragments specifically inhibit microvessel sprouting and network formation in VEGF(165)-mediated mammalian angiogenesis. *Int J Exp Pathol.* 2000; 81: 191–198.

12 Wan MX, Zhang XW, Torkvist L, Thorlacius H. Low molecular weight heparin inhibits tumor necrosis factor alpha-induced leukocyte rolling. *Inflammation Res.* 2001;50:581–584.

13 Fukumura D, Jain R. Imaging angiogenesis and the microenvironment. *APMIS.* 2008; 116: 695–715.

14 Norrby K. Heparin and angiogenesis: a low-molecular-weight fraction inhibits and a high-molecular-weight fraction stimulates angiogenesis systemically. *Haemostasis.* 1993; 23: 141–149.

15 Khorana AA, Sahni A, Altland OD, Francis CW. Heparin inhibition of endothelial cell proliferation and organization is dependent on molecular weight. *Arteriosclers Thromb Vasc Biol.* 2003; 23: 2110–2115.

16 Soker S, Goldstaub D, Svahn CM, Vlodavsky I, Levi BZ, Neufeld G. Variations in the size and sulfation of heparin modulate the effect of heparin on the binding of Vegf(165) to its receptors. *Biochem Biophys Res Comm.* 1994; 203: 1339–1347.

17 Lepri A, Benelli U, Bernardini N, Bianchi F, Lupetti M, Danesi R, *et al.* Effect of low molecular weight heparan sulphate on angiogenesis in the rat cornea after chemical cauterization. *J Ocul Pharmacol.* 1994; 1 (10): 273-80.

18 Jayson G, Gallagher J. Heparin oligosaccharides: inhibitors ofthe biological activity of bFGF on Caco-2 cells. *Br J Cancer.* 1997; 75: 9-16.

19 Norrby K, Ostergaard P. Basic-fibroblast-growth-factor-mediated de novo angiogenesis is more effectively suppressed by low-molecular-weight than by high-molecular-weight heparin. *Int J Microcirc Clin Exp.* 1996; 16: 8–15.

20 Saif M. Anti-VEGF agents in metastatic colorectal cancer (mCRC): are they all alike? *Cancer Manag Res.* 2013; 3: 103-115.

21 Vlodavsky I, Korner G, Ishai-Michaeli R, Bashkin P, Bar-Shavit R, Fuks Z. Extracellular matrix-resident growth factors and enzymes: possible involvement in tumor metastasis and angiogenesis. *Cancer Metastasis Rev.* 1990; 3(9): 203-26.

22 Bar-Ner M, Eldor A, Wasserman L, Matzner Y, Cohen I, Fuks Z, *et al.* Inhibition of heparanase-mediated degradation of extracellular matrix heparan sulfate by non-anticoagulant heparin species. *Blood.* 1987; 2(70): 551-7.

23 Collen A, Smorenburg S, Peters E, Lupu F, Koolwijk P, Van Noorden C, *et al.* Unfractionated and low molecular weight heparin affect fibrin structure and angiogenesis *in vitro. Cancer Res.* 2000; 60: 6196–6200.

24 Carmeliet P, Jain R. Molecular mechanisms and clinical applications of angiogenesis. *Nature.* 2011; 473: 298-307.

25 Jain RK. Normalization of tumor vasculature: an emerging concept in antiangiogenic therapy. *Science.* 2002; 5706 (307): 58-62.

26 Gillies RJ, Raghunand N, Karczmar GS, Bhujwalla ZM. MRI of the tumor microenvironment. *J Magn Reson Imaging.* 2002; 16: 430–450.

27 Kwee RM: Prediction of tumor response to neoadjuvant therapy in patients with esophageal cancer with use of (18)F FDG PET: a systematic review. *Radiology.* 2010; 254: 707–717.

28 Mees G, Dierckx R, Vangestel C, Van de Wiele C: Molecular imaging of hypoxia with radiolabelled agents. *Eur J Nucl Med Mol Imaging.* 2009; 36: 1674–1686.

29 Yue J, Yang Y, Cabrera AR, Sun X, Zhao S, Xie P, Zheng J, Ma L, Fu Z, Yu J: Measuring tumor hypoxia with 18 F-FETNIM PET in esophageal squamous cell carcinoma: a pilot clinical study. *Dis Esophagus.* 2012; 25: 54–61.

30 Harry VN, Semple SI, Parkin DE, Gilbert FJ: Use of new imaging techniques to predict tumour response to therapy. *Lancet Oncology.* 2010; 11: 92–102.

31 Hylton N: Dynamic contrast-enhanced magnetic resonance imaging as an imaging biomarker. *J Clin Oncol.* 2006; 24: 3293–3298.

32 Ceelen W, Smeets P, Backes W, Van Damme N, Boterberg T, Demetter P, Bouckenooghe I, De Visschere M, Peeters M, Pattyn P: Noninvasive monitoring of radiotherapy-induced microvascular changes using dynamic contrast enhanced magnetic resonance imaging (DCE-MRI) in a colorectal tumor model. *Int J Radiat Oncol Biol Phys.* 2006; 64: 1188–1196.

33 Sourbron SP, Buckley DL: Tracer kinetic modelling in MRI: estimating perfusion and capillary permeability. *Phys Med Biol.* 2012; 57:R1–R33.

34 Kemperman H, Wijnands YM, Roos E. alpha V integrins on HT-29 colon carcinoma cells: Adhesion to fibronectin is mediated solely by small amounts of alpha V beta 6, and alpha V beta 5 is codistributed with actin fibers. *Exp Cell Res.* 1997; 234: 156-164.

35 Haier J, Nasralla M, Nicolson GL. Different adhesion properties of highly and poorly metastatic HT-29 colon carcinoma cells with extracellular matrix components: role of integrin expression and cytoskeletal components. *Br J Cancer.* 1999; 80: 1867-1874.

36 Liu Z, Jia B, Shi J, *et al.* Tumor Uptake of the RGD Dimeric Probe (99m)Tc-G(3)-2P(4)-RGD2 is Correlated with Integrin alpha(v)beta(3) Expressed on both Tumor Cells and Neovasculature. *Bioconjug Chem.* 2010; 21 (3): 548–555.

37 Zhou Y, Kim YS, Chakraborty S, Shi J, Gao H, Liu S. 99mTc-labeled cyclic RGD peptides for noninvasive monitoring of tumor integrin $\alpha_v\beta_3$ expression. *Mol Imaging.* 2011; 10:386-397.

38 Dunehoo A, Anderson M, Majumdar S, Kobayashi N, Berkland C, Siahaan TJ. Cell adhesion molecules for targeting drug delivery. *J Pharm Sci.* 2006; 95: 1856-1872.

39 Winter PM, Caruthers SD, Kassner A, *et al.* Molecular Imaging of angiogenesis in nascent vx-2 rabbit tumors using a novel alpha(v)beta(3)-targeted nanoparticle and 1.5 tesla magnetic resonance imaging. *Cancer Res.* 2003; 63: 5838-5843.

40 Mulder WJM, Strijkers GJ, Habets JW, *et al.* MR molecular imaging and fluorescence microscopy for identification of activated tumor endothelium using a bimodal lipidic nanoparticle. *FASEB J.* 2005; 19: 2008-2010.

41 Zhang CF, Jugold M, Woenne EC, *et al.* Specific targeting of tumor angiogenesis by RGD-conjugated ultrasmall superparamagnetic iron oxide particles using a clinical 1.5-T magnetic resonance scanner. *Cancer Res.* 2007; 67: 1555-1562.

42 Jiang T, Zhang CF, Zheng X, Xu XF, Xie X, Liu HC, Liu SY. Noninvasively characterizing the different alpha v beta 3 expression patterns in lung cancers with RgD-USPIO using a clinical 3.0T MR scanner. *Int J Nanomed.* 2009; 4: 241-249.

43 Kiessling F, Huppert J, Zhang CF, *et al.* RGD-labeled USPIO Inhibits Adhesion and Endocytotic Activity of alpha(v)beta(3)-Integrin-expressing Glioma Cells and Only Accumulates in the Vascular Tumor Compartment. *Radiology.* 2009; 253: 462-469.

44 Wong C, Stylianopoulos T, Cui J, *et al.* Multistage nanoparticle delivery system for deep penetration into tumor tissue. *Proc Natl Acad Sci USA.* 2011; 108: 2426-2431.

45 Sharma R, Saini S, Ros PR, *et al.* Safety profile of ultrasmall superparamagnetic iron oxide ferumoxtran-10: Phase II clinical trial data. *J Magn Res Im.* 1999; 9: 291-294.

46 Kuderer NM, Khorana AA, Lyman GH, Francis CW. A meta-analysis and systematic review of the efficacy and safety of anticoagulants as cancer treatment: impact on survival and bleeding complications. *Cancer.* 2007 Sep 1;110(5):1149-61.

47 Chen JL, Fan J, Chen MX, Dong Y, Gu JZ. Effect of non-anticoagulant N-desulfated heparin on basic fibroblast growth factor expression, angiogenesis, and metastasis of gastric carcinoma *in vitro* and *in vivo. Gastroenterol Res Pract.* 2012;2012:752940.

48 Phillips PG, Yalcin M, Cui H, Abdel-Nabi H, Sajjad M, Bernacki R, Veith J, Mousa SA. Increased tumor uptake of chemotherapeutics and improved chemoresponse by novel non-anticoagulant low molecular weight heparin. *Anticancer Res.* 2011 Feb;31(2):411-9.

49 Sudha T, Yalcin M, Lin HY, Elmetwally AM, Nazeer T, Arumugam T, Phillips P, Mousa SA. Suppression of pancreatic cancer by sulfated non-anticoagulant low molecular weight heparin. *Cancer Lett.* 2014 Aug 1;350(1-2):25-33.

50 De Palma M, Hanahan D. The biology of personalized cancer medicine: facing the complexities underlying hallmark capabilities. *Mol Oncol.* 2012; 6:111-27.

51 Hanahan D. Rethinking the war on cancer. Lancet. 2014; 383: 558-563.

52 Garraway LA, Jänne PA. Circumventing cancer drug resistance in the era of personalized medicine. *Cancer Discov.* 2012 Mar;2(3):214-26.

53 Bottsford-Miller JN, Coleman RL, Sood AK. Resistance and escape from antiangiogenesis therapy: clinical implications and future strategies. *J Clin Oncol.* 2012 Nov 10;30(32):4026-34.

54 Mittal K, Ebos J, Rini B. Angiogenesis and the tumor microenvironment: vascular endothelial growth factor and beyond. *Semin Oncol.* 2014 Apr;41(2):235-51.

55 Hanahan D, Coussens LM. Accessories to the crime: functions of cells recruited to the tumor microenvironment. *Cancer Cell.* 2012 Mar 20;21(3):309-22.

56 Togo S, Polanska UM, Horimoto Y, Orimo A. Carcinoma-associated fibroblasts are a promising therapeutic target. *Cancers (Basel).* 2013 Jan 31;5(1):149-69.

57 Gomes FG, Nedel F, Alves AM, Nör JE, Tarquinio SB. Tumor angiogenesis and lymphangiogenesis: tumor/endothelial crosstalk and cellular/microenvironmental signaling mechanisms. *Life Sci.* 2013 Feb 7;92(2):101-7.

58 De Wever O, Van Bockstal M, Mareel M, Hendrix A, Bracke M. Carcinoma-associated fibroblasts provide operational flexibility in metastasis. *Semin Cancer Biol.* 2014 Apr;25:33-46.

59 Schumann P, Lindhorst D, von See C, Menzel N, Kampmann A, Tavassol F, Kokemüller H, Rana M, Gellrich NC, Rücker M. Accelerating the early angiogenesis of tissue engineering constructs *in vivo* by the use of stem cells cultured in matrigel.*J Biomed Mater Res A.* 2014 Jun;102(6):1652-62.

60 Patel N, Harris AL, Gleeson FV, Vallis KA. Clinical imaging of tumor angiogenesis. *Future Oncol.* 2012 Nov;8(11):1443-59.

Summary

CHAPTER 6: SUMMARY

During multiplication of neoplastic cells, all necessary nutrients and oxygen are delivered by passive diffusion, which is sufficient for distances up to 100-200 μm. After reaching a critical tumour mass, the formation of new blood vessels (angiogenesis) is needed to feed the tumour. Inhibition of tumour-associated angiogenesis (TAA) or normalization of the pathological microvasculature is a logic next step in treating cancer. To develop antiangiogenic molecules, and to adequately follow patients during treatment strategies, it is crucial to find early anti-angiogenic molecular effects and validated biomarkers.

First, we investigated tumour associated angiogenesis and the anti-angiogenic effects of therapy using *in vivo* microscopy (IVM), a non-invasive method which allows detailed repetitive examination of microvasculature. The antitumour effect of nadroparin, a frequently used LMWH, is thought to rely on vascular normalization (**chapter 3.1**). We studied tumoural angiogenesis and the effects of nadroparin via *in vivo* fluorescence microscopy in a dorsal skinfold chamber model in hamsters using contrast agent that is tagged with a fluorescent marker (FITC–labelled dextran). Morphological (length of microvessels, number of vessels per area, diameter, vascular area fraction), dynamic (red blood cell velocity and volumetric blood flow), and immunohistochemical data (pericyte coverage index, fractal dimension, and microvesssel density) were gathered to assess tumour microenvironment and the effects of nadroparin therapy on AMel-3 (hamster melanoma) and HaP-T1 (hamster pancreatic carcinoma) tumours. In this tumour model, nadroparin revealed to have anti-angiogenic effects, leading to a normalized tumour microvasculature, including a smaller increase in diameter, a higher PCI (maturation), and less vessel tortuosity (smaller fractal dimension). In **chapter 3.2**, we examined the effects of nadroparin and enoxaparin, frequently used LMWHs, using IVM and the dorsal skinfold chamber model, but this time we used a human colorectal cancer model in athymic mice. Our results suggest that both nadroparin as enoxaparin exert an anti-angiogenic effect in human colorectal carcinoma, as evidenced by a significantly lower vascular area fraction, microvessel density, length and number of microvessels when compared with control animals.

The validation of reliable biomarkers of TAA is an important challenge for the future, enabling an early and effective detection of anti-angiogenic effects. Different aspects of tumour physiology, rather than morphology, can be measured in a non-invasive way through various types of imaging modalities, as discussed in the overview given in **chapter 4.1**. One imaging technique, molecular imaging, was studied in **chapter 4.2**, using a new contrast agent targeting integrin $\alpha_v\beta_3$ (P1227), expressed in tumoural endothelial cells and not in normal endothelium. Colorectal cancer xenografts (HT29) were subcutaneously grown in the hind leg of nude mice and MRI was performed before contrast agent administration and at several time intervals after injection of P1227 or Gd-DOTA, an aspecific blood pool CA. ROIs were drawn and the normalized enhancement ratio (NER) was calculated in the tumour. After quantification of tumour associated angiogenesis via P1227, images were taken after injection of cilengitide, a specific inhibitor of $\alpha_v\beta_3$ mediated cell adhesion. Using P1227, specific enhancement of the angiogenic tumour rim, but not of normal muscle was observed whereas Gd-DOTA enhanced tumour and normal muscle. After administering cilengitide, enhancement

with P1227, but not with DOTA was significantly suppressed during the first 20 minutes. When using P1227, a significant correlation was observed between normalized enhancement of the tumour rim and immunohistochemical $\alpha_v\beta_3$ integrin expression. We showed that molecular MR imaging using a small monogadolinated tracer targeting $\alpha_v\beta_3$ integrin holds promise in assessing colorectal TAA.

Future work of our group will include a complete study of the tumour microenvironment and vessel normalization after antiangiogenic regiments using *in vivo* fluorescent microscopy, measurements of laser Doppler erythrocyte flow, plasma and interstitial oncotic pressure, neovascular permeability (K^{trans} in DCE-MRI) and oxygenation in the tumour region.

Ultimately, these IVM findings can than be used as a gold standard for correlation with functional and molecular imaging of tumour neoangiogenesis and effects of multimodal treatment strategies.

CHAPTER 7

Samenvatting

CHAPTER 7: SAMENVATTING

Tijdens neoplastische celdeling worden zuurstof en nutriënten aangebracht via passieve diffusie, die toereikend is over afstanden tot 100-200 μm. Na het bereiken van een kritisch tumorvolume is vorming van nieuwe bloedvaten (angiogenese) nodig om de tumor te voeden. Het inhiberen van tumorale angiogenese of de normalisatie van deze pathologische bloedvaten is dan ook een logische stap in de behandeling van kanker. Zowel voor de ontwikkeling van antiangiogene moleculen als voor het adequaat opvolgen van kankerpatiënten is het van groot belang vroegtijdige anti-angiogene moleculaire effecten en gevalideerde biomerkers op te sporen.

Wij onderzochten in **hoofdstuk 3** tumorale angiogenese en de anti-angiogene effecten van therapie door middel van *in vivo* microscopie (IVM), een niet-invasieve methode waarbij gedetailleerd repetitief onderzoek van microvasculatuur mogelijk is. Het anti-tumorale effect van nadroparine, een frequent gebruikt laag moleculair gewichts heparine (LMWH), zou berusten op het bevorderen van tumorale vasculaire normalisatie (**hoofdstuk 3.1**). We bestudeerden tumorale angiogenese en de effecten van nadroparine via *in vivo* fluorescentie microscopie in een dorsal skinfold chamber model in hamsters, waarbij een contraststof werd aangewend die gemerkt is met een fluorescente merker (FITC– dextraan). Morfologische (lengte van microvasculatuur, aantal bloedvaten, diameter, vasculaire fractie), dynamische (rode bloedcel snelheid en debiet), en immunohistochemische gegevens (pericyten coverage index, fractale dimensie, en bloedvatendensiteit) werden verzameld om de tumorale micro-omgeving en de effecten van behandeling met nadroparine te beoordelen op AMel-3 (hamster melanoma) en HaP-T1 (hamster pancreascarcinoom) tumoren. In deze tumor modellen bleek nadroparine anti-angiogene effecten te hebben met een genormaliseerde tumor microvasculatuur tot gevolg, waaronder een beperktere toename in bloedvatdiameter, een hogere PCI (maturatie) en minder tortueuze bloedvaten (lagere fractale dimensie). In hoofdstuk 3.2 onderzochten we opnieuw de effecten van zowel nadroparine als enoxaparine, courant gebruikte LMWHs, via IVM en het dorsal skinfold chamber model, maar ditmaal werd een humaan colorectaal carcinoommodel gebruikt in athymische muizen. Onze resultaten suggereerden dat zowel nadroparine als enoxaparine antiangiogene effecten teweegbrengen ook in een humaan colorectaal carcinoom, zoals gestaafd werd door een significant lagere vasculaire fractie, bloedvatendensiteit, lengte en aantal microvaten na vergelijking met de controle dieren.

Het valideren van betrouwbare biomerkers van tumorale angiogenese is een belangrijke uitdaging voor de toekomst om snel en effectief effecten van anti-angiogene therapie op te sporen. Verschillende aspecten van tumor fysiologie, in plaats van tumor morfologie, kunnen op een niet-invasieve manier worden gemeten via verschillende types beeldvorming, zoals werd besproken in **hoofdstuk 4.1**. Eén ervan, moleculaire beeldvorming, werd door ons onderzocht (**hoofdstuk 4.2**) door middel van een nieuwe contrastof gericht tegen het $\alpha_v\beta_3$ integrine (P1227), dat tot expressie wordt gebracht in tumoraal endotheel en nauwelijks in normaal endotheel. Hierbij werd in naakte muizen een humane HT29 colorectale tumor in de flank geïnduceerd en vervolgens MR beeldvorming uitgevoerd vóór contrasttoediening en op geregelde tijdstippen na injectie

van P1227 of Gd-DOTA, een aspecifieke contraststof. Aan de hand van deze beelden werd de normalized enhancement ratio (NER) berekend in de tumor. Na quantificeren van tumorale angiogenese aan de hand van P1227, werd ook beeldvorming uitgevoerd na toediening van cilengitide, dat specifiek $\alpha_v\beta_3$-gemedieerde celbinding blokkeert. Na toediening van P1227 kon specifieke aankleuring van de angiogene tumorrand maar niet van normaal spierweefsel aangetoond worden, terwijl Gd-DOTA zowel tumor als spierweefsel deed aankleuren. Na toedienen van cilengitide werd de contrastaankleuring van P1227 significant onderdrukt tijdens de eerste 20 minuten; bij Gd-DOTA werd dit verschil niet waargenomen. Tenslotte werd ook een significante correlatie gevonden in de P1227 groep, tussen NER van de tumorrand en immunohistochemische $\alpha_v\beta_3$ integrine expressie. Hierbij kunnen we besluiten dat moleculaire MRI via een kleine monogadolinium tracer die op $\alpha_v\beta_3$ integrine bindt, een beloftevolle techniek is in het evalueren van colorectale tumorale angiogenese.

Toekomstig werk van onze groep zal zich focussen op een complete studie van de tumorale micro-omgeving en bloedvatnormalisatie na antiangiogene therapie via *in vivo* fluorescente microscopie, metingen via laser Doppler doorbloeding, plasma en interstitiële oncotische druk, neovasculaire permeabiliteit (K^{trans} in DCE-MRI) en oxygenatie in de tumorregio.

Uiteindelijk zullen deze resultaten van het IVM onderzoek gebruikt kunnen worden als gouden standaard voor correlatie met functionele en moleculaire beeldvorming van tumorale angiogenese en de effecten van multimodale behandelingsstrategieën.

Curriculum Vitae

1. Personal Data:
   - Name: Debergh
   - First names: Isabelle Maria Cornelia
   - Born: September, 4th, 1982, Veurne
   - Nationality: Belgian
   - Marital status: married (Thomas De Wolf), 3 children (Ernest, °2010; Renee, °2012; Gisele, °2014)
   - Adress: Antwerpsesteenweg 985, B-9041 Oostakker, Belgium
   - E-mail: isabelle.debergh@ugent.be
   - Tel: 0032 498 80 61 97

2. Training:
   - 1994-2000: Humaniora Science-Maths (8h), Sint-Stanislas College, Poperinge
   - 2000-2007: Medical School Study, Ghent University
   - 2007-2010: surgical trainee UZ Ghent, Prof. Dr. B. de Hemptinne
   - 01/10/2007-31/07/2009: PhD-student; project: tumoural angiogenesis
   - 2010-2012: surgical trainee AZ St-Lucas Ghent, Dr. M. Kint
   - 2012-2014: surgical trainee UZ Ghent, Prof. Dr. P. Pattyn
   - 2014-2015: fellowship AZ St-Jan Bruges, Dr. B. Dillemans

3. Certificates and Postgraduate Courses:
   - 2003 ECG-certificate
   - 2007 Doctor in Medicine, with high honours
   - 2007 Certificate Radioprotection
   - 2006-2007 Postgraduate course Urgency medicine
   - 2008 Certificate Laboratory Animal Science

4. Scientifical Work:
   - Paper 2002-2005: "The positive/negative influence of inducible NO-synthase in motility disorders in inflammatory bowel diseases."
     Promotor: Prof. Dr. R. A. Lefebvre; Co-Promotor: K. Van Crombruggen
   - PhD-student 2007-2009 (BOF grant): "Integrated study of the effects of antiangiogenic therapy on microvascular physiology in human cancer models."
     Promotor: Prof. Dr. W. Ceelen; Co-Promotor: Prof. Dr. P. Pattyn

5. Awards:
   - The Belgian Week of Gastroenterology Prize for the best oral presentation in the field of Basic Science Gastroenterology, February 13th 2009
   - VVGE award 2009 Young Scientist (Vlaamse Vereniging voor Gastro-Enterologie)

6. Motto:
   - "Was mich nicht umbringt, macht mich stärker." (Friedrich Nietzsche)
   - "Less is more." (Ludwig Mies van der Rohe)

7. Articles:
   - Debergh I, Van Damme N, De Naeyer D, Smeets P, Demetter P, Robert P, Carme S, Pattyn

P, Ceelen W. Molecular imaging of tumor-associated angiogenesis using a novel magnetic resonance imaging contrast agent targeting αvβ3 integrin. Ann Surg Oncol. 2014 Jun;21(6):2097-104. doi: 10.1245/s10434-013-3444-1. Epub 2013 Dec 20.

- Debergh I, Fierens K. Laparoscopic repair of a Bochdalek hernia with incarcerated bowel during pregnancy: report of a case. Surg Today. 2014 Apr;44(4):753-6. doi: 10.1007/s00595-012-0441-0. Epub 2013 Jan 5.

- Debergh I, Vanhove C, Ceelen W. Innovation in cancer imaging. Eur Surg Res. 2012;48(3):121-30. doi: 10.1159/000338193. Epub 2012 Apr 24. Review.

- De Naeyer D, Debergh I, De Deene Y, Ceelen WP, Segers P, Verdonck P. First order correction for T2*-relaxation in determining contrast agent concentration from spoiled gradient echo pulse sequence signal intensity. J Magn Reson Imaging. 2011 Sep;34(3):710-5. doi: 10.1002/jmri.22681. Epub 2011 Jul 18.

- Bouquet W, Deleye S, Staelens S, De Smet L, Van Damme N, Debergh I, Ceelen WP, De Vos F, Remon JP, Vervaet C. Antitumour efficacy of two paclitaxel formulations for hyperthermic intraperitoneal chemotherapy (HIPEC) in an in vivo rat model. Pharm Res. 2011 Jul;28(7):1653-60. doi: 10.1007/s11095-011-0401-1. Epub 2011 Mar 18.

- Debergh I, Van Damme N, Pattyn P, Peeters M, Ceelen WP. The low-molecular-weight heparin, nadroparin, inhibits tumour angiogenesis in a rodent dorsal skinfold chamber model. Br J Cancer. 2010 Mar 2;102(5):837-43. doi: 10.1038/sj.bjc.6605535. Epub 2010 Feb 2.

Acknowledgments

I wish to express my sincere gratitude to a number of colleagues, dear friends, and my beloved family, for all support and encouragement I have received to accomplish this thesis:

Prof. Dr. W. Ceelen, promotor, for excellent supervision and for always believing in me. The way you combine persistent scientifical work and surgical clinic, is an inspiration for us all. Over the last 7 years, a beautiful surgical lab was founded, and it is thriving rapidly. I am proud I was a little part of this in the beginning days. It has been an honour working with you.

Prof. Dr. P. Pattyn, co-promotor and brilliant surgeon, for logistical support during my PhD-candidate-position and surgical training, and thereby supplying me with invaluable research time in the department of surgery. I am looking forward for future collaborations.

Natacha Rosseel, Ellen Terrie, and Nancy Van Damme, for superb help and advices in the research lab, with immunostaining, culturing cell lines, animal care and experiments. Your support was crucial for the completion of these studies. I really enjoyed working with you!

The lab of Gastroenterology, Marc Peeters, Christophe Van Steenkiste, Dieter De Naeyer, and Pieter Demetter, for providing me essential practical advice, for help with interpretation and technical support concerning histology and immunohistochemistry in my early days of research.

Peter Smeets, and the team of the MRI department, for giving me a fast track course in handling the Magnetom Symphony MRI scanner, and giving me the opportunity and the trust to use your expensive equipment during the long nights of scanning mice.

Sabin Carme and Philippe Robert (Guerbet), for providing me contrast agent and information concerning MRI scanning.

Wouter Willaert and Felix Gremonprez, my research colleagues, for inspiring and helpful discussions concerning surgery and laboratory work, for nice moments in the 'cellar'.

Colleague-trainees, nurses, and secretaries of the department of surgery, for help with patients during my research absence, for practical issues and for relieving laughs and discussions during my training as a surgeon!

Staff members of the department of surgery, University Hospital and AZ Sint-Lucas, Ghent and AZ Sint-Jan, Bruges, for your time and patience, for your support in fulfilling this project, for teaching your surgical skills, and for being an inspiration for young surgeons in handling work-life balance.

Members of the reading and exam commission, Prof. Dr. T. Boterberg, Prof. dr. O. De Wever, Prof. dr. A. Geerts, Prof. dr. J. Van de Voorde, Prof. dr. C. Vanhove, and Prof. dr. P. Van Schil, for your constructive remarks and thorough evaluation.

All my friends and near family, for valuable moments and positive energy, for your empathy and patience, for being there for me and my family in stressful times. Big hug!

Papa and mama, Annelies, Stephanie, and Catherine, for giving me a solid foundation of a warm family to build on, for teaching me how to deal in life, with time for pleasure and grief, relaxing and working hard. Thank you for always believing in me!!

Ernest, Renee, and Gisele, our precious kids, for being the sunshine in our lifes. Your appearances provoke instant happiness! An extra kiss for you, Gisele, for being such a good girl the first three months of your life while mummy had to do the final exam for surgery and finish this thesis.

Thomas, my beloved husband and soulmate, for being Thomas. I am so lucky to have you accompanying me on this beautiful journey of life. You learn me what truly matters; you put adversity in perspective when my mind is blurred. Thank you xxxxxxx